

**Investigations on some amino acid based single
crystals for nonlinear optical applications and amino
acid capped nanocrystals**

Thesis Submitted to

Cochin University of Science and Technology

*In partial fulfilment of the requirements for the
award of the degree of*

DOCTOR OF PHILOSOPHY

By

Sreevalsa V.G



Department of Physics

Cochin University of Science and Technology

Cochin-682022

November 2012

Investigations on some amino acid based single crystals for nonlinear optical applications and amino acid capped nanocrystals

Ph.D. thesis in the field of Material Science

Author:

Sreevalsa V.G

Division for Research in Advanced Materials

Department of Physics

Cochin University of Science and Technology

Cochin-682022

e-mail : sreevalsavg@gmail.com

Supervising Guide:

Dr. S. Jayalekshmi

Professor

Department of Physics

Cochin University of Science and Technology

Kochi: 682 022, Kerala, India

Email: sjayakartha@gmail.com

jayalekshmi@cusat.ac.in

November 2012

Dedicated to my beloved Parents and Teachers



DEPARTMENT OF PHYSICS

Cochin University of Science & Technology
Kochi – 682 022, Kerala, India

Dr. S. JAYALEKSHMI
Professor

Phone: 91-484-2577404 Extn. 34
Email: sjayakartha@gmail.com
jayalekshmi@cusat.ac.in

Date:

Certificate

Certified that the work presented in the thesis entitled “Investigations on some amino acid based single crystals for nonlinear optical applications and amino acid capped nanocrystals” is based on the original work done by Mrs. Sreevalsa, V.G under my guidance and supervision at the Department of Physics, Cochin University of Science and Technology, Cochin-22, India and no part of it has been included in any other thesis submitted previously for the award of any degree.

Dr. S. Jayalekshmi
(Supervising Guide)

DECLARATION

Certified that the work presented in the thesis entitled “Investigations on some amino acid based single crystals for nonlinear optical applications and amino acid capped nanocrystals” is based on the original work done by me under the guidance of Prof. S.Jayalekshmi, Professor, Department of Physics, Cochin University of Science and Technology, Cochin–22, India no part of it has been included in any other thesis submitted previously for the award of any degree.

*Kochi– 22
2012*

Sreevalsa.V.G

Acknowledgement

When mind is full, words are scarce, true, when expressing gratitude to all those who have directly or indirectly involved in all walks of my research career.

I am highly indebted to my guide, Prof. S.Jayalekshmi; under whose supervision the work reported here became fruitful and invaluable. I am grateful to her for the support and excellent guidance throughout my research career. Her humble nature, simplicity, sincerity, the way she treats students are worthy to be followed in life. She is my friend, guide and philosopher in the true sense.

I am also thankful to the present Head of the department of Physics, Prof.B.Pradeep and the former Head Prof. M.R.Anantharaman, for extending all the necessary facilities. Thanks are also due to Prof.V.C.Kuriakose, the doctoral committee member and my teacher, for all the blessings. I express my sincere thanks to all the faculty members of the Department of Physics, for their support and encouragement.

I extend my sincere thanks to the University Grants Commission, for providing Teacher fellowship under the Faculty Improvement Programme.

I am extremely thankful to the Principal and staff of my college, K.K.T.M Govt. College, Pullut, Kodungallur for the support and inspiration.

I take this opportunity to thank Prof. K.Babu Joseph, former Vice Chancellor and Head of the Department of Physics, CUSAT who has paved my way to research. I acknowledge my gratitude to Prof.V.P.N.Nampoori, Prof. V.M.Nandakumar and Prof. P.Radhakrishnan, of International School of Photonics, CUSAT, for the encouragement and support during my research tenure.

I thank Dr. Reji Philip and Miss. Lekshmi of Raman Research Institute, Bangalore, Vishnu Kavungal and Mathew of ISP, CUSAT and Prof. P.K. Das, IISc Bangalore for the help extended in characterising the nonlinear optical properties.

I am also thankful to Dr. Deepthy Menon (formerly of ISP,CUSAT), Dr. Reethamma, of ISP,CUSAT for all the help and support rendered.

Thanks are also due to the non teaching staff, Department of Physics, CUSAT for the help and services rendered throughout the period of research.

Being with all the members of our DREAM lab- Jeeju, Sajimol Augustine, SreekanthVarma, Aanand, Dr.Dhanya.T, Anilkumar,K,M, Francis Xavier and Rajiv Tomy was a nice and enriching experience. I cherish the moments spent with my teacher friends Jeeju and Sajimol Augustine, especially the lunch breaks, sharing dishes and also ideas. Thanks to Sukesan (Jeeju's husband) of CUSAT for the safe and joyful drive to University and back home.

I am extremely thankful to my senior research scholars Dr.Arun.K,J, Dr.Amritesh and Late Dr.Raveendranath who have stamped a rich research culture in our lab.

I take this opportunity to thank Dr Sreeja, Dr Aneesh, Subha, Krishna Prasad, Sanal, Hasna and Ganesh, former and present research students of the Department of Physics for the sincere help extended, whenever necessary.

The services rendered by STIC, CUSAT, SAIF, IIT Madras, SCTIMST Trivandrum and CIPET Bhuvanewar are gratefully acknowledged.

No words are adequate to express my indebtedness to my family, especially my husband and daughter who were always with me with invaluable support, care and affection, without any complaints, even when their needs were overlooked in the tight schedule. I am also grateful to my sister, brother in law and son in law for the

consideration and care extended. Also I remember the prayers of my parents, who are no more now but, were highly concerned about my research.

Above all, I bow my head before the Almighty for the everlasting blessings showered on me, without whose grace, this report would not have emerged in this form.

Sreevalsa.V.G

Contents

Preface

List of Publication

Chapter 1 INTRODUCTION	1
1.1 <i>Theory of crystal growth</i>	2
1.2 <i>Thermodynamics of crystal growth.....</i>	3
1.3 <i>Nucleation.....</i>	4
1.4 <i>Crystal growth theories</i>	6
1.5 <i>Crystal growth techniques</i>	12
1.6 <i>Defects in crystals</i>	21
1.7 <i>Nonlinear optics</i>	22
1.7.1 <i>Frequency Conversion.....</i>	25
1.7.2 <i>Self Action Effects</i>	27
1.8 <i>Nonlinear optical materials.....</i>	28
1.9 <i>Advantages of organic nonlinear materials</i>	31
1.10 <i>Objectives of the present investigations.....</i>	32
1.11 <i>References.....</i>	33
Chapter 2 CHARACTERIZATION TECHNIQUES.....	39
2.1 <i>Structural characterization</i>	39
2.1.1 <i>Single crystal X-ray crystallography</i>	40
2.1.2 <i>Powder X-ray diffraction.....</i>	42
2.1.3 <i>Transmission Electron Microscope.....</i>	42
2.2 <i>Elemental Analysis</i>	44
2.2.1 <i>CHN analysis.....</i>	45
2.2.2 <i>Energy Dispersive Analysis by X-rays (EDX).....</i>	45

2.2.3	<i>Inductively Coupled Plasma Atomic Emission Spectroscopy (ICP AES)</i>	46
2.3	<i>Vibrational Spectral Analysis</i>	46
2.3.1	<i>Fourier transform infra red spectroscopy (FTIR)</i>	47
2.3.2	<i>Raman spectroscopy</i>	49
2.4	<i>Optical characterization</i>	50
2.4.1	<i>UV-Vis absorption spectroscopic studies</i>	51
2.4.2	<i>Photoluminescence studies</i>	53
2.5	<i>Characterization of Nonlinear optical properties</i>	54
2.5.1	<i>Second harmonic efficiency (SHG)</i>	54
2.5.2	<i>Open aperture Z scan method</i>	55
2.6	<i>Thermal Characterization</i>	57
2.7	<i>Dielectric studies</i>	58
2.8	<i>Etching studies</i>	59
2.9	<i>References</i>	59

Chapter 3 L-CITRULLINE OXALATE MONOHYDRATE– A NEW NONLINEAR OPTICAL CRYSTAL 61

3.1	<i>Introduction</i>	61
3.2	<i>Crystal Growth</i>	63
3.3	<i>Characterization</i>	65
3.3.1(a)	<i>CHN analysis</i>	65
3.3.1(b)	<i>EDX spectral studies</i>	65
3.3.2	<i>Single crystal X-ray diffraction</i>	66
3.3.3	<i>Powder X-ray diffraction studies</i>	73
3.3.4	<i>Vibrational assignments</i>	75
3.3.5	<i>Thermo gravimetric analysis</i>	78
3.3.6	<i>UV-Vis Absorption Studies</i>	79

3.3.7	Second Harmonic Generation.....	80
3.3.8	Open aperture Z scan technique.....	80
3.3.9	Dielectric studies.....	82
3.3.10	Etching studies.....	83
3.4	Comparative study with other NLO crystals.....	84
3.5	Conclusions.....	86
3.6	References.....	87
Chapter 4 LITHIUM DOPED L-CITRULLINE OXALATE MONOHYDRATE		
NONLINEAR OPTICAL CRYSTALS.....		89
4.1	Introduction.....	89
4.2	Crystal growth.....	91
4.3	Characterization.....	92
4.3.1	Powder X-ray diffraction.....	92
4.3.2	ICP AES analysis.....	94
4.3.3	FT- IR and Raman spectral studies.....	94
4.3.4	UV-Vis Absorption studies.....	97
4.3.5	TGA analysis.....	98
4.3.6	Second harmonic generation efficiency (SHG).....	99
4.3.7	Open aperture Z scan studies.....	100
4.3.8	Dielectric studies.....	101
4.3.9	Etching studies.....	102
4.4	Conclusions.....	103
4.5	References.....	104
Chapter 5 EFFECT OF AMINOACID DOPING ON THE PROPERTIES OF		
POTASSIUM DIHYDROGEN PHOSPHATE NONLINEAR		
OPTICAL CRYSTALS.....		107
5.1	Introduction.....	107

5.2	<i>Crystal Growth</i>	109
5.3	<i>Characterisation</i>	110
5.3.1	<i>Powder XRD studies</i>	110
5.3.2	<i>EDX spectral studies</i>	111
5.3.3	<i>FTIR spectral studies</i>	113
5.3.4	<i>UV-Vis absorption spectral studies</i>	115
5.3.5	<i>TGA studies</i>	117
5.3.6	<i>Studies on Second harmonic generation efficiency</i>	117
5.3.7	<i>Z scan studies</i>	118
5.3.8	<i>Etching studies</i>	120
5.4	<i>Conclusions</i>	121
5.5	<i>References</i>	121

**Chapter 6 STUDIES ON AMINO ACID CAPPED ZINC OXIDE
NANOCRYSTALS..... 123**

6.1	<i>Introduction</i>	123
6.2	<i>Nanomaterials</i>	124
6.2.1	<i>Semiconductor nanocrystals or quantum dots</i>	125
6.3	<i>Objectives of the present work</i>	130
6.4	<i>Studies on various amino acid capped ZnO</i>	131
6.4.1	<i>Synthesis of aminoacid capped ZnO</i>	131
6.4.2	<i>Powder X-ray diffraction</i>	132
6.4.3	<i>Transmission electron microscope images</i>	133
6.4.4	<i>UV-Vis Absorption spectral analysis</i>	134
6.4.5	<i>Photoluminescence (PL) spectral analysis</i>	135
6.5	<i>Characterization of capped ZnO with L-histidine in various molar ratios</i>	137
6.5.1	<i>X-ray diffraction patterns</i>	137

6.5.2	<i>UV-Vis absorption spectra</i>	138
6.5.3	<i>Transmission Electron Microscopy</i>	139
6.5.4	<i>EDX spectra</i>	140
6.5.5	<i>Fourier Transform Infra red Spectroscopy Studies</i>	141
6.5.6	<i>PL spectra</i>	142
6.5.7	<i>Open aperture Z scan</i>	143
6.6	<i>Studies of L- histidine capped ZnO by varying the molarity of NaOH</i>	144
6.6.1	<i>Synthesis</i>	145
6.6.2	<i>XRD studies</i>	145
6.6.3	<i>UV-Vis absorption spectra</i>	146
6.6.4	<i>PL spectra</i>	147
6.6.5	<i>Biocompatibility studies</i>	148
6.7	<i>Nanocomposite films</i>	149
6.7.1	<i>Preparation of capped ZnO nanoparticles</i>	150
6.7.2	<i>Powder X-ray diffraction studies</i>	151
6.7.3	<i>UV-Vis absorption spectra of capped ZnO nanocrystals</i>	152
6.7.4	<i>PL spectra of capped ZnO nanocrystals</i>	152
6.8	<i>Studies on L-histidine tartrate capped ZnO/PVA nano composite films</i>	153
6.8.1	<i>UV-Vis absorption spectra of the nanocomposite films</i>	154
6.8.2	<i>PL Studies of the nanocomposite films</i>	155
6.9	<i>Conclusions</i>	156
6.9.1	<i>Summary of aminoacid capped ZnO nanocrystals</i>	156
6.9.2	<i>Nanocomposite films</i>	157
6.10	<i>References</i>	157

Chapter 7	GENERAL SUMMARY AND SCOPE FOR FUTURE WORK	163
7.1	<i>Summary</i>	163
7.2	<i>Scope for future work</i>	168

Preface

Non linear optics has been a fascinating area, over the past few decades, due to its varied contributions in all fields of science. The pursuit for new nonlinear optical crystals has the top priority in the present day scenario. Most of the aminoacids show optical nonlinearity as they contain a proton donor carboxyl (COOH) group and a proton acceptor amino (NH₂) group in the structure and hence complexes of aminoacids naturally exhibit nonlinearity. With this view, attempts to grow new aminoacid based nonlinear optical crystals have resulted in the realization of crystals showing nonlinear optical properties appropriate for device applications.

Organic crystals exhibit large nonlinear susceptibilities compared to the inorganic ones. However, these crystals have certain limitations owing to poor mechanical and thermal stability. Inorganic crystals have excellent mechanical and thermal properties but possess relatively low optical nonlinearities because of the lack of electron delocalization. The properties of both types of crystals can be modified with the help of suitable inclusions. Inorganic crystals possessing high thermal and mechanical stability, doped with suitable organic materials can yield high quality nonlinear optical crystals. These motivating ideas have been the prime factors behind the present work on non linear optical crystals.

It is not worthy, if the search for nonlinearity is limited to macrocrystals. This is the millennium powered by the ideas of nano science and nanotechnology. The synthesis of nanomaterials exhibiting optical nonlinearity has attracted global research attention nowadays. Aminoacids as well as zinc oxide are potential candidates for nonlinear optical studies. Part of the present work is hence devoted to the studies on the characteristics of nanostructured zinc oxide capped with aminoacids.

The work reported in the whole thesis is a potrait of the studies on the nonlinear optical materials ranging from the macro domain to the nano domain.

The research work included in the thesis is encapsulated in different sections as follows.

***Chapter 1** includes a brief introduction to the theory of crystal growth, crystal growth techniques and some fundamental aspects of nonlinear optics.*

*A profile of the different characterization techniques employed for the present investigations is outlined in **Chapter 2**. The different characterization techniques utilized are (1) Single crystal XRD (2) Powder XRD (3) Transmission Electron Microscopy (4) CHN analysis (5) EDX (6) ICP AES (7) FTIR spectroscopy (8) Raman spectroscopy (9) UV-Vis Absorption spectroscopy (10) Kurtz Perry powder technique for Second Harmonic Generation (11) Open aperture- Z scan technique (12) Photoluminescence spectroscopy (13) Thermal analysis (14) Dielectric studies using impedance meter and (15) Etching studies.*

***Chapter 3** deals with the growth of a new single crystal, L-citrulline oxalate monohydrate, grown for the first time using solution growth technique and its detailed characterization studies.*

*The effect of doping with lithium and the consequent modifications in the properties of L-citrulline oxalate monohydrate single crystals are portrayed in **Chapter 4***

***Chapter 5** gives an account of the details of the growth and important properties of Potassium dihydrogen phosphate (KDP), nonlinear optical single crystals doped with amino acids, L-citrulline, and L-lysine*

Zinc oxide nanocrystals capped with different amino acids and their complexes are synthesized and the suitability of these capped nanocrystals for

*optoelectronic and biological applications is investigated. The details of these studies form the essence of **Chapter 6**.*

*A brief outline of the whole work carried out, the important results obtained and the conclusions arrived at are summarized in **Chapter 7**. The scope for further investigations based on the results of the present study is also highlighted in this section.*

LIST OF PUBLICATIONS

Papers published in National/International peer reviewed Journals

- [1] *Studies on the thermal, optical and dielectric properties of a new nonlinear optical crystal—L-citrulline oxalate grown by slow evaporation technique.* **Sreevalsa V G**; Jayalekshmi S, Transactions of the Indian Institute of metals 2011, vol. 64, n^o1-2, p. 205-208.
- [2] *Characterization Of Transparent PVA/Amino acid complex capped ZnO nano composite films* **Sreevalsa V G** ;Sajimol Augustine; Jayalekshmi S, Int J Plast Technol (January 2011) 15 (Suppl 1)p 10-18
- [3] *Investigations on the growth and characterization of l-citrulline oxalate monohydrate single crystal,* **Sreevalsa V G**; Jayalekshmi S; Journal of Crystal Growth, v. 324, iss. 1, 2011,p. 172-176.
- [4] *L-Histidine Modified Biocompatible Zinc Oxide Nanocrystals,* **Sreevalsa V G**; Jeeju, P.P,Sajimol Augustine, Anilkumar.K.M, Jayalekshmi S, Journal of Experimental Nanoscience, 29, 2012, p 1-10.
- [5] *Size dependent optical properties of transparent, spin coated Polystyrene/Zinc Oxide nanocomposite films,* Jeeju, P, P, Sajimol. A.M, **Sreevalsa. V.G**, S.J.Varma, S. Jayalekshmi Polym Int. **60**: 2011, p 1263– 1268
- [6] *Excellent UV absorption in spin coated thin films of oleic acid modified ZnO nanorods embedded in poly vinyl alcohol,* M. Sajimol Augustine; P.P. Jeeju; **V.G. Sreevalsa**, S. Jayalekshmi, Journal of Physics and Chemistry of solids, Volume, March 2012, p 396–401 .

- [7] *Studies on L- citrulline Capped Zinc Oxide Nanocrystals*, **V.G Sreevalsa**, P.P Jeeju, M. Sajimol Augustine and S. Jayalekshmi, *Science and Society*, 9: 2011, p 183-189
- [8] *Solvent dependent optical properties of highly luminescent nanocrystals of ZnS doped with Manganese*, M. Sajimol Augustine, P.Indu, **V.G Sreevalsa**, P.P Jeeju, S.Jayalekshmi, *Science and Society*, 9: 2011, p 109-113
- [9] “Micelle- assisted synthesis of polypyrrole nanoparticles and their characterization, P.P. Jeeju, P.A. Francis Xavier, A.M. Sajimol, **V.G. Sreevalsa**, Jayalekshmi, “*Science and Society*, 9: 2011, p 113-121

Papers presented in National/ International seminars

- [1] *Effect of Histidine capping on the optical properties of ZnO nano crystals*, **Sreevalsa.V.G.**, S.Jayalekshmi Proceedings of the National Seminar on Quantum Chemistry and Nano Techniques SNM College Maliankara 2009.
- [2] *On the optical properties of amino acid complex capped Zinc Oxide(ZnO) with varying the precursor molarity-* **Sreevalsa.V.G.**, S.Jayalekshmi, Proceedings of the National Seminar on Nano structured Materials and Nanophotonics at St.Terasas college Ernakulam Feb 2010.
- [3] *Characterization Of Transparent PVA/Amino acid complex capped ZnO nano composite films* **Sreevalsa.V.G.**, Sajimol Augustine.M , S.Jayalekshmi, Proceedings of the Inter National Seminar on Advancements in Polymeric Materials, CIPET, Bhuvanewar. February 2010.

- [4] *Studies on the thermal, optical and dielectric properties of L-histidine tartrate hemihydrate nonlinear optical crystals*, **Sreevalsa.V.G.**, S.Jayalekshmi, Proceedings of the Inter National Seminar ICMST VSSC Trivandrum ,October 2010
- [5] *Studies on the thermal, optical and dielectric properties of a new nonlinear optical crystal — L-citrulline oxalate grown by slow evaporation technique*, **Sreevalsa.V.G.**, S.Jayalekshmi ,Presented at ISRS, IIT, Madras ,December 26-28, 2010
- [6] *Effect Of Various Capping Agents On The Optical Properties of Zinc oxide Nanocrystals* **Sreevalsa.V.G**, Jeeju.P.P, Sajimol Augustine.M and S.Jayalekshmi Proceedings of the Inter National Seminar Cochin Nano 2011 on August 14-16, 2011
- [7] *Studies on L-citrulline capped Zinc oxide nanocrystals*, **Sreevalsa.V.G** Jeeju.P.P, Sajimol Augustine.M and S. Jayalekshmi, Proceedings of the National Seminar Nanotech at Nirmala College, Muvattupuzha on September 1-2, 2011
- [8] *Enhanced UV-shielding properties of ZnO/PS-PMMA nanocomposite films*, Jeeju.P.P, **Sreevalsa.V.G**, Sajimol.A.M and S.Jayalekshmi, Proceedings of the Third International conference on frontiers in Nano Science and Technology. Cochin Nano - 2011, August 14-17, Cochin, Kerala.
- [9] *Micelle-assisted synthesis of polypyrrole nanoparticles and their characterization*, P.P. Jeeju, P.A. Francis Xavier, A.M. Sajimol, **V.G. Sreevalsa**, S.Jayalekshmi, Proceedings of the National symposium on Nano Science and Technology Nanotech–2011, 1-2 September, Nirmala College Muvattupuzha, Kerala.

- [10] *Highly luminescent PANI/ZnO Nanocomposite Films Prepared from Oleic Acid Capped ZnO Nanoparticles*, M. Sajimol Augustine, P.P Jeeju, **V.G Sreevalsa**, S.Jayalekshmi, Proceedings of the Third International conference on frontiers in Nano Science and Technology. Cochin Nano - 2011, August 14-17, Cochin, Kerala.
- [11] *Solvent Dependent Optical Properties of Highly Luminescent Nanocrystals of ZnS Doped with Manganes*, M. Sajimol Augustine, P. Indu, **V.G Sreevalsa**, P.P Jeeju and S. Jayalekshmi, Proceedings of the National symposium on Nano Science and Technology Nanostech – 2011, 1-2 September, Nirmala College Muvattupuzha, Kerala.
- [12] *Effect of lithium doping on the optical properties of L-citrulline oxalate monohydrate nonlinear optical crystals*, **V.G.Sreevalsa**, P.P.Jeeju, S.Jayalekshmi, Proceedings of the National seminar on Emerging Trends in Theoretical and Experimental Physics- September 26-27,2012, Farook College, Calicut.

*Linearity is beautiful
Nonlinearity is exciting....*

**The investigations reported in this dissertation are
oriented in two directions.**

Phase 1

*Growth and characterization of some amino acid based single
crystals showing nonlinear optical properties*

Phase 2

*Synthesis and characterization of amino acid capped
nanocrystals*

Phase 1

Growth and characterization of some amino acid based single crystals showing nonlinear optical properties

“Limitations are only in our minds. If we use our imaginations, the possibilities become limitless.”

This is true for any technology, especially crystal technology.

Phase 2
*Synthesis and characterization of amino acid capped
nanocrystals*

Nano – the buzz word of the present day technology



<i>Contents</i>	1.1 Theory of crystal growth
	1.2 Thermodynamics of crystal growth
	1.3 Nucleation
	1.4 Crystal growth theories
	1.5 Crystal growth techniques
	1.6 Defects in crystals
	1.7 Nonlinear optics
	1.8 Nonlinear optical materials
	1.9 Advantages of organic nonlinear materials
	1.10 Objectives of the present investigations
	1.11 References

A general introduction to the subject dealt with in the thesis is portrayed in this chapter. The general aspects of crystal growth and crystal growth techniques are briefly outlined. A glimpse of the theory of nonlinear optics and the nonlinear optical properties of single crystals is addressed. The objectives of the present investigations are also highlighted in this section.

Crystals hold the key to unlock new arenas of science and technology and hence they form the pillars of the present day technology. Current applications require crystals in their purest form. Progress in crystal growth technology has led to a variety of crystals suitable for device applications. All the same, the developments in the technology have also in turn paved the way for the growth of defect free crystals.

Crystals with nonlinear optical properties find applications in photonic related areas as they have stamped their potential in this field and hence

nonlinear optical (NLO) materials have become the key elements for the current technological revolution. One of the main objectives of the present study is the pursuit of new nonlinear optical (NLO) crystals.

1.1 Theory of crystal growth

Crystal growth is a very complex process and it involves optimization of several parameters such as temperature, pressure, chemical potential etc. Crystalline solids are formed by cooling and solidification from the molten state where there is a discontinuous change in volume at the melting point. The phase transition is followed by an advancement of an interfacial region whose structure and properties differ from its parent phase. The parameters characterizing each phase are density, entropy and specific free energy which vary continuously from equilibrium values for one phase to other. If both phases are amorphous, the transition does not alter the thermo dynamical potential of the system. If the final phase is crystalline, the collective interaction causes the potential to be a periodic function of the positions of the boundary. Any deviation from the equilibrium causes a transition to the favored phase.

If the crystal is in dynamic equilibrium with its parent phase, no growth will occur, as the free energy is a minimum. For growth to occur, the equilibrium must be disturbed by a change in temperature, pressure, chemical potential, saturation, strain etc. The system will release energy to the surroundings, to compensate for the decrease in entropy occasioned by the ordering of atoms in the crystal and as a result, heat of crystallization is evolved. Hence crystal growth is a non equilibrium process, heat of crystallization is evolved to the surroundings and it should be presumed at near equilibrium conditions.

1.2 Thermodynamics of crystal growth

Crystal growth is basically governed by thermodynamics. Gibbs equation relates the free energy of a system to the internal energy and the entropy as

$$G = H - TS \quad (1.1)$$

where H is the enthalpy, S is the entropy and T is the temperature[1]. The formation of a crystal can be considered as a controlled change of liquid phase to the solid state. At equilibrium, the Gibbs free energies of the solid and liquid phases are equal.

$$G_L = G_S \quad (1.2)$$

where the subscript L denotes liquid phase and S denotes solid phase.

Crystallization is a near equilibrium process and occurs by the lowering of the free energy of the system during the phase transformation.

The free energy change associated with such a transition is

$$\Delta G = \Delta H - T\Delta S \quad (1.3)$$

where $\Delta H = H_L - H_S \quad (1.3a)$

$$\Delta S = S_L - S_S \quad (1.3b)$$

$$\Delta G = G_L - G_S \quad (1.3c)$$

At equilibrium

$$\Delta G = 0 \quad (1.4)$$

$$\therefore \Delta H = T_e \Delta S \quad (1.5)$$

where T_e is the equilibrium temperature.

$$\Delta G = \Delta H \cdot \Delta T / T_e \quad (1.6)$$

where $\Delta T = T_e - T$. The free energy change can also be represented as the product of the entropy change and super cooling ΔT .

$$\Delta G = \Delta S \cdot \Delta T \quad (1.7)$$

This representation is convenient for melt growth. The equation can be modified based on the concentration (C) for solution growth and the pressure (P) for vapor growth. Thus

$$\Delta G \sim RT \ln C/C_0 \quad (1.8a)$$

$$\Delta G \sim RT \ln P/P_0 \quad (1.8b)$$

In general

$$\Delta G \sim RT \ln S \quad (1.9)$$

where S is the super saturation ratio. Thus the free energy changes depend on the parameters like super cooling and super saturation which are significant in the process of crystallization.

1.3 Nucleation

Growth comprises of three steps

1. achievement of supersaturation
2. formation of crystal nuclei
3. successive growth of crystals to yield faces.

A supersaturated solution is that which contains solute at a higher saturation concentration, and on slight disturbance causes crystallization of excess solute. Nucleation is the preliminary step for crystal growth. It is the

process of formation of the first sub-microscopic speck or nucleus of the solid crystal by the conglomeration of atoms or molecules. Nucleation can be either homogeneous or heterogeneous. Volmer and Weber put forward a theory for the formation of a nucleus by considering the total free energy for a group of atoms [2]. Embryos are cluster of molecules, formed by fluctuations within the supersaturated solution. The probability that an embryo will grow to form a stable nucleus is decided by the change in free energy associated with its formation. For each unit area of solid-liquid interface formed, the free energy of the system ΔG , decreases by an amount for each unit volume of the solid created, but increases by an amount equal to the interfacial energy σ . Hence the change in Gibbs free energy associated with the formation of a spherical embryo of radius r is given by

$$\Delta G = 4\pi r^2 \sigma - 4\pi r^3 \Delta G_v \quad (1.10)$$

The contribution due to both surface and volume to the free energy change are represented graphically in Fig.1.1

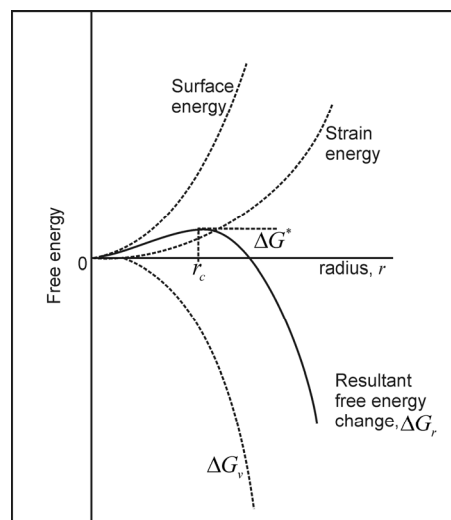


Fig: 1.1 Schematic representations of the different energies involved in crystal growth

From equation 1.10, it is found that the surface energy term increases with r^2 and the volume energy term decreases with r^3 . The size of the nucleus corresponding to the maximum free energy change is known as the "critical nucleus". If the size of the nucleus formed is below the critical dimension, no further growth is possible and it will re-dissociate into the solution. The minimum size of a stable, critically sized nucleus is obtained from the equation 1.10 by maximizing it for r , leading to

$$r^* = 2 \sigma / \Delta G_v \quad (1.11)$$

Now the free energy change ΔG^* leading to the formation of the critical nucleus amounts to

$$\Delta G^* = 16 \pi \sigma^3 / 3 \Delta G_v^2 \quad (1.12)$$

Equation 1.12 can be rearranged by introducing the Gibbs-Thomson relation and it reduces to

$$\Delta G^* = 16 \pi \sigma^3 \Omega^2 / 3 (kT \ln S)^2 \quad (1.13)$$

where Ω is the molecular volume and S , the supersaturation ratio. It can also be seen that the critical supersaturation for spontaneous nucleation depends on the temperature, interfacial energy, volume etc.

1.4 Crystal growth theories

Crystal growth involves optimization of various parameters such as temperature, pressure, chemical potential etc. and, being a non equilibrium process, control of crystal growth environment and consideration of growth kinetics, both at microscopic and atomic levels are significant. The successive growth of the critical nuclei of microscopic size leads to the formation of a crystal. Several theories have been developed, which includes surface energy

theory, diffusion theory, etc., in order to understand the mechanism and the kinetics of growth. Later Kossel and others analyzed the atomic inhomogeneity of a crystal surface and explained the role of step and kink sites on the growth process. A complete explanation for the continuous growth of a crystal surface came as a breakthrough, when Frank showed that crystal dislocations were capable of providing the sources of steps required for the continuous growth of a crystal [3,4].

(a) Surface energy theory

Several theories were put forward based on the thermodynamical treatment of equilibrium states. Gibbs put forward the surface energy theory. It is based on the fact that a growing crystal assumes the shape which has minimum energy, similar to the formation of droplet in a mist. The shapes and end forms of crystals in equilibrium with solution or vapor, consistent with Gibbs criterion was calculated by Curie [5]. Extensions to Curies idea were put forward by Wulff and many others [6-8]. Different faces have different solubilities and the growth rate of different faces is related to surface free energies. Growth is mainly governed by surface energy when the difference in solubility is low. When the supersaturation is high, growth becomes rapid and well defined faces are developed. Further, velocity of the growth of different faces depends on the reticular density which in turn inversely depends on the surface energy.

(b) Diffusion theory

According to diffusion theory, matter is deposited at a rate proportional to the difference in concentration between the point of deposition and the bulk

solution. The amount of solute molecules that gets deposited over the surface of a growing crystal in the supersaturated solution can be written as

$$dm/ dt =D/\delta [A(C-C_0)] \quad (1.14)$$

where dm is the mass of the solute deposited over the crystal surface of area A during time dt , D is the diffusion coefficient of the solute, C and C_0 , are the actual and equilibrium concentration of the solute and δ , the thickness of the stagnant layer adjacent to the crystal surface. This theory was proposed by Noyes, Whitney and Nernst, based on the fact that the growth process is a reverse process of dissolution following certain assumptions that there is a concentration gradient in the vicinity of the growing crystal surface [9-10]. But this theory also could not explain all the experimental observations.

(c) Adsorption layer theory

Another model put forward by Kossel, Volmer and Stranski based on the atomistic point of view, rather than thermodynamical, is the surface nucleation model based on adsorption layer theory[11-13]. The theory depends on the fact that crystal growth is a discontinuous process taking place by the adsorption of matter layer by layer on the crystal surface. The growth units reaching the crystal surface do not incorporate immediately into the lattice, but become adsorbed and migrate over the surface. The migration distance x_s of the adsorbed molecule is given by

$$x_s^2 = D_s \tau_s \quad (1.15)$$

where D_s is the surface diffusion coefficient and τ_s , is the mean life time of an adsorbed molecule on the surface. In this model

$$x_s^2 \sim a \exp (3\phi/2kT) \quad (1.16)$$

where a is the nearest neighbor distance and ϕ is the nearest neighbor interaction parameter, k is the Boltzmann constant and T is the absolute temperature. The probable sites associated with the adsorption of atoms are kink sites, ledge sites and terrace sites. An atom reaching a kink site is attracted by three out of the six nearest neighbors, while for a ledge it is two and one for a terrace site. Since maximum binding energy between the adatom and the existing crystal surface is for a kink site, the adatoms over the crystal surface migrate towards a step to a kink site and get incorporated. This stepwise stacking will continue until the whole layer is completed. Extensive studies were carried out by Burton, Cabrera and Frank regarding the mode of advance of a step [14]. A step advances by incorporating more and more adatoms at kink sites. The rate of advance of a step can be expressed assuming a diffusional flow of adatoms along the step, as

$$V_{\alpha} = (\alpha-1) x_s \gamma e^{-W/kT} \quad (1.17)$$

where γ is a frequency factor which is of the order of atomic frequency of vibration $\sim 10^{13} \text{ sec}^{-1}$ for monoatomic substances and W is the total evaporation energy, α is the saturation ratio.

Steps are created by thermodynamic fluctuations. When the step has covered the whole surface, a new layer has to be formed, and it requires additional energy. Once the nucleus is formed due to thermodynamic fluctuations it will spread and again leave the surface smooth. The growth rate of crystals is governed by nucleation rate rather than the growth velocity of surface steps. On analyzing crucially the nucleation process, it can be seen that the nucleus formed is not circular and the rate of nucleation depends on several factors such as, the

surface area of crystal face, the area per molecule in the layer, the maximum surface free energy at critical radius of the nucleus etc.

The nucleation rate is a sensitive function of super saturation and below a super saturation of 25-50 %, the probability of nuclei formation is negligible which is not in agreement with experimental observations [15]. The growth rate was found to be proportional to super saturation much lower than the critical super saturation as calculated from the surface nucleation theory, which leads to the fact that the growth of real crystals differ from ideal crystals.

(d) BCF theory

A revolutionary breakthrough in the field of crystal growth was put forward by Burton Cabrera and Frank called BCF theory. They applied the concepts, results and methods of theoretical physics to crystal growth and proposed the famous spiral growth theory which had a stronger statistical and mechanical foundation. The first step includes the mechanism of step generation and transport of atoms into steps. Second part is concerned with the transport of molecules from bulk to kinks in steps of spiral. The continuous growth of a crystal surface is based on two dimensional nucleation theory. Frank proposed that dislocations having a screw component can act as a continuous source of steps on the surface of the crystal [16]. A screw dislocation emerging at a point on the crystal surface acts as a step on the surface. The screw dislocation is at the emergence point of the dislocation and, hence further growth can occur only by the rotation of step around the dislocation point. The transport of molecules from bulk to kinks, is in steps of spiral.

Based on spiral growth mechanism Burton, Cabrera and Frank established a relation between the rate of growth R and the relative super saturation which is expressed as

$$R = C (s^2/s_1) \tanh (s_1/s) \quad (1.18)$$

where the parameter s_1 is defined as

$$s_1 = 19 \gamma \Omega / 2kTx_s \quad (1.18a)$$

$$\text{and } C = D S_{se} \Omega \beta / x_s \quad (1.18b)$$

where s - relative super saturation

s_1 - a constant for BCF model

S_{se} - equilibrium concentration of growth units on surface.

β - retardation factor

Ω - volume of the growth unit

D - constant

According to BCF theory the growth rate is proportional to the square of the supersaturation for low super saturation, changing to a linear dependence at higher super saturations. The Frank model has excellent agreement between theory and observations on growth rate as well as on the direct observation of spiral pattern, characteristic of this mechanism [17-19]. However, it is also observed that edge dislocations can act as persistent sources of steps for crystal growth and the surface stresses provides the extra energy required for the formation of the growth nuclei when the dislocation component is perpendicular to the surface[20, 21]. Recent developments in

the theory of crystal growth using the framework of the BCF theory have reduced the gap between theory and experiment [22, 23].

1.5 Crystal growth techniques

Crystalline state is characterized by a regular three dimensionally periodic arrangement of atoms in space. The characteristics such as symmetry, structural simplicity and purity endow crystals with unique physical and chemical properties. The process of crystal growth is a controlled change of state, or phase change, to the solid state. This transition may occur from the solid, liquid or vapor state. The crystal growth methods can generally be classified into four main categories depending on the phase transitions involved in the process [24, 25].

- 1) Solid growth
- 2) Melt growth
- 3) Vapor growth
- 4) Solution growth
- 5) Gel growth

(a) *Solid growth techniques*

In solid growth technique, single crystals are developed by straining and annealing the material. The growth can be achieved in a preferential direction and at low temperatures. Large crystals of metals have been grown by this method [26].

(b) Growth from vapour

Successful growth from vapor phase requires knowledge of the thermodynamic equilibrium among the reacting vapor constituents. Vapour growth techniques can be adopted for the growth of materials which lack a suitable solvent and sublime before melting at normal pressure. Vapour growth methods have been employed to produce bulk crystals and to prepare thin layers on crystals with a high degree of purity. Growth from vapour phase can be classified into two-

- Physical vapour transport
- Chemical vapour transport

In Physical vapour transport technique, the crystal is grown from its own vapours. The processes involved are sublimation-condensation and sputtering [27]. Sputtering techniques have been used to prepare thin films or materials with low vapour-pressures [28, 29]. Chemical vapour transport technique is achieved through a chemical reaction between the material to be crystallized and a transporting agent. The material to be crystallized is converted into one or more gaseous products, which diffuse to the colder end. At the cold end, the reaction is reversed so that the gaseous products decompose, depositing the parent material and liberating the transporting agent. This method is mainly used in the production of thin layers [30, 31].

(c) Melt growth technique

Single crystals with high degree of perfection and purity can be obtained by this method. Melt growth is a field of crystal growth based on fusion and resolidification of solids, which can be melted and crystallized. This method has been employed for the growth of metals and semiconductors.

Melt growth methods are categorized into two

- Normal freezing method
- Zone-growth method

Based on normal freezing method, there are mainly two techniques-

- ✓ Bridgman technique
- ✓ Czochralski technique.

Bridgman technique is named after its inventors Bridgman and Stockbarger. It is most frequently applied for the growth of metals, semiconductors and alkaline earth halides [32, 33]. But this method cannot be used for materials having high melting point and high expansion coefficient. Bridgman technique sticks to random nucleation to produce a single crystal. The crucible tip is designed such that only one crystal propagates. Solidification is obtained by slowly withdrawing the molten material through a temperature gradient [34]. The technique is of low cost and the system is density stable and also less prone to convection effects.

Czochralski method was developed in 1918[35]. It is basically a crystal pulling system and is the most powerful method for growing single crystals. A seed fixed to a holder is brought into contact with the melt in a crucible and when equilibrium is reached, the seed is pulled along with rotation. Rotation of the seed eliminates any radial temperature gradient. The advantage of this method over the Bridgman method is that it can accommodate the volume expansion associated with the solidification. Czochralski method has gained wide recognition particularly in growing single crystals of semiconductors like silicon [36-38].

Zone growth can be classified as

- ✓ Zone melting technique
- ✓ Floating zone technique.

Zone melting technique was enunciated by Pfann in 1952. It produces dislocation free crystals with a low defect density and accurate axial and radial distribution of elements. In this method, a small zone of the solid material is melted and this molten zone travels together with the heating elements. This method is suitable for uniform doping of a known impurity [39].

Floating zone technique was developed by Keck and Golay. This is an alternate method of the zone melting technique in which no crucible is used[40]. The seed crystal is supported vertically upwards and the polycrystalline ingot vertically downwards so that it touches the top of the seed. A zone is moved downwards through the ingot until the seed begins to melt. The direction of the zone is reversed and the seed grows as the zone moves upwards. This method is especially suitable for the preparation of high purity silicon and germanium.

(d) Growth from solution

The most simple and oldest technique of growth of crystals is from solution. Solution growth is particularly suited to those materials which decompose at high temperatures and which undergo phase transformation below the melting point.

It is mainly a diffusion controlled process. In this process, a saturated solution of the material in a suitable solvent is used from which, crystallization takes place as the solution becomes critically supersaturated. The medium

must be viscous to enable faster transference of the growth units from the bulk solution by diffusion. The super saturation can be achieved either by lowering the temperature of the solution or by slow evaporation. The advantage of the method is that crystals can be prepared from a solution at temperatures well below its melting point and even at room temperature.

Super saturation is an important parameter for the solution growth process. The solubility data at various temperatures are essential to determine the level of super saturation. Hence the solubility of the material in the solvent must be determined before starting the growth process. The solubility diagram can be divided into three zones namely, under saturated zone, metastable zone and labile zone. Crystallization is not possible in the under saturated zone. In the metastable zone, spontaneous nucleation is not possible whereas it is more probable in the labile region.

Generally solution growth is classified as

- High temperature growth
- Low temperature growth

In high temperature growth method crystals can be grown from the molten state of the salt at high temperatures [41]. The materials to be crystallized are dissolved in a proper solvent at a temperature slightly above the saturation temperature and then slowly cooled so that growth occurs as a spontaneously formed nucleus.

A variety of crystals can be grown at room temperature. In this low temperature growth method, a saturated solution of the material is prepared in a suitable solvent and crystallization is brought about by slow cooling of the

solution or by slow evaporation of the solvent. Large and perfect crystals of industrially important materials are grown by this method [42-44].

Materials having moderate to high solubility in the temperature range from ambient to 100°C at atmospheric pressure can be grown by low temperature solution method. The crystallization mechanism is predominantly through diffusion, also there is evidence that the growth takes place by surface diffusion as well [45-47]. In addition, the interaction between ions or molecules of the solute and solvent is based on the thermo dynamical parameters like pressure, temperature, solvent concentration etc. One of the advantages of this crystallization method is the control over temperature during growth. Besides, growth at room temperature reduces the structural imperfections, though the growth rate is low.

Low temperature solution growth is classified as follows

- Slow cooling technique
- Slow evaporation technique
- Temperature gradient technique

i) Slow cooling technique

Here supersaturation is produced by a change in temperature in the crystallizer. Supersaturation requires systematic cooling since the volume of the crystallizer is finite and the amount of the substance is limited. This can be achieved by a crystallizer with thermostat.

(ii) Slow evaporation technique

In this method crystals grow at a fixed temperature and can be effectively used for materials having moderate temperature coefficient of

solubility. An excess of the solute is established by utilizing the difference between the rates of evaporation of the solvent and the solute. The vapour pressure of the solvent above the solution is higher than the vapour pressure of the solute and therefore the solvent evaporates more rapidly and the solution becomes supersaturated[48]. Typical growth conditions involve a temperature stabilization of 0.05 °C and rate of evaporation of a few mm³/hr.

(iii) Temperature gradient technique

This technique makes use of the different temperature regions in the crystallizer. It is based on the transport of the material from the source material at the hot region to the supersaturated solution at a cooler region. The main advantages of this method are

- Growth of crystals at fixed temperature
- No direct effect due to changes in temperature
- Use of solvent and solute is economical

e) Hydrothermal methods

Growth of crystals is made possible at elevated temperatures and pressures. This method is suited for the growth of high quality quartz crystals [49]. The hot saturated solution initiates the growth of crystals. The solution simply acts as a transporting agent for the solid phase.

f) Gel growth

Gel growth is another version of solution growth with controlled diffusion. This technique is applicable to the growth of certain class of materials having poor solubility and unstable thermal behavior. In gel

technique supersaturation is achieved either by the slow inter diffusion of solutions of two reacting species, which on mixing react to form the solute, or by the inter diffusion of a solution with a solvent in which the solute is insoluble or less soluble. Using gel technique small but highly perfect crystals of relatively insoluble materials can be grown .Gel method can be classified as follows [50-52].

- ❖ Chemical reaction method
- ❖ Chemical reduction method
- ❖ Solubility reduction method
- ❖ Complex dilution method

Two methods are employed in chemical reaction method-

- (i) Single diffusion method
- (ii) Double diffusion method

In the single diffusion method, one of the components AX or BY which is highly soluble in water and chemically inactive with the gel is impregnated in the acidified gel medium. After the gelation, the other component in solution form is placed over the set gel. This solution reacts with the other component on diffusion through the gel medium, resulting in the formation of the required constitution in crystal form. The byproducts of the reaction are highly soluble in water and will be present in the gel medium. The reaction can be expressed as follows



The double diffusion method is used when both the reactants are found chemically reactive with the hydrogel. Here the two components meet each other at the bent portion of the U tube by diffusion, resulting in the formation of the crystal.

Some of the prominent factors that control the nucleation and growth of the crystal are concentration of the feed solution, the pH of the gel, aging of the gel and the gel density. The various parameters can be optimized by trial and error.

Chemical reduction method is used for growing metal complexes. The metallic complex is taken along with the sodium meta silicate (SMS) solution and is reduced by a proper reducing agent into the gel. Slow reduction results in the formation of crystals. Crystals of copper, nickel, cobalt, gold etc. have been grown by this method [53]

Solubility reduction method is employed for the growth of water soluble substances. The substance to be grown is dissolved in water and incorporated with the gel to form solution. When gelation is over, a solution which reduces the solubility of the material is added over the set gel. Potassium dihydrogen phosphate and potassium acid pthalate have been grown by adding ethyl alcohol over the gel[54].

In the complex dilution method, a chemical complex of the material to be grown is prepared with a complexing agent which diffuses into the gel. Decomplexing is achieved by steadily increasing the dilution which leads to the high supersaturation, necessary for crystal growth. Cuprous chloride has been grown by this method.

1.6 Defects in crystals

The concept that an ideal crystalline solid distinguished by the periodic arrangement of atoms, wherein every lattice point is occupied by a basis of atoms, is valid only at absolute zero. At finite temperatures, a certain configurational disorder exists. Any deviation from a chemically pure, stoichiometric perfect crystal is called an imperfection or defect. The presence of defects, influences many physical properties such as mechanical and thermal strength, optical absorption and electrical conductivity.

The various types of defects[55-57] are

- Point defects
- Line defects
- Plane defects
- Volume defects

If the deviation from the periodic arrangement is localized to certain points within the crystal lattice, it is called point defect. The different point defects are vacancy, Schottky defect, self-interstitial, Frenkel defect, interstitial impurity, non-stoichiometry, color centres etc.

Line defects are lattice imperfections along closed lines which end on the crystal surface. The crystal structure is disturbed around these lines in a volume whose radial extension is of the order of about one atomic separation. These one dimensional lattice defects are called dislocations. The main line defects are edge dislocations and screw dislocations.

Plane defects are two dimensional lattice defects at which periodic structure is disturbed. Grain boundaries, stacking faults and etch pits are some plane defects.

Volume defects such as cracks or large voids or cluster of missing atoms may occur during the growth process. These have important effects on the properties of crystalline solids.

For the fabrication of electronic devices, defect free crystals are required for better performance. Hence interest has increased for detecting defects in crystals. Frank had observed that growth at very low supersaturation can contain screw dislocations. The parts near the dislocation move with greater angular velocity than parts farther away, causing spiral hills. The growth at higher super saturation is fairly smooth without spirals.

Etching is a technique used for the detection and characterization of crystal defects. Etch pits correspond to a point where a dislocation terminates on the surface. A carefully controlled chemical attack often brings forth preferential etch pits.

1.7 Nonlinear optics

Nonlinear optics (NLO) deals with the study of phenomena that occur as a consequence of the modification of the optical properties of a material system by the interaction of high intensity electromagnetic radiation. The electric field strength should be of the order of the atomic or inter-atomic field ie. $\sim 10^9$ to 10^{12} V/m for a system to exhibit nonlinear effects. Consequently the polarization developed is not linear with the field strength E and higher order terms become appreciable [58].

Nonlinear optics has been a fascinating area currently, due to the exciting properties exhibited by materials having nonlinear response. Some of the interesting nonlinear optical effects observed include higher harmonic generation, production of combination frequencies, optical rectification, parametric amplification, optical limiting etc. The generation of second harmonics by Franken et al [59] in 1961, after the discovery of laser by Maiman [60] in 1960, paved the way for the current developments in nonlinear optics. Nonlinear optics is attracting attention in view of its applications in the areas of laser technology, optical communication and data storage technology.

A dielectric medium when placed in an electric field gets polarized. Each constituent molecule acts as a dipole of moment p_i . The orienting effect of the external field E on the molecular dipoles depends on the properties of the medium and on the field strength.

$$P = \sum_i p_i = \epsilon_0 \chi E \quad (1.20)$$

where P is the polarization and χ the susceptibility. P and χ hold a linear relationship in linear optics. But when the intensity of the incident radiation is sufficiently high, the relation is generalized as

$$\begin{aligned} P &= \epsilon_0 [\chi^{(1)} E(t) + \chi^{(2)} E^2(t) + \chi^{(3)} E^3(t) + \dots] \\ &= P^{(1)}(t) + P^{(2)}(t) + P^{(3)}(t) + \dots \end{aligned} \quad (1.21)$$

where $\chi^{(1)}$, $\chi^{(2)}$, $\chi^{(3)}$ are the susceptibility tensors corresponding to first, second and third order nonlinearity[61].

In general, the net polarization can be written as

$$P = P_L + P_{NL} \quad (1.22)$$

where the linear polarization

$$P_L = \epsilon_0 \chi^{(1)} E(t) \quad (1.23)$$

and the nonlinear part

$$P_{NL} = \epsilon_0 [\chi^{(2)} E^2(t) + \chi^{(3)} E^3(t) + \dots] \quad (1.24)$$

$\chi^{(1)}$ is a second rank tensor containing 9 elements

$\chi^{(2)}$ is a third rank tensor containing 27 elements

$\chi^{(3)}$ is a fourth rank tensor containing 81 elements and so on

Ideally, nonlinear optical interactions can be described in terms of the nonlinear polarization only for a material system that is lossless and dispersionless. Second order nonlinearity occurs only in non-centrosymmetric crystals, i.e. crystals that do not display inversion symmetry.

When a light wave propagates through an optical medium, the oscillating electromagnetic field exerts a polarizing force on all the electrons in the medium. Since the inner electrons are tightly bound to the nuclei, the major polarizing effect is exerted on the valence electrons. Non linear optical phenomena are nonlinear in the sense that they occur when the response of a material system to an applied optical field depends in a nonlinear manner upon the strength of the optical field.

The macroscopic NLO properties of many organic crystals are given by the tensor sum of the properties of the constituent molecules, local field factors and molecular orientation. It is this feature of organic materials that allows molecular engineering approach to the optimization of macroscopic properties.

The nonlinear optical crystals cover a wide range of nonlinear optical applications and are used for higher harmonic generation, including frequency doubling (SHG) and tripling (3HG), frequency mixing and in devices including Optical Parametric Oscillators (OPO) and Optical Parametric Amplifiers (OPA). The NLO crystals used in frequency conversion for lasers include KTP, LBO, BBO, KDP, KNbO₃, LiNbO₃, AgGaS₂, AgGaSe₂, LAP etc. The right NLO crystals should be chosen by taking into consideration the criteria such as transparency, damage threshold to incident radiation, efficiency of the nonlinear effect, phase matching range, laser beam quality etc.

1.7.1 Frequency Conversion

The frequency conversion processes include frequency doubling, sum frequency generation (SFG), differential-frequency generation (DFG) and optical parametric generation (OPG) which are demonstrated in the following equations:

Consider the mutual interaction of three waves of frequencies $\omega_1, \omega_2, \omega_3$ where $\omega_3 = \omega_1 + \omega_2$

Let the optical field be incident upon a nonlinear optical medium characterized by $\chi^{(2)}$

$$E(t) = E_1 \exp(-i\omega_1 t) + E_2 \exp(-i\omega_2 t) + \text{complex conjugate(cc)} \quad (1.25)$$

$$P^{(2)}(t) = \chi^{(2)} [E(t)]^2 = \chi^{(2)} [E_1^2 \exp(-2i\omega_1 t) + E_2^2 \exp(-2i\omega_2 t) + 2E_1 E_2 \exp(-i(\omega_1 + \omega_2)t) + 2E_1 E_2^* \exp(-i(\omega_1 - \omega_2)t) + 2[E_1 E_1^* + E_2 E_2^*] + \text{c.c}] \quad (1.26)$$

$$P(2\omega_1) = \chi^{(2)} E_1^2 \text{ (SHG)} \quad (1.27)$$

$$P(2\omega_2) = \chi^{(2)} E_2^2 \text{ (SHG)} \quad (1.28)$$

$$P(\omega_1 + \omega_2) = \chi^{(2)} E_1 E_2 \text{ (SFG)} \quad (1.29)$$

$$P(\omega_1 - \omega_2) = 2\chi^{(2)} E_1^* E_2^* \text{ (DFG)} \quad (1.30)$$

$$P(0) = 2[E_1 E_1^* + E_2 E_2^*] \text{ (OPG)} \quad (1.31)$$

In second harmonic generation, radiation at an incident frequency ω is converted to radiation at twice the frequency of the incident radiation. Here 2 photons of frequency ω are destroyed and a photon of frequency 2ω is simultaneously created in a single electromagnetic process. It is observed only in non centro symmetric crystals. Second harmonic generation efficiency η_{SHG} is proportional to the phase mismatch parameter between the fundamental and the second harmonic signals generated, Δk given by the relation 1.32[62].

$$\eta_{\text{SHG}} \propto [\text{Sin}(\Delta k l / 2) / (\Delta k l / 2)]^2 \quad (1.32)$$

where l is the coherence length of the medium. As Δk deviates from zero, the conversion efficiency steadily decreases. A schematic diagram of the second harmonic generation is represented in Fig: 1.2

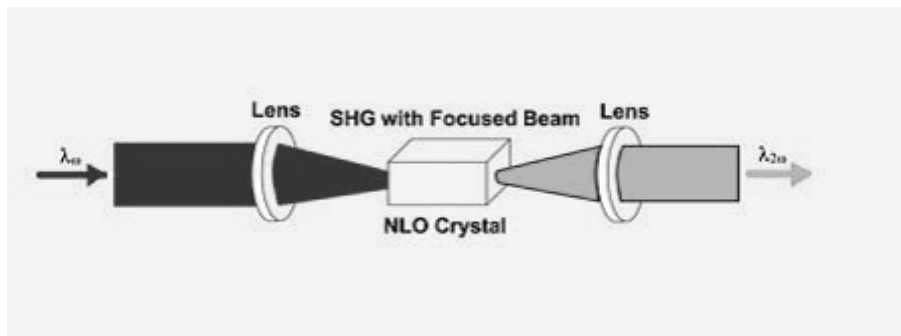


Fig: 1.2 Schematic diagram of the second harmonic generation

1.7.2 Self Action Effects

Self-action effects are due to nonlinear polarization at the same frequency as that of the incident light wave which affect the propagation characteristics of the incident beam i.e. direction of propagation, degree of focusing, state of polarization or bandwidth. A beam of light modifies its own propagation by means of the nonlinear response of a material medium. The various types of self-action effects depend on whether the susceptibility is real or imaginary and also on the temporal and spatial distribution of the incident light. The real part of the nonlinear susceptibility gives rise to spatial effects like self focusing, self defocusing, spectral broadening and changes in the polarization vector. The imaginary part of the susceptibility attributes to nonlinear absorption.

(a) Self-focusing

Self focusing occurs in a medium whose refractive index varies with the electric field intensity and the medium acts as a focusing lens for an electromagnetic wave as a result of a positive value of nonlinear refractive index. The condition is the same as that of a focusing lens. Thus the light beam creates its own positive lens in the nonlinear medium. As the beam gets focused, the strength of the nonlinear lens increases causing stronger focusing and increasing the strength of the lens still further. This behavior results in catastrophic focusing in which the beam collapses to a very small intense spot in contrast to gentle focusing that occurs in normal lenses. Self focusing is observed in a wide range of materials including glasses, crystals, liquids, gases and plasmas [63].

(b) Self defocusing

This phenomenon occurs as a result of a combination of negative refractive index and a beam profile that is more intense at the centre than at the edges. This condition is the same as that of the propagation of light through a lens with negative focal length and hence the beam gets defocused.

(c) Nonlinear Absorption

Nonlinear effects can cause materials that are strongly absorbing at low intensities to become transparent at high intensities, an effect called saturable absorption. The reverse of the phenomenon called multiphoton absorption can also occur. Saturable absorption involves a decrease in absorption at high optical intensities, for materials that have high absorption at low intensities. This occurs when the upper state of the absorbing transition gains enough population to become filled, preventing the transfer of any more population into it. Saturable absorbers are used to mode lock solid state and pulsed dye lasers [64]. It also finds use in optical phase conjugation processes. The reverse also occurs for some materials where absorption will be a maximum leading to a state called reverse saturable absorption.

1.8 Nonlinear optical materials

Nonlinear optical crystals find applications in many fields of science and technology. The unique and intriguing properties are of significant application in the optoelectronic and photonic industries.

Advances in the development of NLO materials can be categorized as follows

- Search for new NLO materials

- Growth of promising NLO crystals
- Improving the characteristic properties of these NLO crystals

The search for new materials with high optical nonlinearities has captured top priority because of their practical applications in higher harmonic generation, amplitude and phase modulation, laser technology, switching and other signal processing devices. Non linear optical crystals, with high conversion efficiencies for second harmonic generation (SHG) and transparent in the visible and ultraviolet ranges are required for various devices in optoelectronics and photonics [65-67]. Amino acid family crystals have been the subject of extensive investigations for their NLO properties in the last two decades [68-70].

Generally, higher power density, longer crystal length, larger nonlinear coefficients and smaller phase mismatching parameter will result in higher conversion efficiency. However, there are always some limitations and the efficiency is determined by the nonlinear crystal itself. Also the input power density has to be lower than the damage threshold of the crystal. Therefore, it is important to select the right crystals for specific applications.

Relevant characteristics of NLO crystals suitable for device applications are the following[71]-

- Good crystal growth properties.
- High nonlinear response for frequency conversion
- Wide optical transparency region
- High laser damage threshold
- Wide phase matchable angle

- High thermal stability and mechanical strength.
- Non-hygroscopic nature
- Non toxicity and good environmental stability
- Low cost of production.

In the beginning, studies were mainly concentrated on inorganic materials such as quartz, potassium dihydrogen phosphate (KDP) etc. With the design of Kurtz Perry technique in 1968 for detecting the generation of second harmonics, a new qualitative screening for second order NLO effects came into use. Most commercial NLO materials are inorganic ones, especially for high power applications. Inorganic compounds are thermally and mechanically more stable compared to organic compounds. Organic compounds have the amenability for synthesis and the ability for multi functionalisation. Further, organic materials have a wide range of interesting properties which can be suitably tuned to meet the requirements. Organic materials are often formed by weak van der Waals forces and hydrogen bonds and hence possess a high degree of charge delocalization. However, many of the organic crystals have poor mechanical and thermal stability. By combining organic and inorganic compounds, a new class of materials for electronic industries, called semi organic materials are also being developed which possess the advantageous properties of both.

In recent years, organic crystals have received a great deal of interest as they provide a potential source of materials with interesting optical properties.

Majority of organic materials crystallize in centrosymmetric space groups and hence fail to exhibit SHG. But this centrosymmetric nature can be removed by employing several techniques. The methods like introducing

hydrogen bonding, chirality, guest-host systems, organo metallic structures and co-crystallization can be utilized to introduce noncentro symmetry. From the materials perspective, the chirality and hydrogen bonds are identified to contribute substantially for remarkable second harmonic generation (SHG) activity. Organic NLO crystals have the added advantage of being easy to be synthesized compared to inorganic crystals. Considerable interest has been shown recently in studying the effects of dopants on the nucleation, growth, and the NLO properties of both inorganic and organic crystals [72-74].

1.9 Advantages of organic nonlinear materials

The main advantages of organic NLO materials are [75]

- ❖ High second order nonlinearity
- ❖ Moderate resistance to laser damage
- ❖ Birefringence
- ❖ Possibility of engineering molecular properties
- ❖ Cost effective synthesis route
- ❖ Availability of simple conventional techniques for purification

Organic materials having electron donor and acceptor groups, have high order of nonlinearity and large hyperpolarizability. The enhancement in the nonlinearity in organic materials as compared to inorganic materials is due to the presence of π conjugation between electron donor and acceptor groups. The second order NLO effects in organic molecules originate from a strong donor acceptor intramolecular interaction. The molecules possessing an electron donor group and an electron acceptor group contribute to large second

order optical nonlinearity arising from intramolecular charge transfer between the two groups of opposite nature.

1.10 Objectives of the present investigations

Nonlinear optical crystals are in the forefront of modern crystal technology owing to their varied applications in optoelectronics and photonics. Recently amino acid complexes are being widely studied because of their significant technological applications. They are identified as systems with delocalized charge carriers showing NLO behavior.

L arginine phosphate(LAP) is an exceptionally good, amino acid complex, NLO crystal with characteristics strong enough to replace the most competent inorganic NLO material, KDP[76-82].Optically active crystals which are enantiomorphic like arginine, lysine, citrulline etc seem to be promising non linear optical crystals[83]. Crystals and complexes of L-arginine,L-histidine, L-asparagine etc. are reported as NLO crystals, whereas attempts to characterize salts of L-citrulline are not yet carried out extensively.

In view of this, attempts to grow new crystals of L-citrulline complexes seem worthwhile. Delocalization of charge carriers in these transparent crystals can be increased by reacting with acids like carboxylic, oxalic etc. When amino acids are treated with the acids, a charge transfer complex is formed due to the protonation of the amino group and deprotonation of the acid group in the crystal, creating a donor-accepter group resulting in enhanced hyperpolarizability.

In the present work, attempts have been made to grow single crystals of the aminoacid complex L-citrulline oxalate, using slow evaporation technique,

for the first time. One of the main objectives of the present work is to carry out detailed investigations on the structural and nonlinear optical properties of L-citrulline oxalate in its pure and metal doped forms. It is expected that doping with light metals such as lithium can enhance the NLO response of these crystals significantly.

Potassium dihydrogen phosphate is a well known nonlinear optical crystal. Another objective of the present work is to assess the prospects of doping KDP with the aminoacids, L-citrulline and L-lysine, with the intension of significantly modifying the NLO properties of KDP for all relevant applications.

1.11 References

- [1] Gibbs, J. G "Collected Works", Longmans, Green and Co., NewYork, 1928.
- [2] Volmer, M. and Weber, A., Z. Phys. Chem., 119, (1925) 227.
- [3] Kossel, W, Nachr. Ges. Wiss. Goettingen Math. Phys., K1 11 A (1927), 135.
- [4] Frank, F. C., Discussions Faraday Soc., 5 (1949)11 48.
- [5] P. Curie,Bull.Soc.franc. Miner.8, (1885)145.
- [6] Wulff, W, Z. Kristallogr, 34 (1901) 449.
- [7] 11. Berthoud, A, J. Chem. Phys., 10 (1912) 624
- [8] Valetton, J, J. P. K. Sachs Gus, Wiss Match. Physik, kipzing, 67 (1951) 1.
- [9] Noyes, A. A. and Whitney, W. R., Z. Physik. Chern., 23 (1891) 689.
- [10] Nernst, W, Z. Physik. Chem., 67 (1909) 470.

- [11] Kossel, W, Nachr. Ges. Wiss. Goettingen Math. Phys., K1 11 A (1927)135.
- [12] Volmer, M, Die Kinetik der Phasenbildung, Steinkopff, Dresden, 1939.
- [13] Stranski, I. N., Z. Phys. Chem., 136 (1928) 259.
- [14] Burton, W. K. Cabrera, N., Frank, F. C., Phil. Trans. Roy. Soc.A 243(1951) 299
- [15] M.Volmer and W.Shultz, Z.Phys.Chem.A156,(1931),1
- [16] Frank, F. C, Discussions Faraday Soc., 5 (1949)1148
- [17] Verma, A. R.J. Phil. Mag., 42 (1951) 1005.
- [18] Arnelinckx, S., Nature, Loodon, 167 (1951) 939.
- [19] Forty, A. J, Adv. Phys., 3 (1954) 1.
- [20] Keller, K. W., "Crystal Growth and Characterization" North-Holland, Amsterdam, 1975) 361.
- [21] Frank, F. C, J. Crystal Growth, 51 (1981) 367.
- [22] F.C.Frank,"Growth and perfection of crystals"Wiley,N.Y.,1958
- [23] A.L.Varma, "Crystal growth and dislocations, Butterworths, London, 1953.
- [24] Pamplin, B. R. (Ed.), Crystal Growth, Pergamen Press, Oxford, 1975.
- [25] Brice, J. C, Crystl. Growth Process, John Wiley and Sons, New York, 1986.

- [26] Barrat, C. S. and Massalski, T. B., *Structure of Metals*, McGraw-Hills, New York, 3rd edn., 1966.
- [27] Piper, W. W. and Polich, S. J., *J. Appl. Phys.*, 32 (1961) 1278.
- [28] Bremer, S. S, *The Art and Science of Growing Crystals*, Wiley, New York, 1963.
- [29] Holland, L, *Vacuum Deposition of Thin Films*, Chapman and Hall, London, 1956.
- [30] Kaldis, E, *J. Cryst. Growth*, 17 (1972) 3.
- [31] Kulkarni, A. K., *Bull. Mater. Sci.*, 17 (1994) 1379
- [32] Beny, C, West, W. and Moser, F., "The Art and Science of Growing Crystals" (Gilman, J. J., Ed.), Wiley, New York, 1963.
- [33] Bridgman, P. W, *Roc. Am. Acad. Arts. Sci.* 60 (1925) 305.
- [34] Stockbarger, C, *Rev. Sci. Instr.*, 7 (1938) 133.
- [35] Czochralski, J, *Z. Phys. Chem.*, 92 (1971) 219
- [36] Dash, W. C, *J. Appl. Phys.*, 30 (1959) 459.
- [37] Howe, S. and Elbaum, C., *Phil. Mag.*, 6 (1961) 1227.
- [38] Furukawa, Y, Sato, M., Nitanda, F. and Ito, K., *J. Cryst. Growth*, '5 (1990) 832.
- [39] Pfann, W. G, *Zone Melting*, John Wiley, New York, 2nd edn., 1966.
- [40] Keck, P. H. and Golay, M. 1. E., *Phys. Rev.*, 89 (1953) 1297
- [41] Ellwell, D and Scheel, H.J, *Crystal Growth from High Temperature Solutions*, Academic Press, London, 1975.

- [42] Bahadur, S. A, Rarnakrishnan, V. and Rajmn, R. K., Bull. Mater. Sci., 13 (1990) 161.
- [43] Chaoyang, T. U, Zundu, L, Chen, G. and Wang, G, Cryst. Res. Tech.29 (1994) 47.
- [44] Yokotani, A. Sasaki, T., Fujioka, K., Nakai, S. and Chiyoe, Y, J. Cryst. Growth, 99 (1990) 815.
- [45] Chernov, A.A, The spiral Growth of Crystals, Usp.Fiz.Nauk, 73(1961)277.
- [46] Bennema, P.J.Cryst. Growth, 24(1974)76.
- [47] Vekilov,P.G, Kuznetsov, Yu.G.Chernov,A.A, J.Cryst Growth 121 (1992) 643.
- [48] Petrov,T.G,Treivus, E.B;Kasatkin,A.P,Growing crystals from solution, Consultant's Bureau, Adivision of Plenum publishing Corp., New York, 1969.
- [49] Laudise, R. A., J. Am. Chem. Soc., 81 (1959) 562.
- [50] Henisch,H.K, Crystal growth in Gels and Leisengang Rings, Cambridge University,1988.
- [51] Selvasekharapandian,S;Vivekanandan,K,Kolandaivel,P,Cryst.Res.T echnol,34, (1999)873.
- [52] Roopakumar.R,Raman.G,Gnanam.F.D,Cryst.Res.Technol27, (1992)92.
- [53] Kalkura.S.N, Devanarayanan.S,J.Cryst.Growth 83, (1987)446.
- [54] Armington.A.F,O'Connor.J.J,Mater.Res.Bull,3, (1968)923.
- [55] Polanyi.M,z.Physik,89, (1934)660.

- [56] Orowan.E,Z.Physik,89, (1934)634.
- [57] Mott,N.F.Nabarro,The strength of solids,Physical Soc.London1948.
- [58] Laud,B.B.,Lasers and nonlinear optics, Welly Easter Ltd., New Delhi, 1985.
- [59] P.A.Franken,A.F.Hill,C.W.Peters,Phys.Rev.Lett. 7, (1961)118.
- [60] T.H.Maiman, Nature, 1877, (1960)493.
- [61] L.Wood, F.J.Sharp, Nonlinear Optics & Electro-Optics hand book, Mc Graw Hill Inc. New York 1994
- [62] N. Bloembergan, Nonlinear Optics, World Scientific, Singapore 1996
- [63] E.G.Sauter, Nonlinear optics, John Wiley& Sons Inc, New York 1996
- [64] Y.R.Shen, Principles of nonlinear optics, John Wiley& Sons Inc, New York 1994
- [65] R.F. Belt, G. Gashurov, Y.S. Liu, Laser Focus 10 (1985) 110.
- [66] R.S. Calark, Photonics Spectra 22 (1988) 135.
- [67] R.J. Gambino, Bull. Mater. Res. Soc. 15 (1990) 20.
- [68] M. Kitazawa, R. Higuchi, M. Takahashi, T. Wada, H. Sasabe, Appl. Phys. Lett. 64 (1994) 2477.
- [69] T. Baraniraja, P. Philominathan, Spectrochim. Acta Part A 75 (2010) 74.
- [70] D. Xu, M. Jiang, Z. Tan, Acta Chem. Sin. 41 (1983) 570.
- [71] Nalwa.H.S,Watanabe.T,Miyata.S,Organic Materials for second order Nonlinear optics,CRC press, Florida, U.S.A,1997

- [72] Manivannan V, Sagayaraj P, Madhavan J, Praveen Kumar P, Bull. Mater. Sci., 32(4) (2009) 431
- [73] Parikh K D, Dave D J, Parekh B B and Joshi M J. Cryst. Res. Technol, 45 (2010) 603.
- [74] Muley G G, Rode M N and Pawar B H, Acta Physica Polonica A116 (2009) 1033
- [75] Owen. J.R, White. A.D, J. Mat. Sci. Lett (1976) 2165.
- [76] D. Xu, M. Jiang and Z. Tan. Acta chem. Sin. 41 (1983) 570.
- [77] S.B. Monaco, L.E. Davis, S.P Velsko, F.T. Wang, D. Eimerl, A. Zalkin, J. Crystal Growth 112(1991) 183.
- [78] S. Haussuhl, J. Chrosch, F. Granam, E. Fiorentini, K. Recker, F. Wallrafen, Crystallogr. Res. 25(1990) 617.
- [79] L.N. Rashkovich, B. Yu. Shekunov, J. Crystal Growth 112(1991) 183.
- [80] G. Ravi, K. Srinivasan, S. Anbukumar, P. Ramasamy, J. Crystal Growth 137(1994) 598.
- [81] O. Angelova, V. Velikova, Ts. Kolev, V. Radomska, Acta Crystallogr C52(1996) 3252.
- [82] G. Arunmozhi, R. Jayavel, C. Subramanian, J. Crystal Growth 178 (1997) 387.
- [83] A.M Petrosyan, R.P. Sukiasyan, H.A. Karapetyan, S.S. Terzyan, R.S. Feigelson, J. Crystal Growth 213 (2000) 103.



2.1 Structural characterization
2.2 Elemental Analysis
2.3 Vibrational Spectral Analysis
2.4 Optical characterization
2.5 Characterization of Nonlinear optical properties
2.6 Thermal Characterization
2.7 Dielectric studies
2.8 Etching studies
2.9 References

• *A bird's eye view on the profile of the various characterization techniques employed for studying the properties of the materials dealt with in the thesis is projected in this chapter.*

The structural, thermal and optical (both linear and nonlinear) characterizations of the samples are carried out using various sophisticated instruments and a comprehensive description of the tools utilized is given in this section.

2.1 Structural characterization

The structural characterization of the materials under study is envisaged using single crystal X-ray diffractometer, powder X-ray diffractometer, transmission electron microscope and FTIR and Raman spectrometers. The elemental analysis has been carried out using CHN analyzer and Energy Dispersive X-ray spectroscopy.

2.1.1 Single crystal X-ray crystallography

The oldest and most precise method of X-ray crystallography is single-crystal X-ray diffraction. It is the most elucidative method of determining the arrangement of atoms within a crystal, in which a beam of X-rays strikes a crystal and gets diffracted into many specific directions and a three-dimensional picture of the density of electrons within the crystal is obtained. From this electron density distribution, information about the mean positions of the atoms, their chemical bonds, and the extent of disorder can be obtained.

Crystals are formed by regular periodic arrangement of atoms. Atoms scatter X-rays. X-ray diffraction results from an electromagnetic wave impinging on a regular array of scatterers, determined by Bragg's law:

$$2d \sin\theta = n\lambda \quad (2.1)$$

Here d is the spacing between diffracting planes, θ is the glancing angle, n is any integer, and λ is the wavelength of the X-ray beam. These specific directions appear as spots on the diffraction pattern.

X-rays are used to produce the diffraction pattern because their wavelength λ is typically of the same order of magnitude as the spacing d between planes in the crystal. These scattered beams make a diffraction pattern of spots as the crystal is gradually rotated and the diffraction patterns can be recorded. X-ray diffraction data can be used to determine the mean chemical bond lengths and bond angles to within a few thousandths of an angstrom and to within a few tenths of a degree, respectively.

The technique of single-crystal X-ray crystallography has three basic steps. The first step is to obtain a large and regular crystal with no significant internal imperfections such as cracks or twinning. In the second step, the crystal is placed in an intense beam of monochromatic X-rays, to produce

regular pattern of reflections. The crystal is gradually rotated and the intensity of every spot is recorded at every orientation of the crystal. When a crystal is mounted and exposed to an intense beam of X-rays, it scatters the X-rays into a pattern of spots or reflections and the relative intensities of these spots provide the information to determine the arrangement of atoms/molecules within the crystal. To collect all the necessary information, the crystal must be rotated step-by-step through 180° , with an image recorded at every step. The intensities of these reflections may be recorded with photographic film, an area detector or with a charge-coupled device (CCD) image sensor. The recorded series of two-dimensional diffraction patterns, each corresponding to a different crystal orientation, is converted into a three dimensional model of the electron density, using Fourier transform. In the third step, these data are combined computationally with complementary chemical information to produce and refine a model of the arrangement of atoms within the crystal. Finally, refined model of the atomic arrangement called the crystal structure is stored in a database.

Data processing begins with indexing the reflections by identifying the dimensions of the unit cell and which image peak corresponds to which position in reciprocal space. A byproduct of indexing is to determine the symmetry of the crystal, i.e., its space group. Having assigned symmetry, the data is then integrated. This converts the hundreds of images containing the thousands of reflections into a single file, consisting of records of the Miller indices of each reflection, and intensity for each reflection. Structure analysis by single crystal X-Ray diffraction is the most powerful technique for structural characterization of crystals. In the present work single crystal X-ray diffraction was carried out using Enraf Nonius CAD-4 diffractometer to study the structure and morphology of the grown crystals. The molecular structure is solved by direct method and refined by SHELXL program [1]

2.1.2 Powder X-ray diffraction

Powder diffraction is a key analytical method to analyze qualitatively the phase purity, particle size, strain etc. of the samples and also to establish the molecular structure of the samples, whose crystal structure has already been determined. Powder X-ray diffractometer utilizes the sample in the powdered form. It consists of a goniometer and a fixed detector to detect the diffracted X-rays. The monochromator provides a specific wavelength and the resulting trace is recorded in intensity for different diffracting angles(2θ). The powdered sample provides all possible orientations of the crystal lattice and the diffracted patterns from all planes are recorded. The powder X-ray diffraction method is useful for qualitative rather than quantitative analysis.

In the present study, powder X-ray diffraction has been carried out using Bruker D8 advance diffractometer with Cu K α radiation ($\lambda = 1.5418 \text{ \AA}$). The crystal structure has been refined by Pawley method [2] using the TOPAZ version 3 program[3]. The Rigaku X-ray diffractometer with Cu K α radiation of wavelength $\lambda=0.15496 \text{ nm}$ has also been used for the structural analysis in the present work.

2.1.3 Transmission Electron Microscope

Transmission electron microscopy (TEM) is a high resolution microscopy technique whereby a beam of electrons is transmitted through an ultra thin specimen and an image is formed by the interaction of the electrons with the specimen. The image is magnified and focused onto an imaging device, such as a fluorescent screen, or a layer of photographic film, or detected by a sensor such as a CCD camera. The transmitted beam which is

used to form the image contains information about electron density, phase and periodicity.

The first TEM was built by Max Knoll and Ernst Ruska in 1931[4]. It has the same principle as that of an optical microscope. The maximum resolution, d , obtained with a light microscope is limited by the wavelength of the photons that are being used to probe the sample λ , and the numerical aperture (NA) of the system, given by

$$d = \frac{\lambda}{2n \sin \alpha} \approx \frac{\lambda}{2NA} \quad (2.2)$$

In TEM imaging technique, electrons play the role as that of photons in an optical microscope. A beam of electrons behave like a beam of electromagnetic radiation whose wavelength is given by

$$\lambda_e \approx \frac{h}{\sqrt{2m_0 E \left(1 + \frac{E}{2m_0 c^2}\right)}} \quad (2.3)$$

where, h is Planck's constant, m_0 is the rest mass of an electron and E is the energy of the accelerated electron. Electrons are generated by an electron gun or by field emission and are accelerated by an electric field. The beam can be focused by electric and magnetic fields on to the sample. The beam is restricted by the condenser aperture, knocking out high angle electrons. The beam strikes the specimen and part of it is transmitted which is focused by the objective lens into an image. Optional objective and selected area metal apertures can restrict the beam. The objective aperture enhances contrast by blocking out high-angle diffracted electrons and the selected area aperture examines the periodic diffraction of electrons by ordered arrangements of

atoms in the sample. The image is passed through the intermediate and projector lenses and directed on to the image screen. The beam transmitted by the sample contains electrons that have not undergone scattering and that have lost energy by inelastic scattering and also electrons reflected by various crystallographic hkl planes. A bright field image is produced when an aperture is inserted and a dark field image when the aperture is positioned to select only beams reflected from a particular hkl plane. The schematic diagram of TEM is shown in Fig: 2.1.

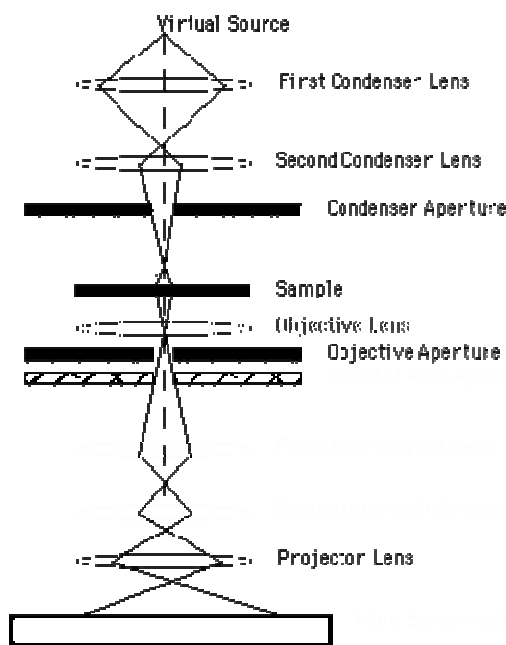


Fig: 2.1 Schematic diagram of Transmission Electron Microscope

2.2 Elemental Analysis

The elemental composition of the samples investigated in the present study has been determined using CHN analysis, EDX and ICP AES.

2.2.1 CHN analysis

This is a very elucidative technique to determine the empirical formula of a compound. The empirical formula is the formula for the compound that contains the smallest set of integer ratios, which gives the correct elemental composition by mass for the elements present in the compound. The CHN analysis is basically a combustion process, where the sample is burnt in an excess of oxygen. The various traps collect the combustion products like carbon dioxide, nitric oxide, water etc. From the weights of these combustion products, the composition of the unknown sample can be calculated.

The analysis is performed by working out a chemical formula that fits with the ratio of the elements of the sample. This technique is important as it helps to determine the composition of the sample and also to confirm the purity of the compound. VarioEL III CHNS analyzer has been used to study the chemical composition of the samples in the present study.

2.2.2 Energy Dispersive Analysis by X-rays (EDX)

This is a technique to identify the elements present in a compound. The system works as an integrated feature of a scanning electron microscope [5]. The principle of EDX is that the electron beam generates X-rays within the specimen. The electron beam incident on the sample excites an electron in an inner shell and ejects it. An electron from an outer, higher-energy shell then fills the hole, and the difference in energy between the higher-energy shell and the lower energy shell may be released in the form of an X-ray. The number and energy of the X-rays emitted from a specimen can be measured by an energy-dispersive spectrometer. The energy of the X-rays are characteristic of the difference in energy between the two shells, and of the atomic structure of

the element from which they are emitted. This helps in determining the elemental composition of the specimen. The EDX system consists of an X-ray detector, a pulse processor and a computer. The X-ray detector intercepts X-rays emitted from the specimen. On entering the detector, X-rays generate a small current, which is then converted into a voltage pulse. The size of the voltage pulse is proportional to the energy of the X-rays. A computer measures the voltage pulses and plots them as a histogram. The histogram shows a spectrum of the X-ray energies and by examining the spectrum, the elements present can be determined. The EDX spectrum displays peaks and each peak is unique to an atom and corresponds to a single element. The higher the peak, the more concentrated is the element present in the specimen.

2.2.3 Inductively Coupled Plasma Atomic Emission Spectroscopy (ICP AES)

It is an analytical technique used for the detection of trace metals. It is a type of emission spectroscopy that uses the inductively coupled plasma to produce excited atoms and ions that emit electromagnetic radiation at wavelengths characteristic of a particular element. The intensity of this emission indicates the concentration of the element within the sample.

2.3 Vibrational Spectral Analysis

This is a method of characterization of materials to get information about the composition and the structure of molecules. The techniques used are Fourier Transform Infra red (FTIR) Spectroscopy and Raman Spectroscopy.

2.3.1 Fourier transform infra red spectroscopy (FTIR)

It is a vibrational spectroscopy that records absorptions of IR light by chemical bonds in all molecules. Different bonds absorb IR light at characteristic but different wavelengths and hence FTIR spectroscopy is often referred to as fingerprint spectroscopy. As a consequence pure compounds have characteristic and unique FTIR spectra. Spectra are collected based on measurements of the coherence of a radiative source, using time-domain measurements of the electromagnetic radiation. FT-IR is a method of obtaining infrared spectra by first collecting an interferogram of a sample signal using an interferometer, and then performing a Fourier Transform (FT) on the interferogram to obtain the spectrum. An FT-IR Spectrometer collects and digitizes the interferogram, performs the FT function, and displays the spectrum.

An FT-IR spectrometer is based on a Michelson Interferometer. The interferometer consists of a beam splitter, a fixed mirror, and a moving mirror that translates back and forth. The beam splitter transmits half of the radiation striking it and reflects the other half as shown in Fig: 2.2. Radiation from the source strikes the beam splitter and gets separated into two beams. One of the beams is transmitted through the beam splitter to the fixed mirror and the second is reflected off the beam splitter to the moving mirror. The fixed and moving mirrors reflect the radiation back to the beam splitter. Half of this reflected radiation is transmitted and half is reflected at the beam splitter, resulting in one beam passing to the detector and the second back to the source. In FTIR spectrometer, the sample is placed between the output of the interferometer and the detector. The sample absorbs the radiation of a particular wavelength. An interferogram of a reference (sample cell and

solvent) is required to revive the spectrum of the sample. After the collection of the data, a fourier transform is performed using a computer program which results in a frequency domain trace.

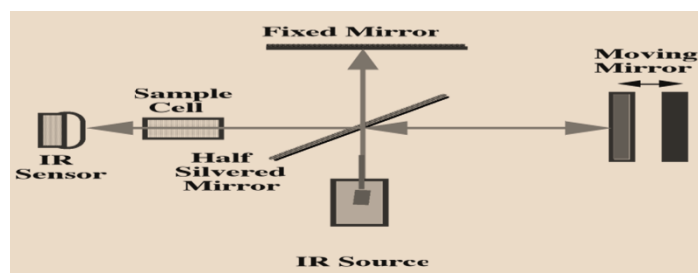


Fig: 2.2 Schematic diagram of FTIR spectrometer

The process of conversion of the interferogram into a spectrum is through the Fast Fourier Transform algorithm introduced by J.W. Cooley and J.W. Tukey in 1965. A number of steps are involved in the conversion process. The advantages of infra red spectroscopy include wide applicability, possibility of measurement under ambient conditions and the capability of providing detailed structural information. The merits of FT technique are higher sensitivity, higher precision, better speed of measurement and better efficiency of data processing [6, 7].

Infra red spectra originate due to the transitions between two vibrational levels of a molecule in the electronic ground state and are observed as absorption bands in the infrared region. For a molecule to have infrared absorption bands, it should have a permanent dipole moment. The dipole interacts with the oscillating electric field of the incident infrared radiation. There must be a change in the dipole moment of the molecule during the vibration of the molecule to be infrared active or to give rise to an observable infrared band.

The vibrational frequency is determined by the force constant and reduced mass and hence the frequency of the fundamental vibration will be higher, if the bond strength is higher. The frequency will be lower when the masses of the atoms attached to the bond increases.

The infrared spectrum can be divided into the functional group region and the finger print region. The region ranging from 1500cm^{-1} to 4000cm^{-1} is called the functional group region and that below 1500cm^{-1} corresponds to the fingerprint region. The functional group region includes stretching vibrations which are localized and gives information about the nature of the components that make up the molecule. The finger print region includes molecular bending vibrations characteristic of the entire molecule [8]

2.3.2 Raman spectroscopy

This spectroscopic technique is named after Sir. C.V.Raman. It is used to study vibrational, rotational, and other low-frequency modes in a system. It relies on the inelastic scattering of monochromatic light in the visible, near infrared, or near ultraviolet range by molecular vibrations, phonons or other excitations in the system, called Raman scattering, resulting in the energy of the photons being shifted up or down. The shift in energy gives information about the phonon modes in the system. Infrared spectroscopy yields similar, but complementary, information.

A Raman spectrometer consists of an illumination source, typically a laser source, a sample chamber, a double monochromator and a spectrometer, a multichannel detector and a photomultiplier tube.

When a molecule is placed in an electromagnetic field, a transfer of energy between the molecule and the field takes place resulting in spectra

which have frequencies higher and lesser than the frequency of the incident field. Raman spectra originate due to the polarization caused by the incident radiation which interacts with a pulsating electron cloud. This interaction is modulated by the molecular vibrations which in turn depend on the chemical structure of the molecules that scatter the radiation.

Raman spectroscopy has become a very powerful tool for the analysis of solids, liquids and solutions and can even provide information on physical characteristics such as crystalline phase and orientation, polymorphic forms, and intrinsic stress [9, 10]. Fig: 2.3 depicts the experimental set up for Raman spectroscopic studies.

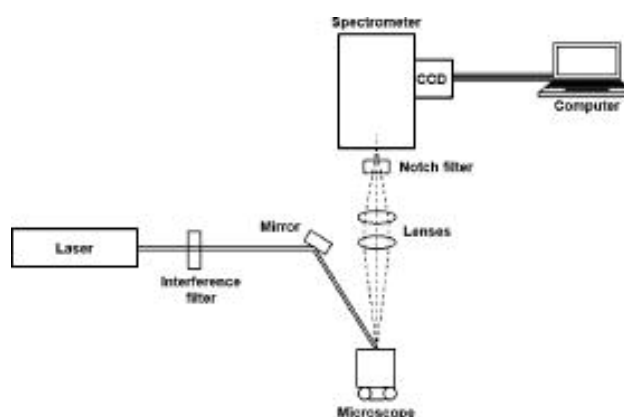


Fig: 2.3 Experimental set up for Raman spectroscopic studies.

2.4 Optical characterization

Optical characterization includes both linear and nonlinear optical properties of the specimen. Linear optical properties are investigated by UV-Vis absorption and photoluminescence studies and the nonlinear optical properties, by employing Kurtz Perry powder technique for estimating the second harmonic generation efficiency and the open aperture Z scan technique for investigating the third order non linear effects.

2.4.1 UV-Vis absorption spectroscopic studies

UV/Vis absorption spectroscopy is based on the Beer-Lambert law which is useful in the quantitative analysis of samples and the absorption spectrum is recorded using a spectrophotometer. Different molecules absorb radiation of different wavelengths. An absorption spectrum will show a number of absorption bands corresponding to structural groups within the molecule [11,12]. The absorption of UV or visible radiation corresponds to the excitation of outer electrons.

When an atom or molecule absorbs energy, electrons are promoted from their ground state to an excited state. In a molecule, the atoms can rotate and vibrate with respect to each other. Possible electronic transitions of π , σ , and n electrons are –

1. $\sigma \rightarrow \sigma^*$ transition
2. $n \rightarrow \sigma^*$ transitions.
3. $n \rightarrow \pi^*$ and $\pi \rightarrow \pi^*$ Transitions

The UV-Vis absorption spectrophotometer consists of the following components:

1. Source (UV and visible)
2. Wavelength selector (monochromator)
3. Sample container
4. Detector
5. Signal processor and readout

Source of UV radiation is the radiation generated by electrical excitation of deuterium or hydrogen at low pressures which produces a continuous spectrum. The tungsten filament lamp is commonly employed as a source of visible light.

Monochromators contain 1) an entrance slit, 2) a collimating lens, 3) a dispersing device (a prism or a grating), 4) focusing lens and (5) an exit slit

The containers or cuvettes for the sample and reference solutions must be transparent to the radiation and hence the material used for cuvettes is quartz.

The detector commonly used is a photomultiplier tube which consists of a photoemissive cathode, several dynodes, and an anode. The schematic diagram of the UV-Vis spectrophotometer is shown in Fig: 2.4.

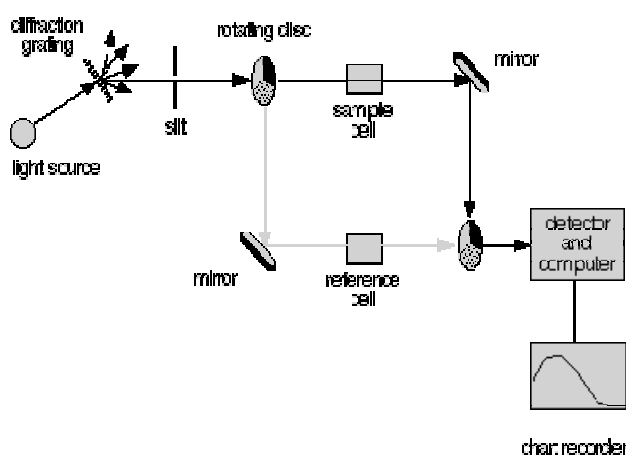


Fig: 2.4 Schematic diagram of a double-beam UV-Vis. Spectrophotometer

The absorbance of an absorbing species in solution, using the Beer-Lambert law is given by

$$A = \log_{10}(I_0/I) = \epsilon \cdot c \cdot L \quad (2.4)$$

where A is the measured absorbance, I_0 is the intensity of the incident radiation at a given wavelength, I is the transmitted intensity, L the path length through the sample, and c the concentration of the absorbing species.

The photon absorption for crystalline materials is found to obey the Tauc relation given by

$$(\alpha h\nu) = A (h\nu - E)^n \quad (2.5)$$

where α is the absorption coefficient, $h\nu$ the photon energy, A is a constant and the index n is related to the distribution of density of states. The value for n is equal to $1/2$ for direct allowed transition, and n is equal to 2 for indirect allowed transition. The linear portion of the plot of $(\alpha h\nu)^2$ versus $h\nu$, when extrapolated to the energy axis, gives the band gap. In the present work, Jasco V 570 UV-Vis-NIR spectrophotometer has been employed for the absorption studies.

2.4.2 Photoluminescence studies

Photoluminescence (PL) is a process in which a substance absorbs electromagnetic radiation and gets excited to a higher energy state, from where it returns to a lower state accompanied by the emission of radiation and the process takes place in a very short duration of the order of a few nanoseconds. Photoluminescence is an important technique for estimating the purity and crystalline quality of semiconductors. Radiative transitions in semiconductors involve localized defect levels. The photoluminescence energy associated with these levels can be used to identify specific defects, and also to determine their concentration [13]. In the present study, the instrument Fluoromax 3 spectrofluorimeter has been used to carry out the PL studies.

2.5 Characterization of Nonlinear optical properties

The second and third order nonlinear optical properties of the samples of the present work have been investigated by determining the second harmonic generation efficiency (SHG), employing Kurtz Perry powder technique and by measuring the nonlinear absorption coefficient by the open aperture Z scan technique respectively.

2.5.1 Second harmonic efficiency (SHG)

Quantitative measurement of the relative second harmonic generation efficiency (SHG) of the sample can be assessed by the Kurtz Perry powder technique [14]. It is a simple method to determine the second order optical nonlinearity of a crystalline material. The crystal is powdered and filled densely in a capillary tube. High intensity laser radiation, like Nd-YAG laser of 1064nm wavelength, 10ns pulse width and 10 Hz pulse rate is made to fall on the sample. The transmitted wave is passed through a monochromator which separates the second harmonic signal from the fundamental. It is again passed successively through filters to remove any residual fundamental beam. The beam is finally focused to a photomultiplier tube which amplifies the second harmonic wave generated by the crystal. The SHG efficiency is determined by comparing the output with that of the reference such as KDP, powdered to the same size, using the formula 2.6. A schematic diagram of the set up is shown in Fig: 2.5

$$\text{SHG efficiency} = I^{2\omega}_{\text{sample}} / I^{2\omega}_{\text{KDP}} \quad (2.6)$$

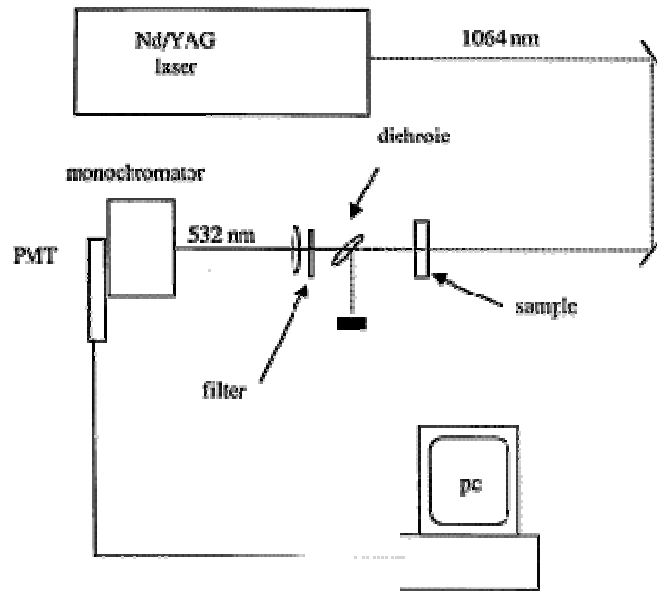


Fig: 2.5 Schematic diagram of the SHG set up

2.5.2 Open aperture Z scan method

Z scan technique is a method used to determine the nonlinear absorption coefficient in the open aperture mode and nonlinear refraction in the closed aperture mode of liquids, films, crystals etc.[15,16].

In a typical Z scan experimental set up, a mode locked Nd-YAG laser beam is focused by a lens. A detector is placed at the far field. The sample is moved along the axial direction of the focused beam. The transmitted intensity is measured as a function of the position of the sample. A laser beam propagating through a nonlinear medium will experience both amplitude and phase variations.

If transmitted light intensity is measured without an aperture, the mode of measurement is referred to as open aperture z-scan. The technique is employed to measure nonlinear absorption in the sample.

When the intensity I of the incident beam is sufficiently high, the response of the nonlinear medium will be such that the absorption becomes intensity dependent, given by

$$\alpha(I) = \alpha_0 + \beta I \quad (2.7)$$

where β is the absorption coefficient.

At sufficiently high intensities, the probability of a material absorbing more than one photon before relaxing to the ground state is greatly enhanced. The different phenomena manifested are

- i. Saturable or reduced absorption
- ii. Reverse saturable or increased absorption
- iii. Two photon absorption (TPA)
- iv. Multiphoton absorption
- v. Free carrier absorption (FCA)

Two photon absorption (TPA) is a third order NLO process. It refers to the simultaneous absorption of two photons from an incident radiation field. The transmitted beam energy, reference beam energy and their ratio can be measured simultaneously by an energy ratio meter. The open aperture z scan technique is employed to measure nonlinear absorption in the sample.

If $I(z)$ is the irradiance, L , the optical length and τ , the time

$$I(z) = 1/(\sqrt{\pi} Q(z)) \int \ln [1+ Q(z)] e^{-\tau^2} d\tau \quad (2.8)$$

where $Q(z) = \beta I(z) [(1 - e^{-\alpha L})/\alpha]$ (2.9)

$$(1 - e^{-\alpha L})/\alpha = L_{\text{eff}}, \text{ the effective path length}$$

In open aperture z scan the phase variations of the beam are not taken in to consideration. Equation 2.9 yields the nonlinear absorption coefficient (β).

If the sample is a reverse saturable absorber, it is manifested in the measurement as a transmission minimum at the focal point. If the sample is a saturable absorber, transmission increases with increase in incident intensity and results in a transmission maximum at the focal region. Schematic representation of the experimental setup for z-scan technique is shown in Fig: 2.6

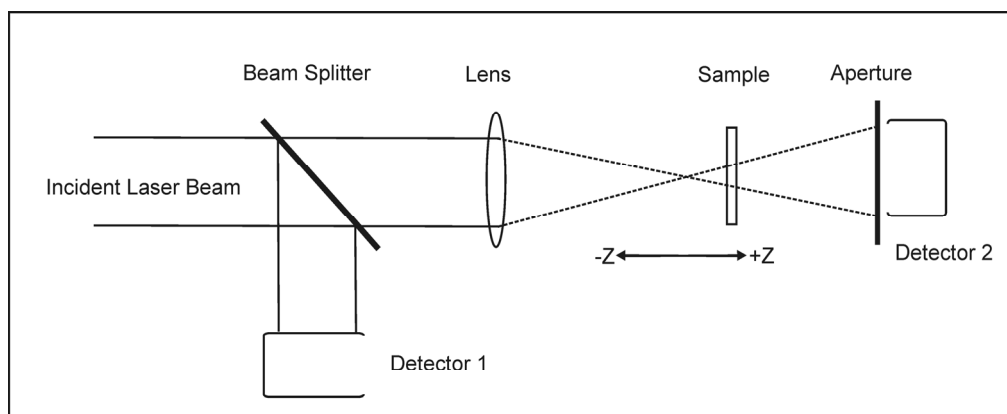


Fig: 2.6 Schematic representation of the experimental setup for z-scan technique

2.6 Thermal Characterization

The thermal characterization is carried out with the help of Thermogravimetric analysis(TGA).

This method basically measures weight changes in a material when subjected to variation in temperature in a controlled atmosphere. From the TGA analysis, the thermal stability and degradation temperature of the material, moisture content in the material, the amount of organic and inorganic

components in the specimen, the decomposition temperature of explosive materials etc can be estimated [17].

The thermal analyzer consists of a high-precision balance with a pan made of platinum which is loaded with the sample. The sample is placed in a small electrically heated oven with a thermocouple to accurately measure the temperature. The atmosphere may be purged with an inert gas to prevent oxidation or other undesired reactions. A computer is used to control the instrument. A graph of the percentage of weight loss versus temperature is plotted from which the different thermal processes can be analysed.

2.7 Dielectric studies

An impedance analyzer is used to study the dielectric properties of the samples in the present study. Dielectrics are substances which do not have free electrons, but in the presence of an electric field E , the material gets polarized and a net dipole moment is induced in the substance. The polarization is given by

$$P = \epsilon_0 \chi_e E \quad (2.10)$$

Where ϵ_0 is the permittivity of free space and χ_e is the electrical susceptibility.

The dielectric constant ϵ_r is also called the relative permittivity and can be calculated using the relation:

$$\epsilon_r = Ct / (\epsilon_0 A) \quad (2.11)$$

where C is the capacitance, t , the thickness of the sample, ϵ_0 , the permittivity of free space and A , the area of cross section.

2.8 Etching studies

Etching is a reverse growth process. When a crystal is placed in contact with a solvent, it dissolves chemically in such a way that the dissolution is consistent with the symmetry of the crystal. Due to the anisotropy of the crystal, the dissolution rates are different in different directions giving rise to depressions known as etch pits [18,19]. The dislocations can also be revealed in the form of etch pits. The shape of the etch pit is consistent with the symmetry of the crystal. There is also the possibility that the etch pits formed may be due to impurity inclusions, point defects etc.

Etching process is a very complex process and the etching study is based on qualitative or empirical aspects. It can mainly be used to reveal the history of growth of the crystals, to determine the density of dislocations and to estimate the impurity distribution in crystalline bodies.

2.9 References

- [1] Sheldrick,G.M,SHELXL97,University of Gottingen,Germany,1997
- [2] G.S.Pawley, J.Appl. Cryst, 14(1981)357.
- [3] Sheldrick,G.M, TOPAZ-R,ver3, University of Gottingen, Germany, 1997
- [4] Egerton, R Physical principles of electron microscopy, Springer 2005.
- [5] D.K.Schroder, Materials and Device Characterisation, Wiley Interscience, New York, 1998.
- [6] Fately.W.G,Mc Devit.N,Bentely.F.F.Appl.Spectrosc,25(1971)155
- [7] Kaneko.N,Takanashi.H,Spectrochem.Acta Part ,40(1984)33
- [8] Stuart.A.V,Sutherland, G.B.M.J.Chem.Phys.24(1956)559.

- [9] Taylor.W,Lockwood.D.J,Labbe.H.J,J.Phys,C17(1984)3685
- [10] Tobin.M.C:Laser Raman Spectroscopy, Wiley Interscience, New Yorkkk,1971.
- [11] I.M.Tsidilkovsk, Band structure of semiconductors, Pergamon Press, Oxford 1982
- [12] A.Ashour, H.H.Afifi and S.A.Mahmoud, Thin Solid Films, 248 (1994) 253.
- [13] D.R.Vij (Ed) Luminescence of solids, Plenum Press, New York, 1998.
- [14] S.K.Kurtz and T.T.Perry, J.appl. Phys.39 (1968)3798.
- [15] M.Sheik Bahae, A.A.Said and E.W.Van Stryland, Opt.Lett.14 (1989) 955
- [16] M.Sheik Bahae, A.A.Said and E.W.Van Stryland, IEEE.J.Quantum Electronics 26 (1990) 760.
- [17] P.E.J.Flewit and R.K.Wild, Physical methods for material characterization, IOP publishing, London, 2003.
- [18] N.Cabrera, The surface chemistry of metals and semiconductors, John Wiley, Holland, 1960.
- [19] S.Amleenikx, Direct observation of dislocations,vol.6,Academic press, New York,1964

**L-CITRULLINE OXALATE MONOHYDRATE—
A NEW NONLINEAR OPTICAL CRYSTAL****Contents**

- 3.1 Introduction
- 3.2 Crystal Growth
- 3.3 Characterization
- 3.4 Comparative study with other NLO crystals
- 3.5 Conclusions
- 3.6 References

This chapter deals with the growth and characterization of a new NLO single crystal, L-citrulline oxalate monohydrate. Growth and structure determination of the crystal and functional group characterization of the crystal using FT-IR and FT-Raman analysis along with the optical and thermal characterization are illustrated in this chapter. Nonlinear optical studies, etching studies and investigations on the dielectric properties are also dealt with, in this section.

3.1 Introduction

Nonlinear optical crystals are of top most interest in the present day scientific scenario due to their wide applications in the domain of optoelectronics and photonics. The development of new materials with high optical nonlinearities has hence gained much importance recently, because of their practical applications in higher harmonic generation, amplitude and phase modulation, laser technology, and in realizing efficient, switching and other signal processing devices. Nonlinear optical crystals with high conversion efficiencies for higher harmonic generation and transparent in the visible and ultraviolet ranges are

required for developing a variety of devices in the field of optoelectronics and photonics [1-3]. Amino acid family crystals have been the subject of extensive investigations for their non linear optical (NLO) properties during the last two decades [4]. The electro- optic and NLO properties exhibited by molecules having asymmetric polarization are brought about by the electron donor and acceptor groups. Aminoacids show appreciable optical nonlinearity as a result of the proton donor carboxyl (COOH) groups and the proton acceptor amine (NH₂) groups present in these materials.

Over the past two decades, much effort has been made to synthesize aminoacid mixed organic/inorganic complex crystals to make them suitable for various device applications. Organic/ inorganic complexes combine the optical nonlinearity of the organic part with the good mechanical properties of the inorganic part. L- arginine phosphate (LAP) is an outstanding amino acid complex crystal possessing unique optical characteristics which make it a strong candidate to replace the well established inorganic NLO material, KDP[5-11].Of late, there has been a trend towards developing organic complexes due to their large nonlinear susceptibilities and diverse and flexible processing possibilities, compared to the inorganic complexes.

Optically active crystals which are enantiomorphic like arginine, lysine, citrulline etc seem to be promising non linear optical crystals [12]. Crystals of L-arginine and L-histidine are reported to be NLO crystals, whereas no serious attempts have been made to characterize salts of L-citrulline. In view of this, attempts to grow new single crystals of citrulline complexes seem worthwhile.

L-citrulline is a non essential amino acid and is optically active. The details of crystal growth and the various characterizations of L- citrulline

oxalate single crystals, grown for the first time using simple solution growth technique are illustrated in this chapter.

3.2 Crystal Growth

Single crystals of L- citrulline oxalate (LCO) were grown using the procedure described below. High pure L- citrulline and oxalic acid were mixed in equimolar ratio in deionised water to form a super saturated solution and maintained at constant temperature with continuous stirring to ensure uniform distribution of the salt over the entire solution. The resulting solution was kept for evaporation. Seed crystals formed were harvested and were used for the solubility test. A key factor for successful growth of any crystal is the proper selection of solvents [13, 14]. The solubility of the crystal was determined in two solvents, methanol and water. A saturated solution of the crystallized salt was prepared in the solvents and solubility was determined at different temperatures. The solubility diagrams for the two solvents are depicted in Fig.3.1.

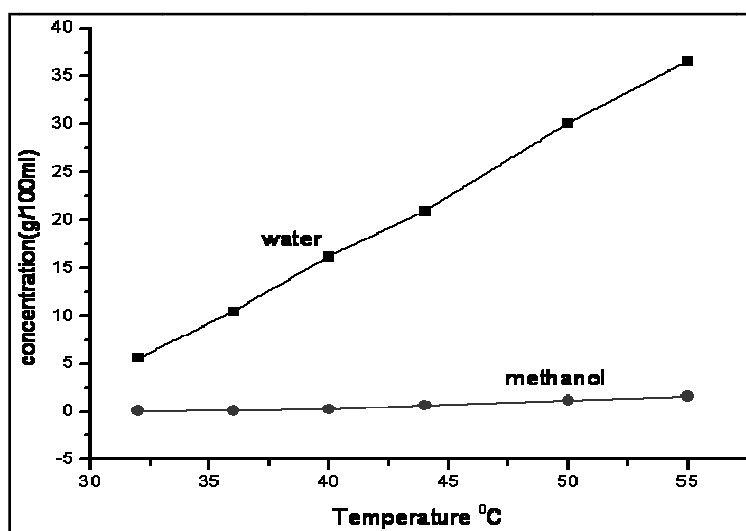
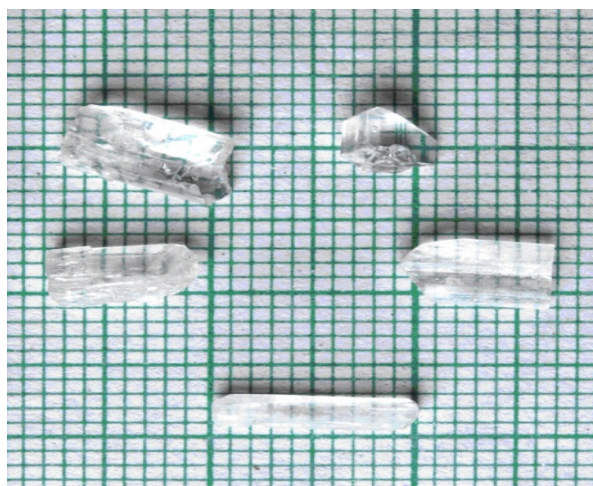


Fig: 3.1 Solubility curves for LCO in 2 different solvents

It was found that the compound has more optimum solubility for crystal growth in water than in methanol. Hence crystals were grown in an aqueous medium. Aqueous solution of the crystallized salt, L- citrulline oxalate (LCO) was prepared and seed crystals were suspended in this solution and kept for slow evaporation to get bigger good quality crystals. The purity of the crystal salt was improved by recrystallization. Transparent crystals of L-citrulline oxalate of size $10 \times 1 \times 0.8 \text{ mm}^3$ were obtained in 3 weeks time and the photograph of the grown crystals is shown in Fig: 3.2. No fungus was seen during the growth process even after an elapse of two months. The grown LCO crystals were found to have good chemical stability and did not show any degradation for several months.

L-citrulline reacts with oxalic acid forming L-citrulline oxalate monohydrate as follows



**L-CITRULLINE
OXALATE**

Fig: 3.2 Photograph of as grown L citrulline oxalate monohydrate single crystals

3.3 Characterization

3.3.1(a) CHN analysis

In order to confirm the chemical composition of the synthesized compound, CHN analysis was carried out on the recrystallized sample using the instrument Elementar Vario EL III CHNS analyzer. The CHN analysis established quantitatively the elemental composition of the synthesized salt. The empirical formula for LCO is $C_8H_{17}N_3O_8$. The experimentally and empirically determined concentrations of C, H and N agree with each other, confirming the formation of L- citrulline oxalate. The result of the CHN analysis is presented in Table 3.1.

Table 3.1 CHN analysis

Element	Experimental value	Computed value
Carbon %	33.88	33.925
Hydrogen %	6.90	6.049
Nitrogen %	14.74	14.83

3.3.1(b)EDX spectral studies

The chemical composition of a material can be determined by EDX. The EDX analysis system works as an integrated feature of a scanning electron microscope (SEM). JEOL Model JED – 2300 was used to take the EDX spectrum. The EDX spectrum is a plot of intensity verses energy of the emitted X-rays. The EDX spectrum was recorded as shown in Fig: 3.3; which confirms the elemental composition of the LCO crystal.

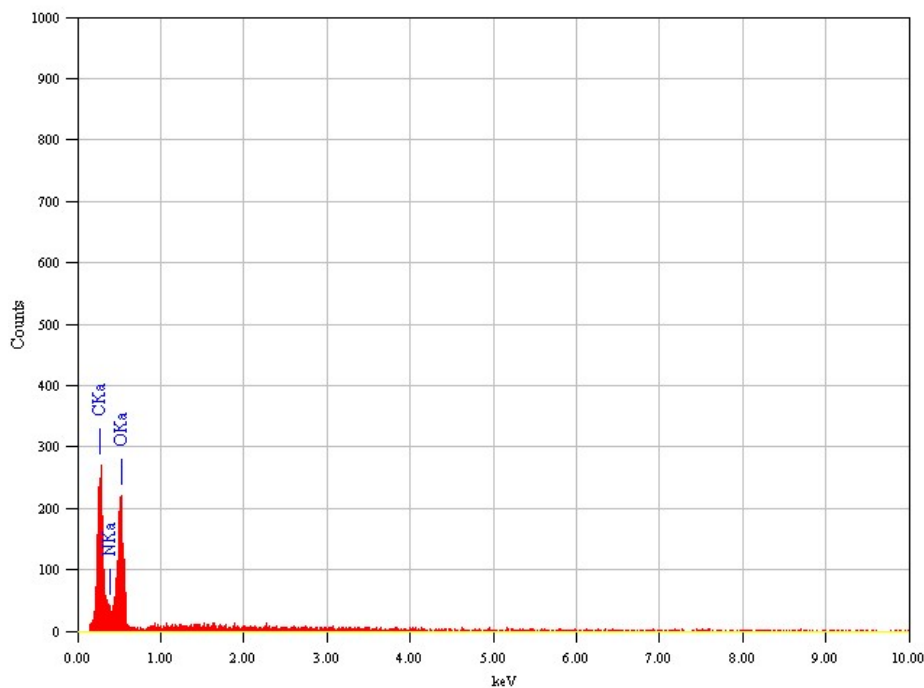


Fig: 3.3 EDX spectrum of LCO crystal

3.3.2 Single crystal X-ray diffraction

The grown single crystal of LCO was subjected to single crystal X-ray diffraction using Enraf Nonius CAD-4 and powder diffraction using Bruker AXS D8 Advance diffractometer with Cu K α radiation ($\lambda = 1.5418 \text{ \AA}$) to understand the crystal structure and morphology.

The unit cell dimensions were obtained by analyzing the single crystal X-ray diffraction data.

The structure of L-citrulline oxalate monohydrate crystal was resolved. The crystal data and refinement details are given in Table 3.2.

Table 3.2 Crystal data and structure refinement for L-citrulline oxalate

Identification code	shelxl
Empirical formula	C ₈ H ₁₇ N ₃ O ₈
Formula weight	283.25
Temperature	293(2) K
Wavelength	0.71073 Å
Crystal system, space group	Orthorhombic, P2 ₁ 2 ₁ 2 ₁
Unit cell dimensions	a = 5.208(5) Å ⁰ alpha = 90.000(5) deg. b = 9.829(5) Å ⁰ beta = 90.000(5) deg. c = 23.879(5) Å ⁰ gamma = 90.000(5) deg.
Volume	1222.4(14) (Å ⁰) ³
Z, Calculated density	4, 1.539 Mg/m ³
Absorption coefficient	0.138 mm ⁻¹
F(000)	600
Crystal size	0.3 x 0.25 x 0.21 mm
Theta range for data collection	1.71 to 34.10 deg.
Limiting indices	-7 < = h < = 8, -15 < = k < = 15, -26 < = l < = 37
Reflections collected / unique	11445 / 5025 [R(int) = 0.0223]
Completeness to theta = 25.00	100.0 %
Absorption correction	Semi-empirical from equivalents
Max. and min. transmission	0.994 and 0.854
Refinement method	Full-matrix least-squares on F ²
Data / restraints / parameters	5025 / 7 / 195
Goodness-of-fit on F ²	1.119
Final R indices [I > 2sigma(I)]	R1 = 0.0457, wR2 = 0.1079
R indices (all data)	R1 = 0.0578, wR2 = 0.1203
Absolute structure parameter	1.0(8)
Largest diff. peak and hole	0.393 and -0.226 e.Å ⁻³

The atom numbering scheme for L-citrulline oxalate is shown in Fig:3.4. The crystal structure data confirms that L-citrulline oxalate molecule behaves as a charge transfer complex with protonation of the amino acid group and deprotonation of the oxalic acid. The structure solution and refinement of the crystal at room temperature indicate orthorhombic symmetry with space group (P2₁2₁2₁).

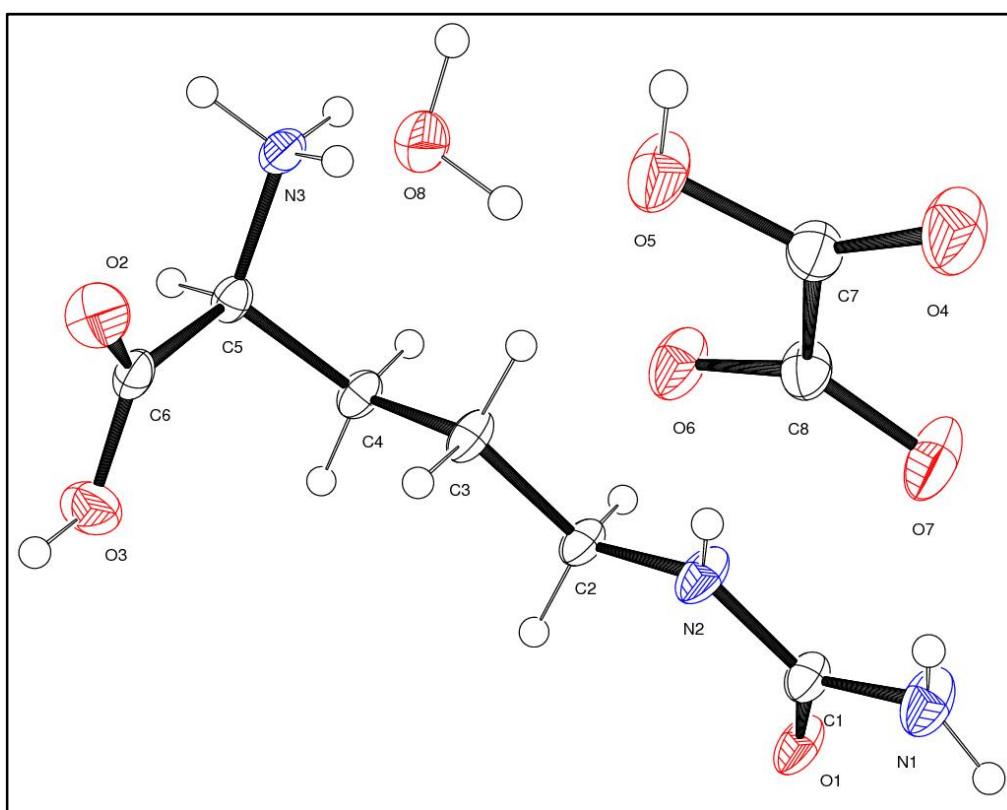


Fig: 3.4 Atom numbering scheme for L-citrulline oxalate

Table3.3 Atomic coordinates ($\times 10^4$) and equivalent isotropic displacement parameters ($\text{Å}^0)^2 \times 10^3$) for L citrulline oxalate crystal .U(eq) is defined as one third of the trace of the orthogonalized U_{ij} tensor.

Atom	x	y	z	U(eq)
C(1)	12702(3)	187(1)	6188(1)	24(1)
C(2)	10732(3)	-1915(1)	5863(1)	24(1)
C(3)	11334(3)	-3419(1)	5881(1)	26(1)
C(4)	9261(2)	-4253(1)	5595(1)	23(1)
C(5)	9915(2)	-5760(1)	5545(1)	21(1)
C(6)	12348(2)	-5996(1)	5212(1)	23(1)
C(7)	19421(3)	-3338(1)	7445(1)	26(1)
C(8)	17447(3)	-2472(1)	7115(1)	26(1)
N(1)	14479(3)	795(1)	6509(1)	36(1)
N(2)	12654(3)	-1167(1)	6182(1)	30(1)
N(3)	10227(2)	-6409(1)	6102(1)	25(1)
O(1)	11121(2)	875(1)	5910(1)	32(1)
O(2)	14146(2)	-6642(1)	5384(1)	35(1)
O(3)	12199(2)	-5404(1)	4719(1)	37(1)
O(4)	20734(3)	-2873(1)	7814(1)	45(1)
O(5)	19454(2)	-4599(1)	7273(1)	39(1)
O(6)	16017(2)	-3073(1)	6783(1)	37(1)
O(7)	17422(3)	-1223(1)	7208(1)	43(1)
O(8)	15090(3)	-5807(1)	6667(1)	35(1)

Table 3.4 Bond lengths [\AA] for L- citrulline oxalate

C(1)-O(1)	1.2550(17)
C(1)-N(2)	1.3313(18)
C(1)-N(1)	1.3422(19)
C(2)-N(2)	1.4560(19)
C(2)-C(3)	1.5111(19)
C(2)-H(2A)	0.9700
C(2)-H(2B)	0.9700
C(3)-C(4)	1.518(2)
C(3)-H(3A)	0.9700
C(3)-H(3B)	0.9700
C(4)-C(5)	1.5245(18)
C(4)-H(4A)	0.9700
C(4)-H(4B)	0.9700
C(5)-N(3)	1.4849(17)
C(5)-C(6)	1.514(2)
C(5)-H(5)	0.9800
C(6)-O(2)	1.2035(19)
C(6)-O(3)	1.3140(18)
C(7)-O(4)	1.2058(17)
C(7)-O(5)	1.3061(19)
C(7)-C(8)	1.551(2)
C(8)-O(6)	1.2376(17)
C(8)-O(7)	1.2475(18)
N(1)-H(1A)	0.849(9)
N(1)-H(1B)	0.847(9)
N(2)-H(2)	0.847(9)
N(3)-H(3C)	0.8900
N(3)-H(3E)	0.8900
N(3)-H(7C)	0.8900
O(3)-H(3)	0.8200
O(5)-H(5A)	0.8200
O(8)-H(8A)	0.848(9)
O(8)-H(8B)	0.859(9)

Table 3.5 Bond angles [deg] for L citrulline oxalate

O(1)-C(1)-N(2)	121.36(13)
O(1)-C(1)-N(1)	120.94(13)
N(2)-C(1)-N(1)	117.69(13)
N(2)-C(2)-C(3)	109.68(11)
N(2)-C(2)-H(2A)	109.7
C(3)-C(2)-H(2A)	109.7
N(2)-C(2)-H(2B)	109.7
C(3)-C(2)-H(2B)	109.7
H(2A)-C(2)-H(2B)	108.2
C(2)-C(3)-C(4)	111.62(11)
C(2)-C(3)-H(3A)	109.3
C(4)-C(3)-H(3A)	109.3
C(2)-C(3)-H(3B)	109.3
C(4)-C(3)-H(3B)	109.3
H(3A)-C(3)-H(3B)	108.0
C(3)-C(4)-C(5)	113.65(11)
C(3)-C(4)-H(4A)	108.8
C(5)-C(4)-H(4A)	108.8
C(3)-C(4)-H(4B)	108.8
C(5)-C(4)-H(4B)	108.8
H(4A)-C(4)-H(4B)	107.7
N(3)-C(5)-C(6)	108.29(11)
N(3)-C(5)-C(4)	111.79(10)
C(6)-C(5)-C(4)	112.16(10)
N(3)-C(5)-H(5)	108.2
C(6)-C(5)-H(5)	108.2
C(4)-C(5)-H(5)	108.2
O(2)-C(6)-O(3)	125.80(13)
O(2)-C(6)-C(5)	123.54(13)
O(3)-C(6)-C(5)	110.66(12)
O(4)-C(7)-O(5)	125.61(14)
O(4)-C(7)-C(8)	122.68(13)
O(5)-C(7)-C(8)	111.71(12)
O(6)-C(8)-O(7)	125.26(13)
O(6)-C(8)-C(7)	117.58(13)
O(7)-C(8)-C(7)	117.16(12)
C(1)-N(1)-H(1A)	116.7(14)
C(1)-N(1)-H(1B)	120.3(13)
H(1A)-N(1)-H(1B)	121.4(15)

C(1)-N(2)-C(2)	121.56(12)
C(1)-N(2)-H(2)	120.3(15)
C(2)-N(2)-H(2)	118.1(15)
C(5)-N(3)-H(3C)	109.5
C(5)-N(3)-H(3E)	109.5
H(3C)-N(3)-H(3E)	109.5
C(5)-N(3)-H(7C)	109.5
H(3C)-N(3)-H(7C)	109.5
H(3E)-N(3)-H(7C)	109.5
C(6)-O(3)-H(3)	109.5
C(7)-O(5)-H(5A)	109.5
H(8A)-O(8)-H(8B)	108.2(14)

Table 3.6 Anisotropic displacement parameters ($\text{\AA}^2 \times 10^3$) for LCO The anisotropic displacement factor exponent takes the form:

$$-2 \pi^2 [h^2 a^{*2} U_{11} + \dots + 2 h k a^* b^* U_{12}]$$

Atom	U11	U22	U33	U23	U13	U12
C(1)	26(1)	18(1)	29(1)	-1(1)	-4(1)	1(1)
C(2)	28(1)	15(1)	31(1)	1(1)	-4(1)	1(1)
C(3)	27(1)	15(1)	37(1)	-2(1)	-5(1)	2(1)
C(4)	20(1)	18(1)	32(1)	-1(1)	-2(1)	3(1)
C(5)	17(1)	18(1)	27(1)	-3(1)	1(1)	-1(1)
C(6)	21(1)	17(1)	31(1)	-6(1)	5(1)	-3(1)
C(7)	30(1)	24(1)	25(1)	-1(1)	-6(1)	2(1)
C(8)	29(1)	23(1)	26(1)	-3(1)	-6(1)	4(1)
N(1)	35(1)	26(1)	45(1)	-4(1)	-18(1)	0(1)
N(2)	34(1)	15(1)	41(1)	2(1)	-14(1)	3(1)
N(3)	27(1)	16(1)	31(1)	0(1)	5(1)	0(1)
O(1)	39(1)	16(1)	43(1)	0(1)	-18(1)	2(1)
O(2)	23(1)	38(1)	43(1)	1(1)	4(1)	6(1)
O(3)	36(1)	39(1)	34(1)	5(1)	11(1)	5(1)
O(4)	56(1)	36(1)	43(1)	-6(1)	-27(1)	3(1)
O(5)	50(1)	25(1)	42(1)	-5(1)	-23(1)	11(1)
O(6)	41(1)	25(1)	44(1)	-4(1)	-20(1)	3(1)
O(7)	51(1)	22(1)	55(1)	-9(1)	-26(1)	5(1)
O(8)	47(1)	28(1)	30(1)	-4(1)	-5(1)	-6(1)

Table 3.7 Hydrogen bond lengths and angles for L-citrulline oxalate [\AA and deg.].

D-H...A	d(D-H)	d(H...A)	d(D...A)	\angle (DHA)
N(3)-H(3E)...O(1)#1	0.89	1.86	2.749(2)	175.1
N(3)-H(7C)...O(8)#2	0.89	2.17	3.054(3)	170.1
O(3)-H(3)...O(1)#3	0.82	1.76	2.578(2)	172.1
O(5)-H(5A)...O(7)#4	0.82	1.79	2.5941(19)	164.9
N(1)-H(1B)...O(8)#5	0.847(9)	2.554(11)	3.376(2)	163.9(19)
O(8)-H(8A)...O(7)#6	0.848(9)	2.285(18)	3.015(2)	144(2)
N(3)-H(3C)...O(8)	0.89	2.07	2.931(3)	162.8
N(1)-H(1A)...O(7)	0.849(9)	2.180(9)	3.012(2)	167(2)
N(2)-H(2)...O(6)	0.847(9)	2.104(11)	2.938(2)	169(2)
O(8)-H(8B)...O(6)	0.859(9)	1.906(10)	2.744(2)	165(2)

3.3.3 Powder X-ray diffraction studies

The powder X-ray diffraction pattern of LCO is shown in Fig.3.5. It was recorded using Bruker D8 advance diffractometer operated at 40 kV and 50 mA, using Cu target and graphite monochromator. The intensity data was recorded by continuous scan from 5° to 60° with a step size of 0.02° and scan speed of $4^\circ/\text{minute}$. The lattice parameters obtained from the single crystal XRD were used for the simulation of hkl values corresponding to various d values. The assignment of the hkl values is displayed in Table3.8

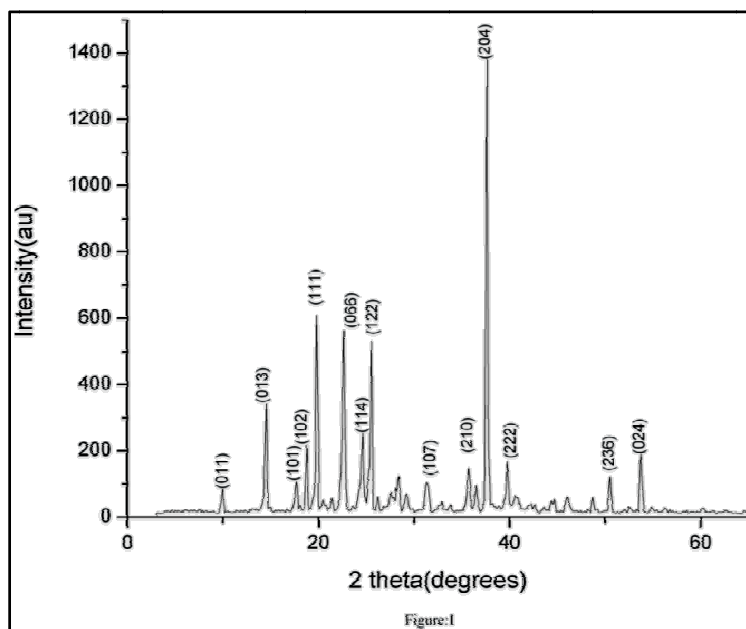


Fig: 3.5 Powder X-ray diffraction pattern of the LCO sample

Table3.8 Assignment of hkl values for the diffraction peaks

2theta	dexp	dcal	hkl
9.947	8.85	9.08	011
14.49	6.107	6.18	013
17.68	5.01	5.08	101
18.76	4.73	4.77	102
19.80	4.47	4.51	111
22.63	3.92	3.97	066
24.6	3.61	3.644	114
25.54	3.48	3.424	122
31.3	2.85	2.853	107
35.73	2.51	2.52	210
37.63	2.388	2.389	204
39.76	2.26	2.25	222
50.49	1.80	1.81	236
53.70	1.705	1.78	024

3.3.4 Vibrational assignments

Functional groups present in the LCO sample were determined from the FT-IR spectrum and confirmed using the Raman spectrum. The FTIR spectrum was recorded using the AVTAR 370 DTGS FT-IR spectrophotometer in the wave number range 400–4000 cm^{-1} . FT Raman spectrum was recorded using BRUKER RFS 100/S with a resolution of 4 cm^{-1} using standard Ge detector with Nd YAG laser.

The FT-IR spectrum of LCO is shown in Fig. 3.6 and the Raman spectrum in Fig.3.7. Different molecular groups present in LCO were identified with the vibrational frequencies of amino acids and their complexes.

Vibrational analysis of L-citrulline oxalate crystals has been done, based on the vibrations of L- citrulline ion, consisting of the amino, methylene, carboxylic acid groups and the oxalate ion. Observed bands are assigned on the basis of characteristic vibrations corresponding to various functional groups and the details are tabulated below (Table3.9).

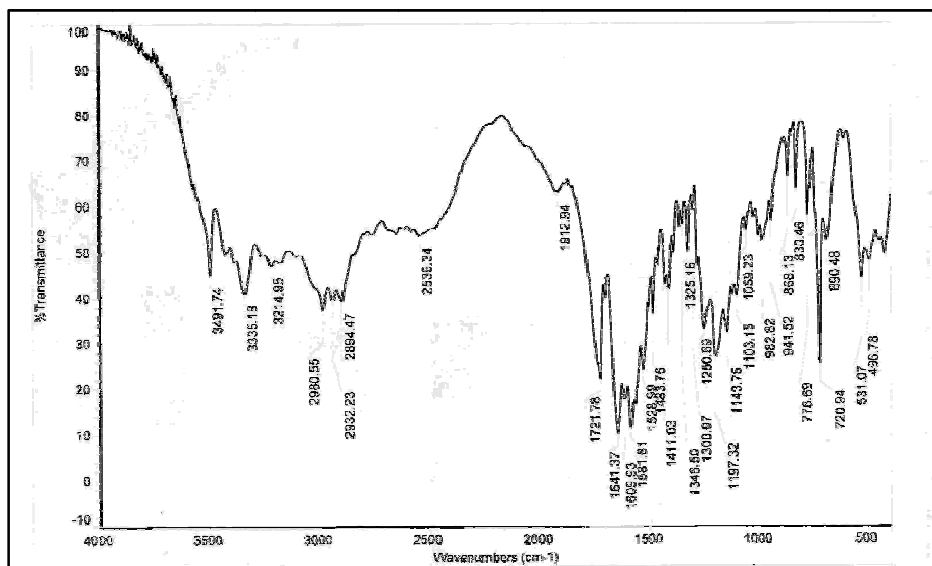


Fig: 3.6 FT-IR transmission spectrum of L-citrulline oxalate

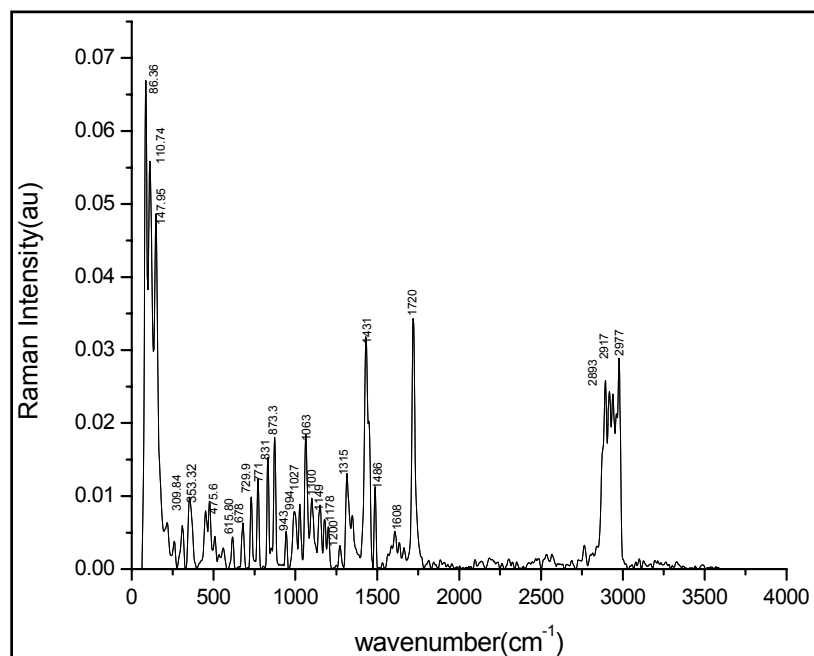


Fig. 3.7 Raman spectrum of L-citrulline oxalate

Strong infrared bands located at 3491cm^{-1} and 3335cm^{-1} are attributed to the asymmetric and symmetric vibrations of the water molecule. The corresponding Raman frequencies are very weak. The vibrational band at 3214cm^{-1} corresponds to the NH_3^+ asymmetric stretching [15, 16]. The NH_3^+ symmetric stretching occurs at 2980cm^{-1} in the IR spectrum and its Raman counterpart occurs at 2978cm^{-1} . The NH_3^+ asymmetric and symmetric bending modes occur in the region 1641cm^{-1} and 1609cm^{-1} respectively [17,18]. The NH_3^+ rocking modes occur at wave numbers around 1100cm^{-1} , similar to those in amino acids. The NH_3^+ parallel rocking modes are assigned to 1103cm^{-1} in IR and 1100cm^{-1} in Raman spectra while the perpendicular modes to 941cm^{-1} in IR and 994cm^{-1} in Raman spectra [19-22]. The IR vibrational spectral analysis establishes the existence of NH_3^+ group in the crystal, confirming the protonation of the amino group for the formation of L-citrulline oxalate. The asymmetric stretching bands at 2932cm^{-1} and 2939cm^{-1} in IR and Raman spectra respectively, and the corresponding

symmetric bands at 2894cm^{-1} and 2893cm^{-1} denote the CH_2 stretching modes for amino acids. The CH_2 rocking mode occurs at 982cm^{-1} in IR and at 994cm^{-1} in Raman spectra. The sharp intense band at 1721cm^{-1} in IR and at 1720cm^{-1} in Raman spectra correspond to $\text{C}=\text{O}$ vibrations. The observation of similar vibrational frequencies in both IR and Raman spectra confirms the non centro symmetric nature of the grown single crystals and highlights the prospects of LCO as a strong NLO material.

Table 3.9 Vibrational assignments of FTIR and FT Raman spectra for L-citrulline oxalate

Wave no (FTIR)(cm-1)	Wave no (FT Raman). (cm-1)	Assignment of vibration	Wave no (FTIR) (cm-1)	Wave no (FT Raman) (cm-1)	Assignment of vibration
3491 ssh		H_2O asymm stretching	1325 wsh	1315 msh	Wagging CH_2
3335 msh		H_2O symm stretching	1300 vw		CN vibration
3214 wb		NH_3^+ asymm str	1250 msh		Wagging NH_2
2980 sb	2978 msh	CH str	1197 ssh	1200 wsh	Rocking NH_3^+
2932 w	2939 msh	CH_2 asymmstr	1143 wsh	1149 msh	Wagging NH_2
2894 w	2893 msh	CH_2 symmstr	1103 vw	1100 msh	CN str
2539 vw		OH str	982 vw	994 msh	Rocking CH_2
1912 wb		C-C overtone	941 vw	943 wsh	O-H defor out of plane
1721 ssh	1720 ssh	C=O of carboxylate	868 msh	873 ssh	C-C str mode
1641 ssh		NH_3^+ asymm deformation	830 vsh	831 ssh	Rocking NH_2
1609 msh	1608 wb	NH_3^+ bending	776 msh	771 msh	Rocking CH_2 /scissoring mode COO^-
1581 msh		COO^- asymm	720 ssh	729 msh	Wagging NH
1528 w		NH_2 symm deformation	690 mb	678 wsh 615 wb	NH_2 out of plane bending O-H bending
1483 wsh	1486 msh	CH_2 in plane deformation	531 msh		Torsion NH_3
1411 wb	1431 sb	Ionized carboxylate symmstr	496 mb	476 mb	Rocking COO^-
1346 vw		O-CH in plane deformation			

s-strong, m-medium, w-weak, v-very, sh-sharp, b-broad, symm-symmetric, asymm-asymmetric, str-stretch

3.3.5 Thermo gravimetric analysis

Thermo gravimetric analysis (TGA) of LCO was carried out using a simultaneous thermal analyzer Q50 V20.10 TGA. A ceramic crucible was employed for heating the sample and the analysis was carried out in an atmosphere of nitrogen at a heating rate of 20°C in the temperature range 30–800°C. The thermal properties of the LCO crystals were studied by analyzing the thermo gravimetric curve shown in Fig.3.8. The crystal is highly stable up to 165°C and there after the decomposition starts. The compound starts to lose single molecules of water of crystallization around 100°C. The weight loss in this temperature range is consistent with the weight of single molecule of water present in the crystal. A second dissociation occurs at 214°C. This weight loss may be attributed to the dissociation of ammonia molecules. Decomposition of main carbon chain starts above 371°C with the evolution of carbon dioxide. This decomposition process continues up to 800°C with the removal of almost all the compounds as gaseous products.

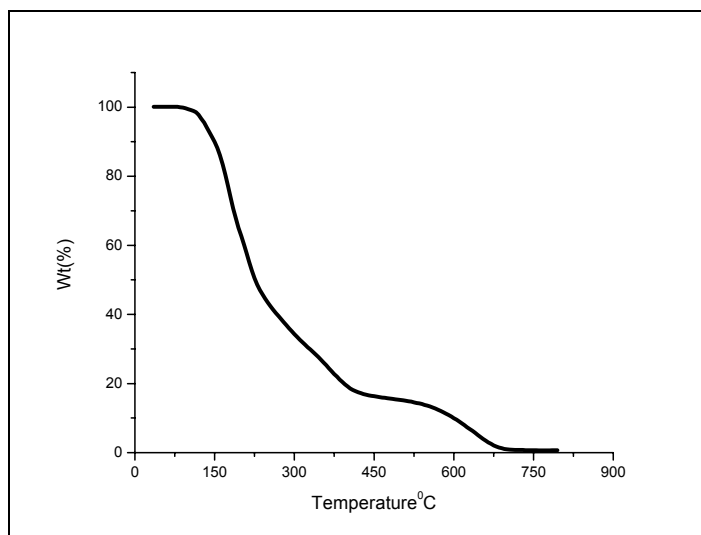


Fig: 3.8 TGA curve for LCO

3.3.6 UV-Vis Absorption Studies

The UV-Vis absorption spectrum of LCO was recorded using JASCO V570 UV-Vis spectrophotometer in the range 200- 1000 nm and the crystal is found to possess a wide transparency region from 311 nm to the far IR region as shown in Fig: 3.9(a). There is no appreciable absorption of light in the entire visible range. A plot of $(\alpha h\nu)^2$ versus $h\nu$ is shown in Fig: 3.9(b). The band gap is estimated by extrapolating the graph, which turns out to be 3.86eV.

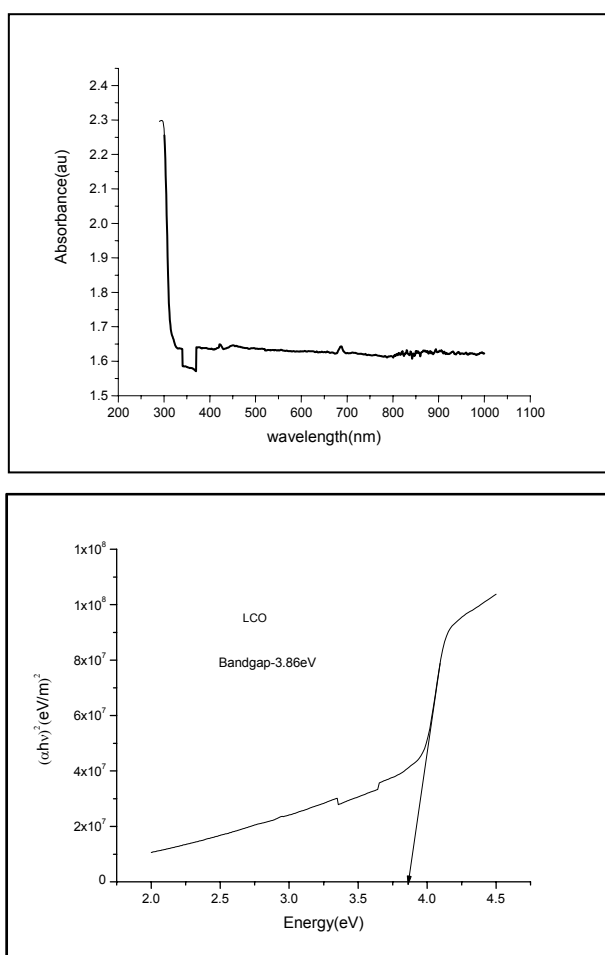


Fig: 3.9(a) UV-Vis Absorption Spectrum of LCO **Fig: 3.9(b)** Plot to determine band gap

3.3.7 Second Harmonic Generation

A prominent property of nonlinear optical crystals is generation of higher harmonics. The second harmonic generation (SHG) efficiency test was performed using Kurtz Perry technique by illuminating the crystal with pulsed Nd: YAG laser of wavelength 1064nm, pulse width 10ns and power~7.5mJ.

The grown single crystal of LCO was powdered to uniform particle size and then packed in a micro capillary of uniform bore and exposed to laser radiation. The generation of the second harmonic was confirmed by the emission of green light. A sample of potassium dihydrogen phosphate (KDP), also powdered to the same particle size as the experimental sample, was used as a reference material in the present measurement. The output voltage measured for LCO crystal was 16 mV and for reference KDP was 40mV. Thus the relative SHG efficiency of LCO crystal was calculated as 0.4 with respect to KDP.

3.3.8 Open aperture Z scan technique

The z scan technique is a method to measure the nonlinear absorption and nonlinear refraction in solids and liquids [23,24]. In the z- scan experimental set up, a laser beam with a Gaussian profile is focused using a lens. The sample is moved along the z axis. At the focal point, the sample experiences the maximum pump intensity. If a light detector is placed at the far field, the transmitted intensity can be measured as a function of the position of the sample along the z axis. As there is no aperture placed near the detector, this method is called the “open aperture z scan” method. The shape of the curve reveals the nonlinearity in the absorption, from which the nonlinear absorption coefficient can be determined.

In the present work, a mode locked Nd-YAG laser(Spectra Physics LAB-1760) of 532 nm and 7ns pulse operating at 10 Hz was used for the z scan studies. The crystal was dissolved in distilled water taken in a cuvette and placed in the sample holder, which was fixed on a microprocessor controlled translation stage of range 30cm and resolution 2 microns. Photodiodes were used to monitor the input laser energy and the transmitted beam energy. Data acquisition was carried out in real time with the help of a PC.

To analyze the data, the normalized transmission of the sample was plotted against the sample position relative to the beam focus. The plot is displayed in Fig: 3.10.

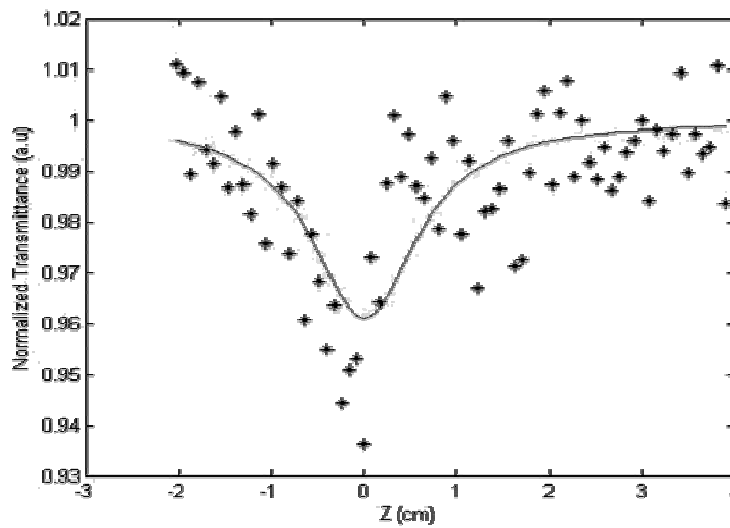


Fig: 3.10 Open aperture z scan plot of LCO

The nonlinear absorption coefficient β can be obtained from the best fitting on the experimental data with the theoretical fit. The characteristic pattern of the curve shows that the nonlinear absorption is reverse saturable absorption. The nonlinear absorption coefficient β is estimated to be

2.9×10^{-10} m/W. The experimental results confirm the presence of third order nonlinearity in the sample.

3.3.9 Dielectric studies

Dielectric studies were carried out using the impedance analyzer(4192A) for frequencies ranging from 100 Hz to megahertz. Samples of known dimension were silver coated on the opposite faces and then placed between the two copper electrodes to form the parallel plate capacitor. The dielectric constant ϵ_r can be calculated using the formula

$$\epsilon_r = Cd/\epsilon_0A \quad (3.2)$$

where C is the capacitance, d –the thickness of the dielectric medium,A area of contact and ϵ_0 ,the permittivity of free space. The plot of dielectric constant with applied frequency for L-citrulline oxalate crystal is shown in figure 3.11. The dielectric studies show that the dielectric constant decreases with increase in frequency and has a comparatively high value at very low frequencies. Quite high value of ϵ_r around 1000 observed at low frequencies in LCO may be due to the dominant presence of various polarizations arising as a consequence of the charge transfer complex nature of LCO. The low value of ϵ_r at higher frequencies may be accorded to the decay of the dominant polarizations gradually. The grown LCO crystal exists as a charge transfer complex, which contributes mostly for polarization in the direction of the applied field. As the frequency increases, a situation will be reached, where the space charges cannot sustain and comply with the external field and hence polarization decreases giving rise to diminishing values of dielectric constant. The high value of dielectric constant is found in many amino based crystal complexes like L-arginine hydrochloride monohydrate[25], bis-glycine hydrogen

chloride[26] etc. In carrier-dominated dielectric materials, the value of dielectric constant is high at low frequencies, and shows frequency dispersion due to space charge polarization.

The dielectric constant of bis- glycine hydrogen chloride is 504 at 100 Hz, and of L arginine hydrochloride monohydrate, 1200 and that of LCO crystal, 1100. The dielectric behaviour of LCO crystal is similar to most of the organic NLO crystals.

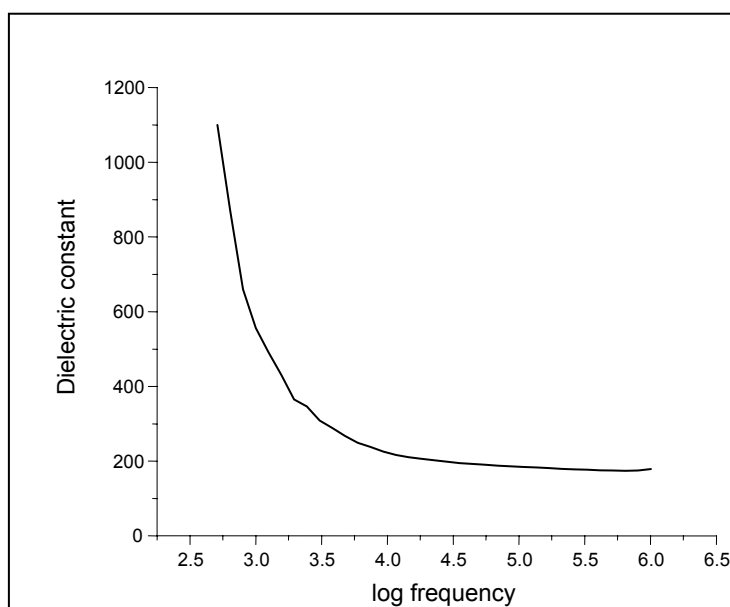


Fig: 3.11 Plot of dielectric constant Vs log frequency of LCO

3.3.10 Etching studies

Microtopographical studies on LCO crystals were carried out to look for the presence of spirals, hillocks, slip lines etc., which yield information about the growth mechanism. Chemical etching studies reveal the symmetry of the crystal faces from the shape of the pits and the distribution of structural defects. For etching studies, the crystal was immersed in the etchant (distilled

water) for 10s and then cleaned, dried and kept under the optical microscope (Magnus, model MIPS-USA, Olympus make). Micro topographical analysis reveals that the growth of the crystals is due to 2 dimensional nucleation and spreading of layers. The dislocation density was estimated to be of the order of $10^2 / \text{cm}^2$ from the microscope images. The etch patterns are displayed in Fig: 3.12. The low value of dislocation density suggests good crystalline perfection of the grown crystals and highlights the prospects for optical device applications.

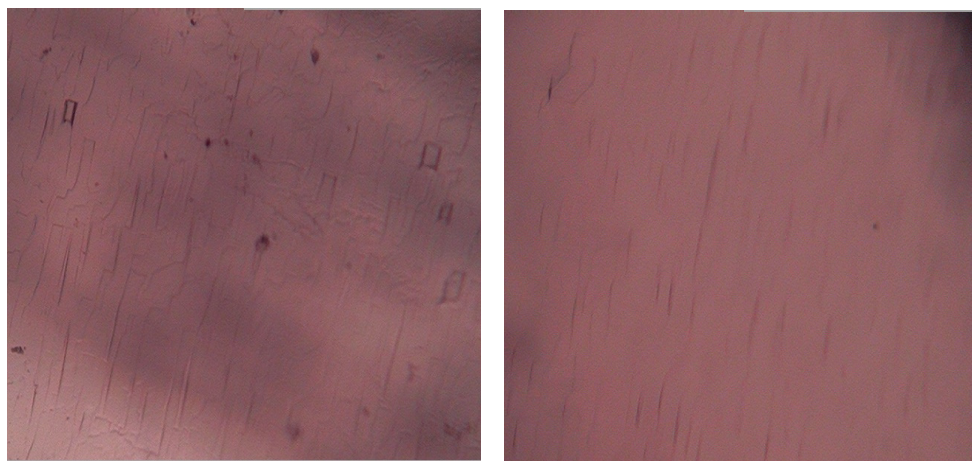


Fig: 3.12 Etch patterns of L-citrulline oxalate crystals

3.4 Comparative study with other NLO crystals

Potassium dihydrogen phosphate is a strong nonlinear optical inorganic compound with high mechanical strength, thermal stability and good transmittance in the visible region, but moderate optical nonlinearity due to lack of extended π electron delocalization.

The major disadvantage of KDP is that it is highly hygroscopic in nature. This limits its suitability for device applications. In this respect L-citrulline

oxalate (LCO) crystal stands out, as it has excellent air stability and it is not hygroscopic at all. The crystal does not degrade when exposed to air for months together. The starting materials used to grow LCO single crystals are cheap and the synthesis can be carried out at room temperature. The crystal growth is also quite cost effective and simple since it involves only slow evaporation from saturated solution. Defect free LCO crystals can be grown to quite big size by optimizing the growth conditions. The non toxicity of the crystal makes it ecofriendly.

The optical, thermal and SHG properties of some known NLO crystals are compared in Table3.10

Table-3.10 Comparison of properties of some NLO crystals

Crystal	UV cut off wavelength (nm)	Temp of decomposition (°C)	Relative SHG
Potassium dihydrogen phosphate	200	310	1
Glycinium oxalate	324	180	0.92
L- alaninium oxalate	318	196	1.2
Glycine sodium nitrate	310	198	2
L-arginine hydrochloride monohydrate	300	230	0.38
L-citrulline oxalate	311	165	0.4

Another strong semiorganic NLO crystal is L-arginine phosphate. But during the growth process it is affected with microbial contamination and coloration which in turn results in poor quality of the grown crystals. The nonlinear optical properties are consequently affected in an adverse way and the laser damage threshold gets reduced. L-citrulline oxalate is not encountered with any microbial growth even after 3 months. This favorable property makes it suitable for device applications.

The newly grown L-citrulline oxalate single crystal satisfies all the criteria for an NLO crystal such as- high solubility in organic /aqueous media, good crystal growth properties, moderate, thermal stability and mechanical strength, optical transmittance , second and third order nonlinear characteristics and non-hygroscopic nature.

Taking into account the above features; the newly grown L-citrulline oxalate single crystal seems to have prospects as an NLO crystal, suitable for device applications.

3.5 Conclusions

L-citrulline oxalate monohydrate single crystals were grown by slow evaporation technique. During the growth, no microbial contamination or discoloration was encountered. The cell parameters were determined by single crystal XRD. The compound crystallizes in a non centro symmetric space group ($P2_12_12_1$) of the orthorhombic system. It has good thermal stability up to 165°C . The crystal possesses a wide transparency region from 311nm to the far IR region and there is no appreciable absorption of light in the entire visible range. The crystal, being a charge transfer complex shows a very high value of dielectric constant of about 1000 mainly due to various polarizations. The second harmonic efficiency is found to be 0.4 times that of KDP. However it is observed that SHG efficiency can be improved to a value close to that of KDP by doping with alkali metals like lithium. This crystal showing wide transparency, significant dielectric properties and moderate thermal stability can be a potential candidate for nonlinear optical applications, once the SHG efficiency is improved to still higher values.

3.6 References

- [1] R. F. Belt, G. Gashurov, and Y. S. Liu, *Laser Focus* 10, (1985) 110.
- [2] R. S. Calark, *Photonics Spectra* 22, (1988) 135.
- [3] R. J. Gambino, *Bull. Mater. Res. Soc.* 15, (1990) 20.
- [4] N. Bloembergen, *J. Nonlinear Opt. Phys. Mater.* 15(1996)1.
- [5] D. Xu, M. Jiang and Z. Tan. *Acta Chem. Sin.* 41(1983)570.
- [6] S. B. Monaco, L. E. Davis, S. P. Velsko, F. T. Wang, D. Eimerl, A. Zalkin, *J. Crystal Growth* 112(1991) 183.
- [7] S. Haussuhl, J. Chrosch, F. Granam, E. Fiorentini, K. Recker, F. Wallrafen, *Crystallogr. Res.* 25(1990) 617.
- [8] L. N. Rashkovich, B. Yu. Shekunov, *J. Crystal Growth* 112(1991)183.
- [9] G. Ravi, K. Srinivasan, S. Anbukumar, P. Ramasamy, *J. Crystal Growth* 137 (1994) 598.
- [10] O. Angelova, V. Velikova, Ts. Kolev, V. Radomska, *Acta Crystallogr.* C52 (1996) 3252.
- [11] G. Arunmozhi, R. Jayavel, C. Subramanian, *J. Crystal Growth* 178 (1997) 387.
- [12] A. M. Petrosyan, R. P. Sukiasyan, H. A. Karapetyan, S. S. Terzyan, R. S. Feigelson, *J. Crystal Growth* 213 (2000) 103.
- [13] Y. Tanaka, M. Matsuoka, *J. Crystal Growth* 99(1990)1130.
- [14] R. Christian, *Solvents and solvent effects in organic chemistry*, VCH, New York, (1990)
- [15] J. Baran, A. J. Barnes, H. Ratajczak, *Spectrochim. Acta A*, 51, (1995) 197.
- [16] A. Novak, *Struct. Bonding* 18, (1973) 177.

- [17] N.B.Colthup, L.H.Daly, S.E. Wiberley, Introduction to Infra red and Raman Spectroscopy, Academic Press, New York, (1990).
- [18] I.Hubert Joe, G.Arulhas, P.Ramasamy, J.Cryst.Res.Technol, 29 (1994) 685.
- [19] G.Lan, H.Wang, spectrochem Acta a,469(1990)1211.
- [20] K.Machida, A.Kagayama, Y.Saito, T.Uno,Spectrochim. Acta A,33 (1977) 569.
- [21] F.R.Dollish, W.G.Fateley, F.F.Bentley, Characteristic Raman Frequencies of Organic Compounds, Wiley, New York, (1974).
- [22] B.Borut Lavrencic, V.S.Robin, Ferroelectrics, 88(1988)37.
- [23] M.Sheik-Bahae, A.A Said and E.W.Van Stryland, Opt. Lett.14 (1989) 955.
- [24] M.Sheik-Bahae,A.A Said, T.H.Wei,D.J.Hagan, E.W.Van Stryland, IEEE, J.Quantum Electron.26(1990)760.
- [25] D. Kalaiselvi, R. Mohan Kumar, and R. Jayavel Cryst. Res. Technol. 43, (2008)851
- [26] K. Ambujama, K. Rajarajan, S. Selvakumar, I. Vetha Potheherb, Ginson P. Joseph, P. Sagayaraj, Journal of Crystal Growth 286, (2006) 440.

**LITHIUM DOPED L-CITRULLINE OXALATE MONOHYDRATE
NONLINEAR OPTICAL CRYSTALS****Contents**

- 4.1 Introduction
- 4.2 Crystal Growth
- 4.3 Characterization
- 4.4 Conclusions
- 4.5 References

This chapter deals with the studies on the effect of lithium doping on the crystal properties of L-citrulline oxalate (LCO) single crystal, grown by slow evaporation technique. The Li doped crystals were characterized by X-ray powder diffraction, TGA, FTIR, Raman and UV-Vis spectroscopic techniques. The presence of lithium in Li doped LCO crystals was estimated using AES. The thermal stability, the width of the optical transparency region and the second harmonic generation efficiency are found to be considerably enhanced for the Li doped crystals, compared to the pristine crystals. Lithium doping can hence be considered as a simple and advantageous technique to improve the thermal, optical and non linear optical (NLO) properties of the LCO single crystals.

4.1 Introduction

Organic nonlinear optical (NLO) materials are of current interest owing to their wide applications in the domain of optoelectronics and photonics. Nonlinear optical crystals find applications in various fields due to their high hyperpolarizability. Amino acids are potential candidates for optical second harmonic generation (SHG) because they contain chiral carbon atoms and

crystallize in noncentro symmetric space groups. Amino acid complexes show good nonlinear response and are promising candidates for blue-green laser generation and frequency doubling applications [1-6]. Most of the organic NLO crystals are constituted by weak van der Waals bonds and hydrogen bonds. Hence, they have poor mechanical and thermal properties. Doping the organic complexes with inorganic elements affects most of the properties positively. Over the past decade, efforts have been made to characterize the structure, and NLO behavior of materials, with a view to the designing of new NLO materials with the desired characteristics. One of the most suitable models is based on the theory of anionic groups, which is based on two fundamental assumptions. The first assumption is that the anionic groups in the crystal structure are mainly responsible for the NLO properties and the observed NLO susceptibility tensor of a crystal is the geometrical superposition of the microscopic NLO susceptibilities of the anionic groups. The second one is that the microscopic second-order susceptibilities of the anionic groups can be calculated from the localized molecular orbitals of the groups, by approximation methods used in quantum chemistry. Some researchers are also of the opinion that the anion groups in the crystal are not the only entities, contributing to the nonlinearity of the crystal. The cations, especially those with large radii and changeable electron-cloud, also play some significant role in originating nonlinearity in the crystal [7].

It has been reported that SHG efficiency can be greatly enhanced by altering the molecular alignment through inclusion complexation [8]. Literature survey on lithium doped materials show that many of the inherent properties of amino acid based materials can be modified by the doping of lithium ions. Lithium is mainly selected to study the effect of cations on the nonlinearity of

crystals, because lithium exists at the upper-left of the periodic table of elements and has the strongest polarity among the metal cations.

Lithium based materials find applications in the fields of optical and acoustic devices and as photorefractive materials. Attempts to dope L-alanine with lithium [9], L-histidine acetate [10] and L-arginine acetate [11] with metals like copper and magnesium have resulted in the advancement of the NLO characteristics of the parent crystals. In the present work, doping the organic NLO crystal, L-citrulline oxalate [LCO], with lithium has been attempted and Li doped LCO single crystals showing moderate nonlinearity, have been grown by the simple slow evaporation technique. Doping the LCO crystal with lithium is found to enhance the nonlinear optical properties and improve the optical and thermal properties. The present work highlights the advantageous effects of lithium doping on the optical and nonlinear properties of L-citrulline oxalate crystals.

4.2 Crystal growth

Aqueous solutions of L-citrulline and oxalic acid were mixed in equimolar ratio to get L-citrulline oxalate (LCO) as mentioned in an earlier report [12, 13]. For growing the doped crystals, 2 mol% of lithium sulphate was added to the LCO solution. The seed crystals of both pure and lithium doped L-citrulline oxalate (LCOL) were obtained by slow evaporation of the respective solutions in doubly distilled water at ambient temperature. Good quality crystals were harvested in a period of 30 days. The photographs of the pure and Li doped LCO single crystals are shown in Fig.4.1. The crystals are found to be transparent and free from defects.

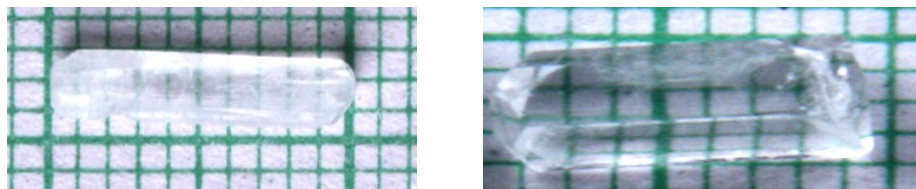


Fig: 4.1 Photographs of as grown (a) pure LCO crystals (b) Li doped LCO crystals

4.3 Characterization

The synthesized crystals were structurally characterized by powder XRD, using Bruker D8 Advance diffractometer with Cu K_{α} radiation ($\lambda = 1.5418 \text{ \AA}$). The infra red spectrum was recorded using the AVTAR 370 DTGS FT-IR spectrophotometer to analyze the bonding nature in the crystal. The Raman spectral analysis was carried out using Horiba JY Raman spectrometer. The UV-Vis-absorption spectrum was recorded using JASCO V570 UV-Vis spectrophotometer. Thermal studies were carried out using Q50 V20.10 TGA instrument in an atmosphere of nitrogen at a heating rate of 20°C in the temperature range $30\text{--}800^{\circ}\text{C}$. The atomic emission spectroscopy (AES) was used to confirm the presence of the dopant in the crystal. The second harmonic generation efficiency of the grown crystals was determined by the Kurtz Perry powder technique.

L-citrulline oxalate has already been identified as a promising organic nonlinear optical material. The work presented here reveals the influence of lithium doping on the growth and properties of LCO single crystals.

4.3.1 Powder X-ray diffraction

X-ray powder diffraction technique was used to ascertain the purity of the grown crystals. The XRD patterns of both the pure and Li doped LCO crystals are shown in Fig: 4.2.

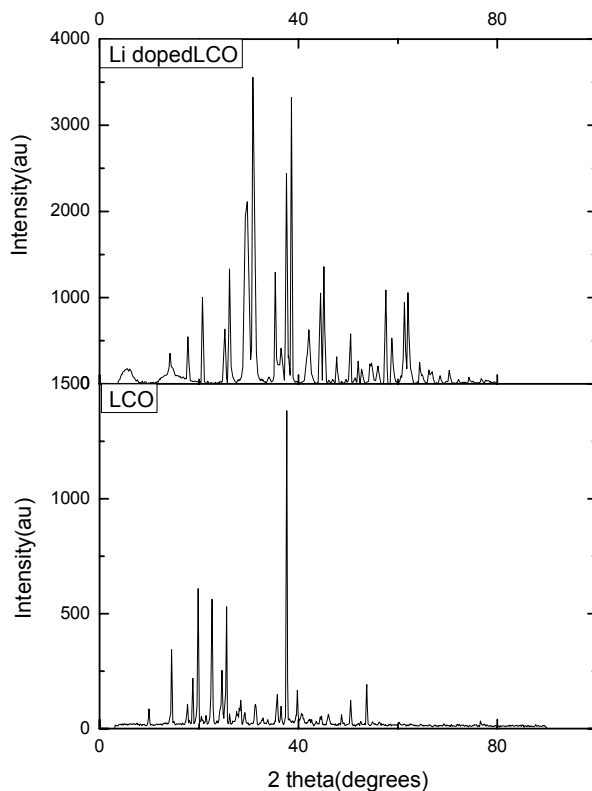


Fig: 4.2 XRD spectra of pure and lithium doped L-citrulline oxalate crystals.

From the powder X-ray diffraction data of Li doped LCO crystals, the structure of the doped LCO crystals was determined by direct method and refined by Pawley method using Topaz version with the single crystal X-ray data for pure LCO. The crystal data of LCO and Li doped LCO are presented in Table.4.1.

Table 4.1 Crystal data of pure and Li doped LCO crystals

Crystal parameters	Pure LCO	Li doped LCO
a (Å)	5.208(5)	5.196
b (Å)	9.829(5)	9.863
c (Å)	23.879(5)	23.848

It is seen that both the pure and doped crystals crystallize in orthorhombic crystal system with $P2_12_12_1$ space group. There are slight variations in the lattice parameters of the lithium doped crystal, compared to those of the pure one, due to the incorporation of Li in the LCO crystal. Lithium doped L-citrulline oxalate has the same crystal structure and comparable lattice parameters as those of LCO.

4.3.2 ICP AES analysis

The presence of lithium in the doped sample was confirmed from the inductively coupled plasma, atomic emission studies (ICPAES) using atomic emission spectrometer (IRIS INTREPID II XSP DUO). From the measurements it is found that the concentration of lithium is 6.583 ppm in the doped sample. The AES result is shown in Table.4.2, which confirms that the metallic dopant is incorporated into the crystal lattice.

Table 4.2 Data of ICP Atomic Emission studies

Sample No	Sample Name	Element Measured
		Li6707
1	Lithium doped LCO	6.583ppm

4.3.3 FT- IR and Raman spectral studies

The Fourier transform infrared (FT-IR) spectra were recorded for the pure and Li doped LCO crystals in the range $400-4000\text{cm}^{-1}$, in order to analyze qualitatively, the presence of functional groups. The recorded spectra are shown in Fig.4.3. The Raman spectra for the samples are depicted in Fig: 4.4.

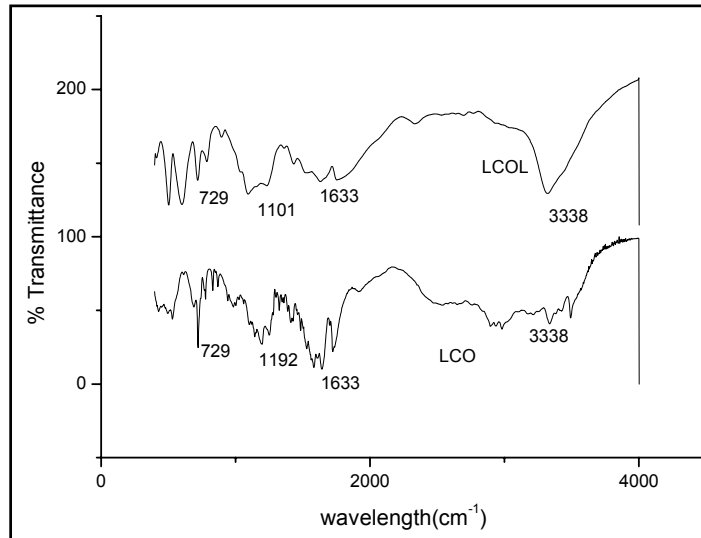


Fig: 4.3 FTIR spectra of pure LCO and lithium doped LCO(LCOL)

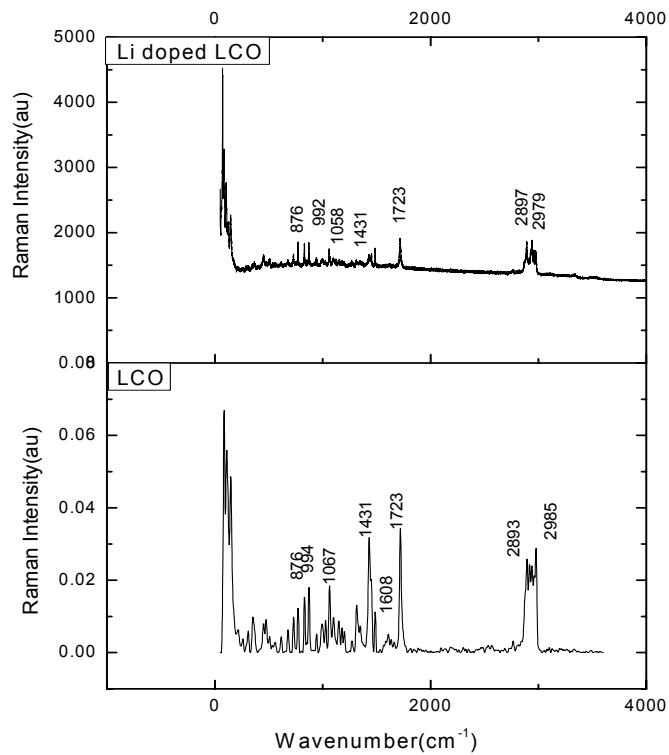


Fig: 4.4 Raman spectra of (a) pure LCO (b) Lithium doped LCO

For saturated amines, the asymmetric NH_2 stretch will give rise to a band between 3380 cm^{-1} and 3350 cm^{-1} while the symmetric stretch will appear between 3310 cm^{-1} and 3280 cm^{-1} [14]. But the protonation of NH_2 group can produce a shift in band position. In the IR spectra of the lithium doped LCO, the vibrational band at 3338 cm^{-1} corresponds to the NH_3^+ asymmetric stretching. The NH_3^+ asymmetric and symmetric bending modes occur in the region around 1633 cm^{-1} . The NH_3^+ rocking modes occur at wave numbers around 1100 cm^{-1} and the wagging NH vibrations are found around 720 cm^{-1} . FT-IR vibrational spectral analysis establishes the existence of NH_3^+ group in the crystal confirming the protonation of the amino group for the formation of pure and doped L citrulline oxalate. The IR spectrum recorded for doped crystals is similar to that of pure L-citrulline oxalate crystals and confirms the presence of all functional groups.

To analyze the presence of functional groups in the doped samples Raman spectra were also recorded for the Li doped LCO in the range $50\text{--}3500\text{ cm}^{-1}$. The NH_3^+ stretching frequencies are found between 3100 cm^{-1} and 2600 cm^{-1} in the form of a broad strong band with multiple peaks. The weak absorption band observed at 2979 cm^{-1} shows the N–H stretching of amino group. The absence of peak at 1608 cm^{-1} for C=O stretching in the Li doped–LCO may be due to the metal linkage with the carboxylic group. The NH_3^+ symmetric stretching occurs at 2985 cm^{-1} for LCO and at 2979 cm^{-1} for the doped one. The NH_3^+ parallel rocking modes are assigned to 1067 cm^{-1} for pure and to 1058 cm^{-1} for doped crystals in Raman spectra respectively. The Raman vibrational spectral analysis establishes the existence of NH_3^+ group in the crystal confirming the protonation of the amino group for the formation of L citrulline oxalate.

The asymmetric stretching bands at 2939 and 2979 cm^{-1} in Raman spectra and the corresponding symmetric bands at 2893 and 2897 cm^{-1} for the pure and doped crystals respectively denote the CH_2 stretching bands for

amino acids. The rocking CH_2 bands occur at 994 and 992 cm^{-1} and the $\text{C}=\text{O}$ vibrational bands at 1723 cm^{-1} in Raman spectra for both pure and Li doped LCO. Also it can be seen that the vibrational frequencies in both IR and Raman spectra are similar, confirming the non centro symmetric nature of the crystals, which is an essential criterion for the crystals to exhibit second order optical non linearity.

4.3.4 UV–Vis Absorption studies

The recorded absorption spectra of pure and lithium doped LCO crystals are shown in Fig: 4.5. It is seen from the spectra that absorption is not observed between 400 nm to 800 nm (visible region). The absence of absorption of light in the visible region is an intrinsic property of all the amino acids [15]. The doped LCO crystals have better transparency window in the visible region which is about 20 nm wider than that of the pure sample. It can be concluded that the lithium doping considerably improves the optical quality of L-citrulline oxalate crystals.

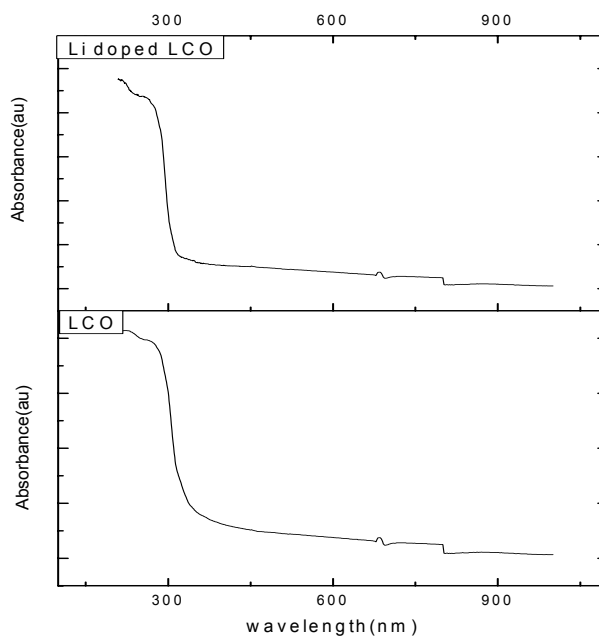


Fig: 4.5 UV-Vis absorption spectra of pure(LCO) and Li doped LCO(LCOL)

The band gap of the doped sample was determined as illustrated in Fig: 4.6. The band gap is found to be 4eV. The band gap of the doped sample has also increased showing that the transparency region has increased, compared to the undoped LCO whose band gap is 3.8eV.

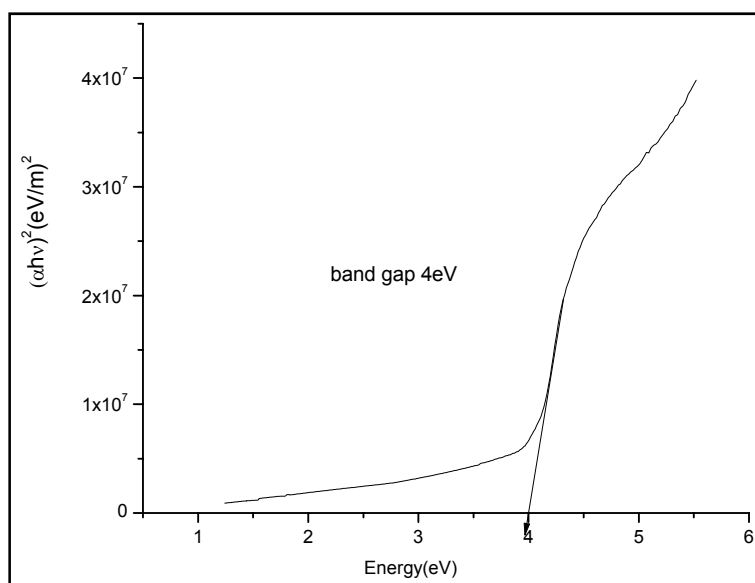


Fig: 4.6 Plot to determine the band gap of Li doped LCO

4.3.5 TGA analysis

The thermo gravimetric analysis of Li doped LCO crystals was done in nitrogen atmosphere in the temperature range 28°C – 800°C as mentioned earlier. The thermo grams of pure and Li doped LCO are shown in Fig 4.7. The decomposition of LCO begins at 165°C . But for lithium doped LCO crystals, the decomposition starts at 205°C . The compound starts to lose single molecules of water of crystallization around 100°C . The weight loss in this temperature range is consistent with the weight of single molecules of water present in the crystal. The increment in the decomposition temperature is

evident for the doped crystals, suggesting that the incorporation of lithium enhances the thermal stability.

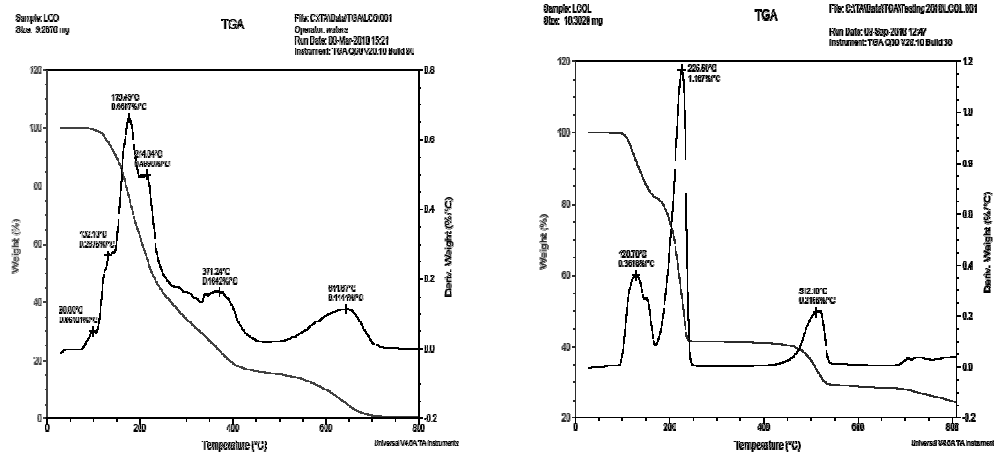


Fig. 4.7 TGA curves for (a) pure and (b) Li doped LCO crystals.

4.3.6 Second harmonic generation efficiency (SHG)

The experiment to determine the SHG efficiency of lithium doped LCO crystal was carried out using the Q-switched Nd:YAG laser as the source by the Kurtz powder technique [16]. The fundamental 1064nm beam from Q-switched Nd:YAG laser (Prolab 170 Quanta ray), pulse width 8ns, repetition rate 10 Hz) was made to fall normally on the crystalline powder, packed in a micro-capillary tube. The experiment was carried out with KDP as reference. For a laser input of 4.2 mJ, the second harmonic signal was obtained at 532 nm with an output peak signal voltage of 21 mV for Li doped LCO. The corresponding output voltage for the reference KDP was 23mV. The data is shown in Table 4.3. The SHG efficiency of doped LCO crystal is 0.9 times that of KDP. Thus, the presence of lithium has increased the SHG efficiency of pure LCO to a value almost comparable to KDP. Due to the presence of

metal like Li in the crystal lattice, there is an increase in the polarizability of the molecule which tends to increase the SHG efficiency.

Table 4.3 SHG efficiency of Li doped LCO

Material	Output (mV)
Li doped LCO	21
KDP reference	23

4.3.7 Open aperture Z scan studies

This is a standard technique to elucidate the third order non linear optical parameters. The photonic sensors have threshold intensity to electromagnetic radiation, above which they get damaged. The sensors can be made to function optimally at higher input intensities by the use of materials which act as optical limiters. The NLO parameters determine the type of applications that can be utilized for. Any NLO effect in an organic material is contributed by a strong donor-acceptor intermolecular interaction.

The open aperture z scan studies of the Li doped LCO were carried out for laser energy of 22 μ J. The Nd-YAG laser beam having a pulse width of 7 ns, a repetition rate of 10Hz, wavelength 532nm and whose spatial distribution has a Gaussian profile was used for the z scan experiment. The sample was placed on a translation stage, controlled by a computer. The laser beam was separated into two beams using a beam splitter, whose energy was measured by energy detectors. The transmittance of the samples was measured as a function of the position of the sample. Data acquisition was made possible in real time with the help of a computer. The shape of the z scan curve shown in Fig 4.8 suggests a high third order optical nonlinearity for the Li doped LCO. The nonlinear absorption coefficient β is found to be 4.9×10^{-10} m/W, which is quite high

compared to that of pure LCO crystal. Doping L citrulline oxalate with lithium has facilitated its prospects for utilization in nonlinear optical devices.

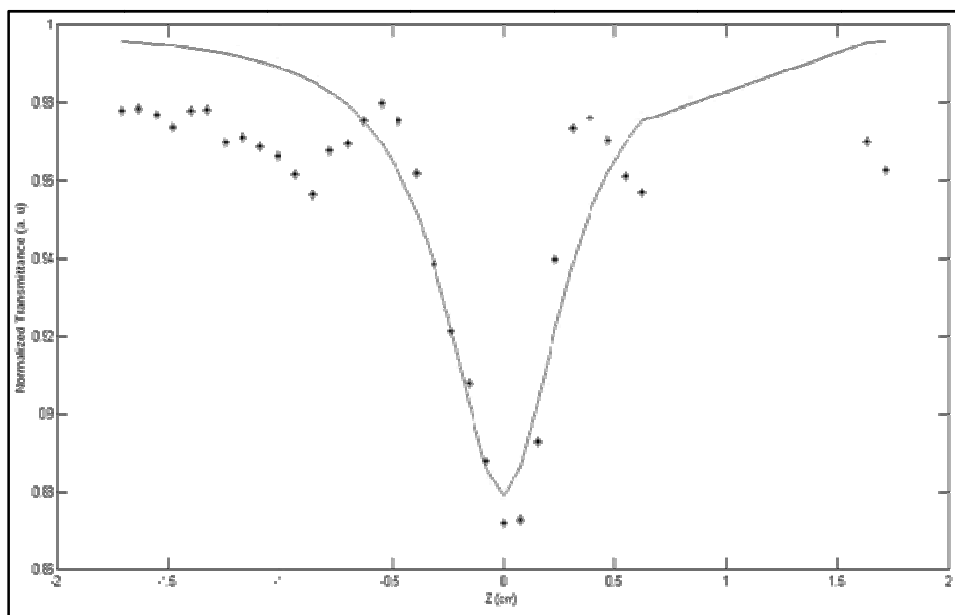


Fig: 4.8 Open aperture Z scan of Li doped LCO

4.3.8 Dielectric studies

The dielectric analysis is significant for the electro-optic properties of a crystal. Dielectric studies were carried out for Li doped LCO using the impedance analyzer (4192A) and the variation of dielectric constant is shown in Fig: 4.9. At low frequencies the dielectric constant is found to be less than that of the pristine LCO crystal. The dielectric measurements indicate that the dielectric constant decreases with increasing frequency similar to the behavior of pure LCO crystal. The lower dielectric constant value of lithium doped LCO (LCOL) indicates higher crystal perfection compared to undoped LCO. The better crystal perfection in LCOL is also evident from the higher intensity of the peaks in the powder XRD pattern.

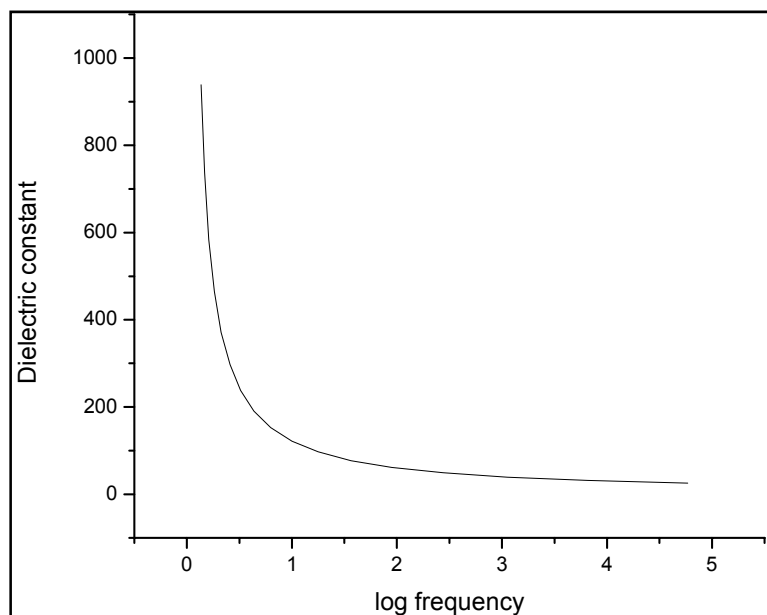


Fig: 4.9 Dielectric constant verses log frequency of LCOL

4.3.9 Etching studies

Etching reveals a host of information about the growth mechanism and defects in crystals. The micro structural aspects of the crystals influence the crystal strength and the electronic and ionic conductivity which in turn affect the performance of the devices. An approach to understand the growth mechanism is to study the patterns observed on the etched surfaces of the crystal. For the etching studies, the Li doped LCO crystal was immersed in distilled water for 10 s and viewed under an optical microscope attached to a computer, as detailed earlier. The etched patterns are shown in Fig: 4.10. From the patterns it is inferred that the growth mechanism is 2 dimensional nucleation and spreading of layers.

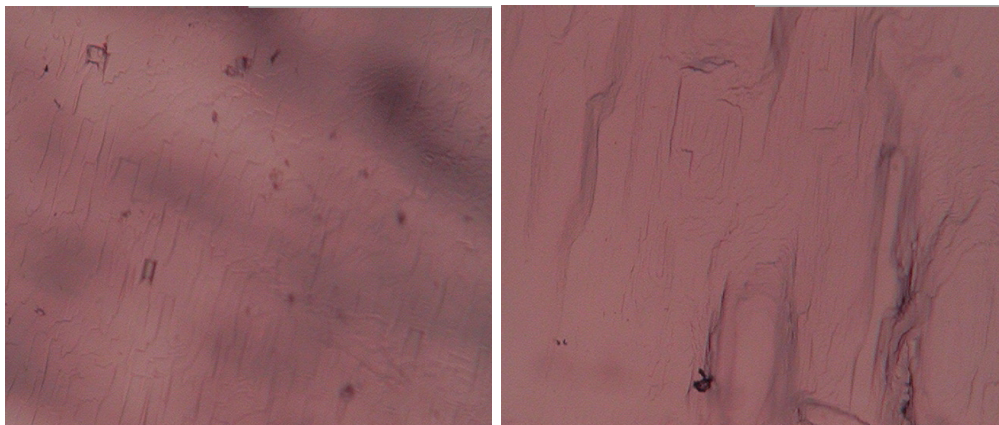


Fig: 4.10 Etch patterns of lithium doped LCO

4.4 Conclusions

Good quality, single crystals of Li doped L-citrulline oxalate (LCO) were grown successfully by slow evaporation technique. The powder XRD studies confirm the structure of the doped crystals to be similar to that of the pure one. The presence of the dopant has marginally altered the lattice parameters without affecting the basic structure of crystal. The thermal stability is found to be better for the doped samples. Also the UV absorption edge has shifted towards the blue region, increasing the transparency region from the IR to the middle of UV. The decrease in the dielectric constant of the lithium doped LCO compared to pure LCO can be attributed to better crystal perfection in the doped sample. The second harmonic generation efficiency for the doped LCO sample has increased to a great extent making the doped crystal suitable for NLO applications. The nonlinear absorption coefficient of the doped crystal is also found to be increased so that it can be used as an optical limiter as well. Good mechanical properties, excellent optical quality, moderate thermal stability and increased SHG efficiency, make the Li doped LCO crystals a strong candidate for NLO device applications.

4.5 References

- [1] R W Boyd Nonlinear optics (San Diego: Academic Press) (1992)
- [2] D S Chemla and J Zyss (eds) Nonlinear optical properties of organic molecules and crystals (New York: Academic Press) Vols 1 and 2
- [3] R. F. Belt, G. Gashurov, and Y. S. Liu, Laser Focus 10, (1985) 110.
- [4] R. S. Calark, Photonics Spectra 22, (1988) 135.
- [5] R. J. Gambino, Bull. Mater.Res. Soc. 15, (1990) 20.
- [6] G. Rameshkumar, S. Gokul Raj, R. Mohan, and R Jayavel, Cryst. Growth Des. 6, (2006) 1308.
- [7] Cheng Wendan and Lu Jiaksi, Chinese J.Struct. Chem,16(1997) 81
- [8] Ying Wang and D. F. Eaton, Chem. Phys. Lett. 120, (1985) 441.
- [9] B. Suresh Kumar, M. R. Sudarsana Kumar, and K. RajendraBabu, Cryst. Res. Technol. 43, (2008) 745.
- [10] P. Praveen Kumar, V. Manivannan, S. Tamilselvan, S. Senthil, Victor Antony Raj, P. Sagayaraj and J. Madhavan Optics communications 281, (2008) 2989.
- [11] P. Praveen Kumar, V. Manivannan,P. Sagayaraj and J. Madhavan Bull. Mater. Sci., 32, (2009) 431.
- [12] Sreevalsa, V. G.,Jayalekshmi, S.Journal of Crystal Growth, 324, (2011) 172.
- [13] Sreevalsa V. G, Jayalekshmi S .Transactions of the Indian Institute of Metals 64, 2, (2011) 205.

- [14] D.RajanBabu and D.Jayaraman, J.Crystal growth 245 , (2002) 121.
- [15] K. Ambujam, S. Selvakumar, D. PremAnand, G. Mohamed, and P. Sagayaraj, Cryst.Res. Technol. 41, (2006) 671.
- [16] S. K. Kurtz and T. T. Perry, J. Appl. Phys. 39, (1968) 3798.

EFFECT OF AMINOACID DOPING ON THE PROPERTIES OF POTASSIUM DIHYDROGEN PHOSPHATE NONLINEAR OPTICAL CRYSTALS



<i>Contents</i>	5.1 Introduction
	5.2 Crystal Growth
	5.3 Characterization
	5.4 Conclusions
	5.5 References

The studies on the effect of aminoacid doping on the crystal properties of the established nonlinear inorganic material, potassium dihydrogen phosphate (KDP), grown by the slow evaporation method, form the essence of this chapter. The structural characterization of doped KDP was done by powder X ray diffraction, FTIR and EDAX techniques. The linear and nonlinear optical characterization of these samples was carried out. The SHG efficiency has been found to be considerably enhanced for the doped KDP samples, showing that they are good nonlinear optical crystals.

5.1 Introduction

Potassium Dihydrogen Phosphate (KDP) single crystal is being considered as one of the best representatives of nonlinear optical crystals. It is used as a standard to characterize other nonlinear materials. It finds several device applications because of its good structural quality. It possesses good mechanical and piezoelectric properties as well. The crystal also has moderate

laser damage threshold and non-linear optical coefficient and is suitable for phase and amplitude modulation applications [1, 2].

The successful growth of large sized KDP crystals [3] as well as KDP crystals with additives [4] has favored the use of these crystals for device application on a large scale. Recently the development of new semi-organic non-linear optical (NLO) materials which possess the advantages of both organic and inorganic materials in terms of high thermal and mechanical stability as well as broad optical frequency range, higher second harmonic generation (SHG) efficiency and high damage threshold has attracted much research attention[5-7]. The quality of KDP crystals grown by solution methods is affected by many factors such as additives, supersaturation, pH value etc which influence the physical properties of the crystals like growth kinetics [8-11] and surface morphology of crystal faces [12-14]. The doping of KDP with suitable dopants modifies the properties positively.

Amino acids exhibit specific features of interest [15] such as

- i) molecular chirality, which attributes noncentro symmetric structure,
- ii) absence of strongly conjugated bonds, which leads to wide transparency ranges in the visible and UV spectral regions, and
- iii) zwitter ionic nature of the molecule, which favors crystal hardness for applications in devices.

Amino acids may be used as dopants in order to modify the nonlinear optical properties of inorganic materials such as KDP [16-18]. In the present work the aminoacids L-citrulline and L-lysine have been used as dopants for the growth of doped KDP single crystals by the slow evaporation technique. Studies on the growth and dielectric properties of L-lysine doped KDP crystals have been reported [19].

5.2 Crystal Growth

Potassium dihydrogen phosphate (1M) was dissolved in distilled water, to which L citrulline (.025M) was added and stirred for 2 hrs and kept for evaporation. Seed crystals were collected and grown in the supersaturated solution. Good quality crystals of L citrulline (CKDP) and L-lysine (LKDP) doped KDP crystals were harvested in 30 days and collected for characterization. No fungus was seen during the growth process even after 2 months. Crystals are found to have good chemical stability when stored at room temperature and do not have any degradation. The photographs of the grown, aminoacid doped KDP crystals are shown in Fig: 5.1(a) and (b).

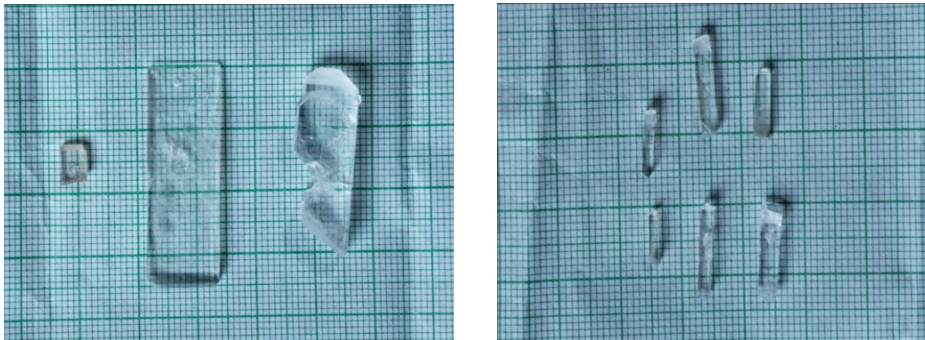


Fig: 5.1(a) Photographs of L citrulline doped KDP crystals



Fig: 5.1(b) Photographs of L-lysine doped KDP crystals

5.3 Characterisation

5.3.1 Powder XRD studies

The crystals were crushed into a fine powder and the powder X-ray diffraction studies were carried out using the Bruker D8 advance diffractometer with Cu K_{α} radiation ($\lambda = 1.5418 \text{ \AA}$). The powder XRD patterns of the doped samples are compared with that of KDP and displayed in Fig: 5.2. From the powder X-ray diffraction data, the structure of the doped KDP crystals was determined by direct method and refined by Pawley method using Topaz version program and the single crystal X-ray data for pure KDP. The crystal data of KDP and L- citrulline and L- lysine doped KDP are presented in Table.5.1.

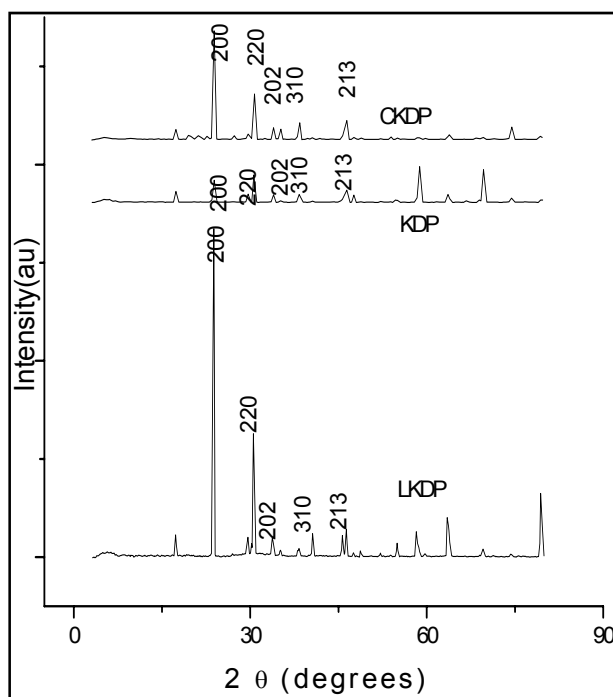


Fig: 5.2 XRD patterns of the pristine and doped KDP samples

Table.5.1. Crystal parameters of KDP and doped KDP samples

Sample	KDP	CKDP	LKDP
a	7.448(A°)	7.467(A°)	7.487(A°)
b	7.448(A°)	7.467(A°)	7.487(A°)
c	6.977(A°)	6.977(A°)	7.029(A°)
α	90°	90°	90°
β	90°	90°	90°
γ	90°	90°	90°
Crystal system / Space group	Tetragonal I42 d	Tetragonal I42 d	Tetragonal I42 d

It is seen that both the pure and doped crystals crystallize in tetragonal crystal system with I42 d space group. There are slight variations in the lattice parameters of the doped crystals, compared to the pure one, due to the incorporation of the dopants in the pristine crystal. The doped crystals have the same crystal structure as that of KDP.

5.3.2 EDX spectral studies

The chemical composition of the material can be determined by EDX. The EDX spectrum is a curve between binding energy and intensity of the emitted photoelectron. The peak heights is a measure of the quantity of the concerned elements in the specimen. To confirm the presence of the dopants in the samples, EDX spectra were recorded using integrated feature of a scanning electron microscope (SEM (JEOL Model JED – 2300)) and are shown in Fig:5.3. The main components of aminoacids like carbon and oxygen are present in the EDX spectrum, showing the effectiveness of doping.

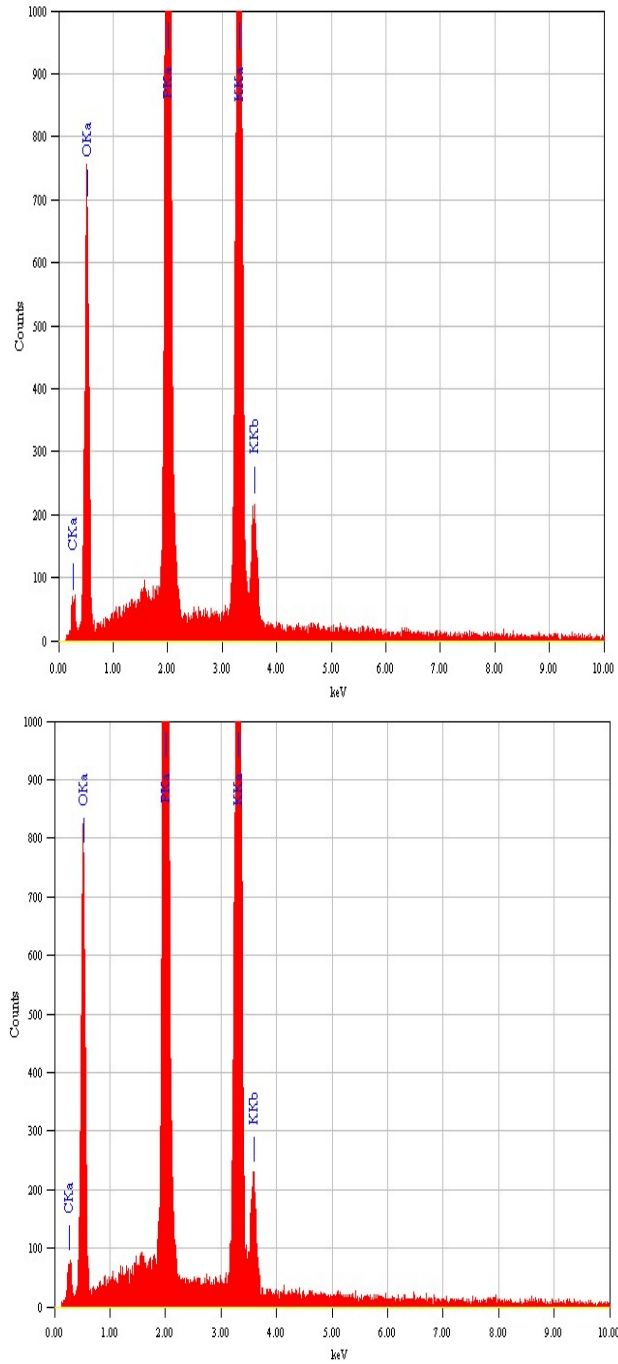


Fig: 5.3 EDX spectrum of (a) L- citrulline doped KDP (b) L- lysine doped KDP

5.3.3 FTIR spectral studies

The FTIR spectra of pure and doped KDP samples were recorded to study the vibrational assignments of the different bonds associated with the samples. The FTIR spectra are portrayed in Fig: 5.4 and the corresponding vibrational assignments are displayed in Table5.2.

The O-H stretching vibration of hydrogen bond for CKDP is at 3319 cm^{-1} , and for LKDP at 3402 cm^{-1} . P-O-H asymmetric stretching occurs at 2950 cm^{-1} for CKDP and at 2755 cm^{-1} for LKDP. N-H bending mode corresponds to 1623 cm^{-1} for CKDP and to 1621 cm^{-1} for LKDP. P=O stretching vibrations are found at 1313 cm^{-1} and at 1096 cm^{-1} for CKDP and at 1303 cm^{-1} and 1099 cm^{-1} for LKDP respectively. The rocking NH_2 mode occurs at 895 cm^{-1} for CKDP and at 904 cm^{-1} for LKDP. On comparing the FTIR data of the doped KDP samples with that of pure KDP, it is observed that there are no significant changes in characteristic group frequency peak positions. Broad bands corresponding to the aminoacid group vibrations are observed around $3300/3400\text{ cm}^{-1}$ in both the doped KDP samples. This gives further confirmation that the aminoacid doping of the KDP crystals has been quite effective.

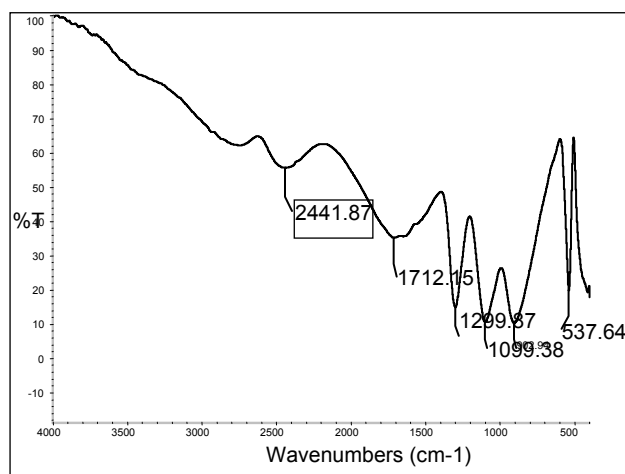


Fig: 5.4(a) FTIR spectrum of KDP

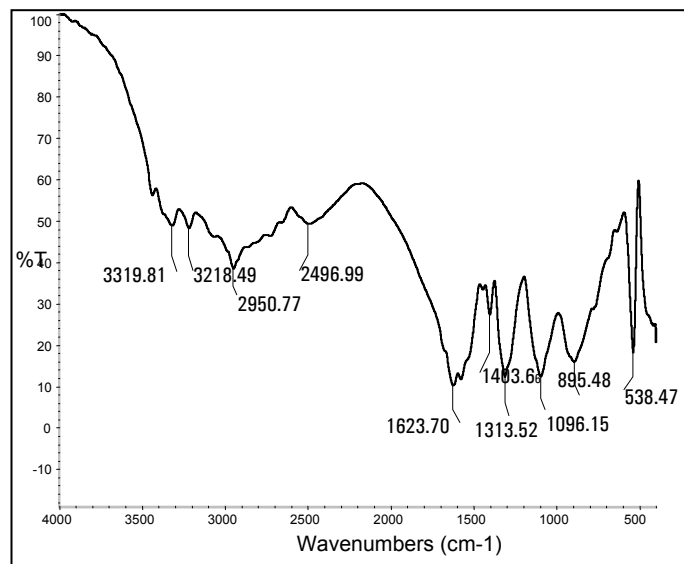


Fig: 5.4(b) FTIR spectrum of L- citrulline doped KDP

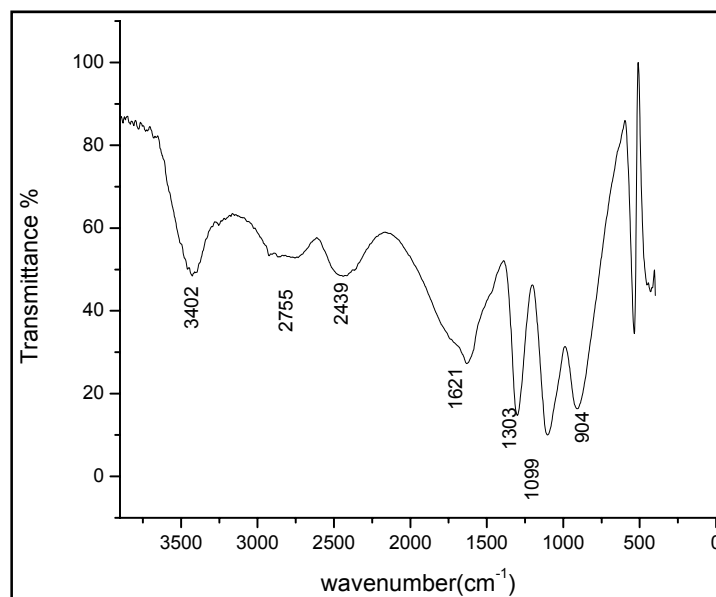


Fig: 5.4(c) FTIR spectrum of L- lysine doped KDP

Table 5.2 Vibrational assignments of the doped samples

Wavenumber (cm ⁻¹) CKDP/LKDP	Vibrational assignments
3319/3402	O-H Stretching of Hydrogen bond
2950/2755	P-O-H asymmetric stretching
2496/2439	O P - OH stretching
1623/1621	N-H Bending of the aminoacid
1313/1303	P=O stretch
1096/1099	P-OH stretching
895/904	Rocking NH ₂

5.3.4 UV-Vis absorption spectral studies

For optical device applications, the crystal should possess a wide transparency region. The absorption spectra of the doped samples were recorded and the spectra are shown in Fig: 5.5. Both the doped crystals are found to be transparent in the entire visible region. The crystal has low absorption in the visible and NIR regions and high absorption in the UV region.

For optical transitions, $\alpha h\nu = A (\alpha h\nu - E_g)^n$ where ν is the frequency of the incident photons, h , the Planck's constant, A and B are constants and E_g is the optical energy gap and $n=1/2$ for direct allowed transition. The band gap of the doped samples is determined by plotting the energy along the X axis and $(\alpha h\nu)^2$ along the y axis as shown in the Fig:5.6, where α is the absorption coefficient and $h\nu$ the photon energy. When the straight portion of the graph

of $(\alpha h\nu)^2$ against $h\nu$ is extrapolated to $\alpha=0$, the intercept gives the band gap. The band gap for CKDP is 4.85eV and for LKDP, 4.1eV.

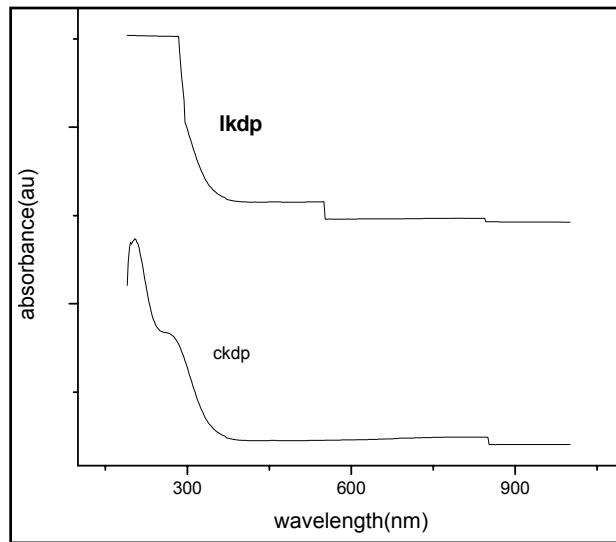


Fig: 5.5 UV-Vis absorption spectra of doped KDP samples

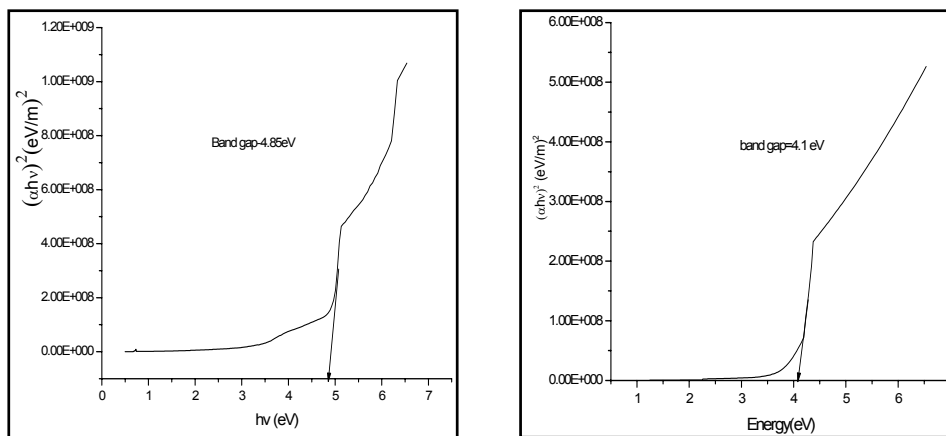


Fig: 5.6 Plots to determine the band gap of (a)CKDP (b) LKDP

5.3.5 TGA studies

The thermal properties were studied using the thermal analyzer as explained earlier and from the thermo grams shown in Fig: 5.7, it is seen that the L- citrulline doped KDP is stable upto 225°C while L- lysine doped KDP is stable up to 221°C . The degradation temperature of pure KDP is 215°C . Doping has increased the thermal stability compared to that of pristine crystal. The good thermal stability establishes the prospects of the use of these crystals in laser applications.

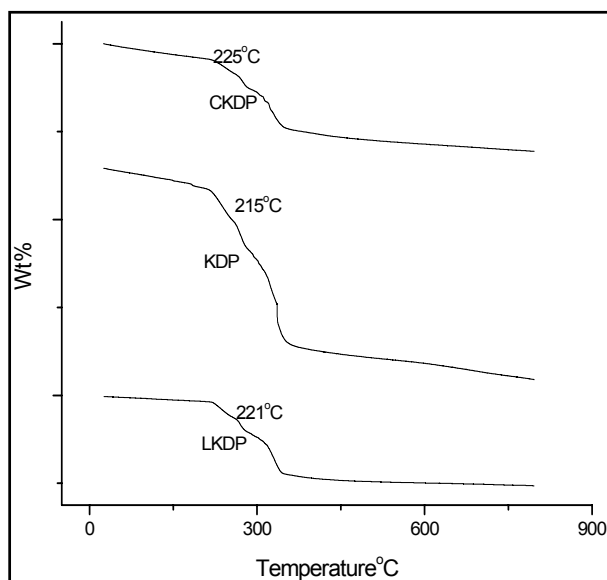


Fig: 5.7 TGA graphs of the samples

5.3.6 Studies on Second harmonic generation efficiency

The second harmonic generation efficiency of the doped samples was determined by Kurtz powder technique using Nd: YAG Q-switched laser source. For a laser input power of 4.2 mJ, the second harmonic signal was obtained at 532 nm for both the samples. The measured output voltages are

shown in Table 5.3. The SHG efficiency of CKDP is found to be 2.2 times that of KDP and that of LKDP is 1.3 times that of KDP. Doping of KDP with aminoacids has enhanced the second harmonic generation efficiency significantly.

Table 5.3 SHG efficiency of CKDP and LKDP

Sample	SHG output (mV)
CKDP	51
LKDP	32
KDP(ref)	23

5.3.7 Z scan studies

The nonlinear optical properties can be well studied by the open aperture z scan technique. In the present work, a Q switched Nd-YAG laser (532nm, 7ns, 10Hz) was used as the light source. The sample was moved in the direction of light. The transmitted beam energy, reference beam energy and their ratio were measured simultaneously by an energy meter. The plot of the transmittance verses z axis in open aperture z scan technique is shown in Fig: 5.8. The open aperture curve exhibits a normalized transmittance valley. The nonlinear absorption coefficient β was obtained by theoretical fitting for two photon absorption. β is found to be equal to 9.7×10^{-10} m/W for CKDP and equal to 4×10^{-10} m/W for LKDP. It is inferred that doping KDP with L-citrulline and L-lysine has enhanced the third order nonlinearity considerably.

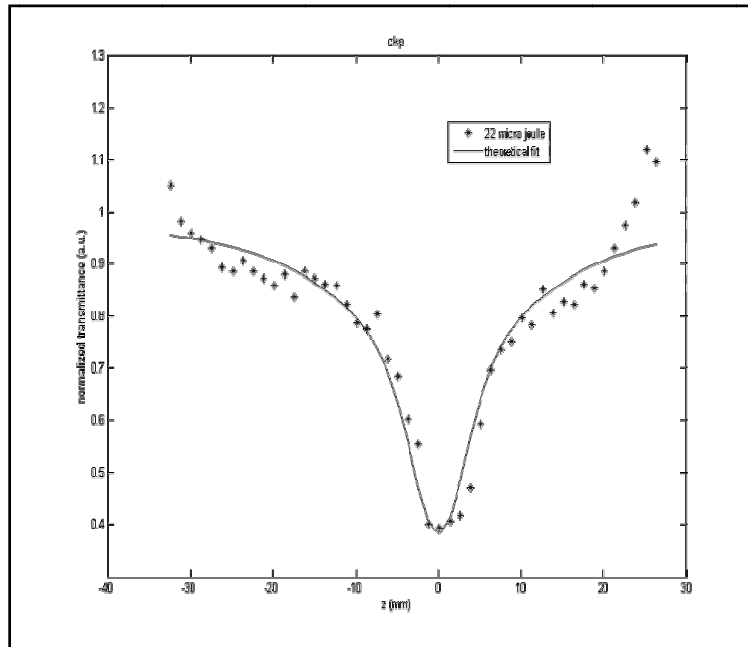


Fig: 5.8(a) Open aperture Z scan curve for CKDP

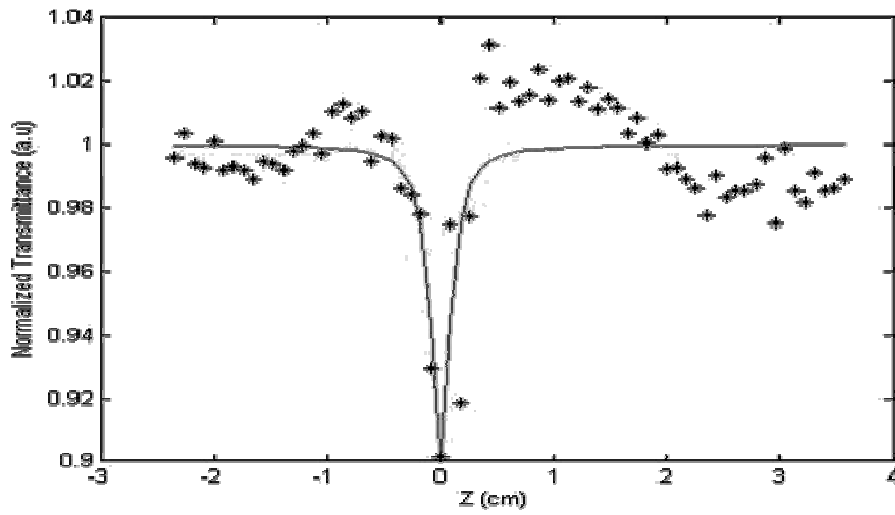


Fig: 5.8(b) Open aperture Z scan curve for LKDP

5.3.8 Etching studies

Etching is the selective dissolution of the crystal which reveals the crystal symmetry and lattice defects. Considerable information on the growth process and growth mechanism of the crystal can be had from the patterns observed on surfaces like spirals, hillocks and step patterns. When a crystal surface is etched, well defined etch patterns are produced at the dislocation sites. The etching studies were carried out on the (1 0 0) plane of the single crystals of L- citrulline doped KDP and L lysine doped KDP using demonized water as the etchant at room temperature for an etching time of 5s. The crystal sample was completely immersed in the etchant and then the etched sample was cleaned using a tissue paper and the etch patterns were observed using an optical microscope in the reflection mode. Well defined etch pits were observed. The etch patterns are depicted in Fig: 5.9. It is seen that the growth mechanism is 2dimensional nucleation.



Fig: 5.9 Etch patterns of (a) CKDP (b) LKDP

5.4 Conclusions

Good quality nonlinear optical crystals of KDP, doped with L-citrulline and L-lysine have been grown by slow evaporation technique. The crystals have been characterized by powder XRD, EDX, FTIR, UV-Vis absorption spectral analysis, SHG, open aperture z scan and etching studies. Doping of KDP by the aminoacids has positively enhanced the optical properties. The doping has increased the SHG efficiency of the KDP crystals to a large extent, highlighting the prospects of aminoacid doped KDP for applications in higher harmonic frequency generation.

5.5 References

- [1] A. K. Ghatak and K. Thyagarajan, *Optical Electronics* (Cambridge Uni. Press, Cambridge, (1989) 462
- [2] S. S. Jha, *Perspective of Optoelectronics* (World Scientific, (1995) 658 .
- [3] N. P. Zaitseva, J. J. De Yoreo, M. R. Dehaven, R. L. Vital, K. E. Montgomery, M. Richardson, and L. J. Atherton, *J. Cryst. Growth* 180, (1997) 255.
- [4] G. Li, G. Su, X. Zhuang, Z. Li, and Y. He, *J. Cryst. Growth* 269, (2004) 443.
- [5] L. F. Warren, *Soc. Adv. Mater. Proc. Eng.* 4, (1990) 388.
- [6] D. Xu, M. Jiang, and Z. Tan, *Acta Chem. Sinica* 41, (1983) 570.
- [7] A. Yokotani, T. Sasaki, K. Yoshida, and S. Nakai, *J. Appl. Phys. Lett.* 55, (1989) 2692.
- [8] J. W. Mullin, *Crystallization*, 3rd Edition (Butterworth Heinemann, London, (1993) 255.

- [9] L. N. Rashkovich, *KDP Family of Single Crystals*, Adam Hilger, New York, (1991).
- [10] K. Sangwal, *J. Cryst. Growth* 242, (2002) 215.
- [11] V. Kannan, R. Bairava Ganesh, R. Sathylakshmi, N. P. Rajesh, and P. Ramasamy, *Cryst. Res. Technol.* 41, (2006) 678.
- [12] I. Owczarek and K. Sangwal, *J. Cryst. Growth* 102, (1990) 574.
- [13] V. I. Bredikhin, V. P. Ershov, V. V. Korolikhin, and V. N. Lizyakina, *Kristallografiya* 32, (1987) 214.
- [14] L. N. Rashkovich, N. V. Kronskey, *J. Cryst. Growth* 182, (1997) 434.
- [15] J. F. Nicoud and R. J. Twieg (Eds.), *In Non-Linear optical properties of Organic Molecules & Crystals Vol. 1*, Edited by D. S. Chemla and J. Zyss (Academic Press, London, 1987) 277.
- [16] K. D. Parikh, D. J. Dave, B. B. Parekh, and M. J. Joshi, *Bull Mat Sci*, vol. 30, 2, (2007) 105.
- [17] K. D. Parikh, D. J. Dave, B. B. Parekh, and M. J. Joshi, *Cryst Res and Technol.* 45, 6, (2010) 603
- [18] B. S. Kumar and K. R. Babu, *Ind J of Pure and Appl Phy.*, 46, 2, (2008) 123.
- [19] N. Kangathara, G. Anbalagan, *Int J Opt.* 2012 (2012) 1.

STUDIES ON AMINO ACID CAPPED ZINC OXIDE NANOCRYSTALS



Contents

- 6.1 Introduction
- 6.2 Nanomaterials
- 6.3 Objectives of the present work
- 6.4 Studies on various amino acid capped ZnO
- 6.5 Characterization of capped ZnO with L-histidine in various molar ratios
- 6.6 Studies of L-histidine capped ZnO by varying the molarity of NaOH
- 6.7 Nanocomposite films
- 6.8 Studies on L-histidine tartrate capped ZnO/PVA nano composite films
- 6.9 Conclusions
- 6.10 References

Zinc oxide nanocrystals capped with different aminoacids and their complexes are synthesized and the suitability of these capped nanocrystals for optoelectronic and biological applications is investigated. The details of these studies form the essence of this chapter.

6.1 Introduction

Nanotechnology is the buzz word of the present millennium. It is a very diverse field, with a vast range of applications in medicine, electronics, biomaterials, energy production etc. New materials are developed by controlling matter at the atomic scale which has at least one of the dimensions in nano scale, where quantum mechanical effects are predominant. The first step towards the concepts found in 'nano-technology' was the words "There's Plenty of Room at the Bottom", in a talk given by the great physicist Richard Feynman at an American Physical Society meeting at California Institute of Technology on December 29, 1959.

Nano science has been a fascinating area of research for material scientists for the last 2 decades due to the intriguing properties exhibited by nano particles. Nanotechnology is evident in nature and its resources. A thorough knowledge of molecular machinery is necessary for implementing nature's ways and this when applied to matter results in functional materials. Nanostructured materials exhibit unique properties which are size dependent and quite different from their bulk counterparts. Nanostructuring often leads to improvements in mechanical, electrical and optical properties. The tremendous progress achieved in material processing has revolutionized the fields of opto electronics and integrated optics which in turn has resulted in breakthroughs in the domain of nanotechnology.

A number of physical phenomena become pronounced as the size of the system decreases. These include statistical mechanical effects, as well as quantum mechanical effects. The quantum effect is not prominent when going from macro to micro dimensions. However, quantum effects become dominant when the nanometer size range is reached, typically at distances of 100 nanometers or less, the so called 'quantum realm'. Consequently many of the physical and chemical properties change, compared to the macroscopic systems.

6.2 Nanomaterials

Nano materials are materials having nanoscale in at least one of the dimensions. A host of routes has been identified for the synthesis of nanomaterials. A variety of interesting nanostructured materials including carbon nanotubes, fullerenes, graphenes and different types of nanorods, nanoribbons and quantum dot structures can be synthesized with tailor made

properties. Nanostructured materials find wide applications in almost all branches of science and technology.

6.2.1 Semiconductor nanocrystals or quantum dots

Quantum dots are zero dimensional structures with quantum confinement in all dimensions. The first set of quantum dots synthesized dates probably, many hundred years ago, when colored glass was prepared by mixing zinc sulfide and zinc selenide with the glass material. Quantum dots grown in glass matrix at high temperature [1, 2], inorganic glass fabrication at ambient temperature known as sol-gel technique are various techniques of growing nanostructured materials. [3, 4]. Besides the growth of nanocrystals in glass matrix, synthesis of semiconductor nanocrystals by wet chemical route is presently one of the most preferred techniques [5-7].

Nanocrystals are clusters of discrete number of atoms. Information about excitonic transitions and local field effects are envisaged by the nonlinear interaction of light with nanocrystals. In semiconductors, the formation of an electron-hole pair called an exciton is by the local excitation of an electron through optical absorption process. In low dimensional structures, the coulomb effects or the excitonic effects become more prominent than in bulk structures, leading to unique optical properties, as a result of confinement effects.

In semiconductors, quantum confinement describes the confinement of the excitons within the physical boundaries. The exciton Bohr radius (a_B) is often used as a meter-stick to judge the extent of confinement in a low dimensional structure. Quantum confinement effects arise as soon as the dimension of the nanocrystals (D) becomes comparable to the Bohr radius of

the exciton wave function a_B , leading to significant changes in the electronic and optical properties. Hence depending on the size of the nanocrystals formed, three different regimes of quantum confinement can be realized

1. Strongly-confined regime: $D < 2 a_B$
2. Intermediate- confined regime: $D \sim 2 a_B$
3. Weakly- confined regime : $D > 2 a_B$

In the strongly-confined regime, the optical properties of the quantum dots are most affected by a marked blue shift of the optical absorption edge with reduction in size of the nanocrystals [8-10]. This leads to an exciting area of research, finding technological applications, where properties can be tuned just by tailoring the size of the nanocrystals.

Chemically synthesized nanostructures show exotic properties and the properties can also be tailored according to the requirements. The prerequisite for knowing the three dimensional confinement effects in semiconductors is understanding the growth process. The growth of nanocrystals is by thermodynamic nucleation followed by diffusion in the surroundings of the nanoclusters.

Wide band gap, II-VI compounds, characterized by direct bandgap with either zinc blend or wurtzite structures and large exciton binding energy are attractive from the scientific point of view, among which zinc oxide (ZnO) plays a dominant role from the point of view of device application.

Nanotechnology has provided a new arena to use the potential of ZnO. Some of the significant characteristics of ZnO include, the wurtzite structure with lattice parameters $a=3.25\text{\AA}$, $c=5.12\text{\AA}$, the direct band gap of 3.37 eV,

the high, room temperature exciton binding energy of 60 meV and specific heat around 40.3J/mol/K. Nano sized ZnO has revolutionized present day technology and has become a part and parcel of everyday life.

The optical properties of semiconductors are influenced by the energy band structure and lattice dynamics. The nanoparticles also exhibit a change in their electronic properties depending on the size of the particles. The studies on the size dependent optical properties also have attracted much attention during the last decades. The absorption spectrum of nanosized semiconductors is characterized by a sharp band edge followed by a series of excitonic states. The spectral position of the absorption peaks gets shifted to higher energies as the size of the particle decreases.

Of late, much advances have taken place in the application of quantum dots in biotechnology. The study of biological systems by imaging via engineering of the optical properties of many materials such as colloidal dispersions, quantum dots (QD) etc is of high relevance in the nanobiotechnology regime. New classes of imaging probes based on nanometer sized photo luminescent nanoparticles showing attractive photo physical properties have been explored [11,12]. Photo stable fluorescence quantum dots are found to replace organic dyes for fluorescent biological labeling [13]. Nano structured materials with tailor made properties used as biolabels have caught attraction recently [14-16]. Semiconductor quantum dots due to their unique absorption and size dependent emission characteristics are significant as promising nanoparticle imaging agents [17-22].

Many labeling experiments can be performed with luminescent nanocrystals which are not possible with organic dyes [23]. Biomarkers which

are more biocompatible and photostable can be realized by the bio conjugation of quantum dots with antibodies and can be used as probes to monitor cellular functions [24,25]. This has led to the development of water soluble and biocompatible quantum dots that find applications as fluorescent based bioimaging materials[26,27]. To make the quantum dots biocompatible, proper surface modification and conjugation with biomolecules have to be made. The bio conjugation represents the attachment of biomolecules (*e.g.*, proteins, antibodies, peptides, DNA) to the nanoparticle surfaces. As the size of these nanoparticles does not exceed the size of the biomolecules, interfacing of the quantum dots and the biological materials, for targeting to biological systems such as cells and tissues is easily achieved. To achieve biocompatibility, hydrophilic surface coatings leading to colloidal stability, having very low toxicity should be identified.

The influence of surface modifications on ZnO nanoparticles using coatings such as silica (SiO₂) and poly methyl acrylic acid (PMAA) [28] has been studied. By capping with biocompatible materials such as amino acids, chitosan [29] etc, it is possible to tailor the optical properties for suitable applications in biological systems.

Zinc Oxide (ZnO) is a wide band gap material with unique properties and extensive applications in photonics and optoelectronics [30-32]. Research on colloidal ZnO nanoparticles began in late 1980s, when Koch et al. [33] and Bahnemann et al. [34], used the colloidal method to prepare ZnO nanoparticles by hydrolyzing zinc salts in basic alcoholic solutions. Since then, this route has been widely adopted to prepare ZnO nanoparticles [35–36]. ZnO based nano structures hold a host of applications as field emission sources, flat screen displays, biological sensors, UV light emitters and switches [37].

Formation of pure and stable ZnO colloidal crystals with controlled size and less agglomeration, especially for bio imaging applications is a major challenge nowadays. The size as well as the colloidal stability can be controlled by using suitable capping agents. The synthesis of ZnO nano crystals using suitable capping agents with the perspective of biological applications has not been studied widely. Recently Kshirsagar et al [38] have reported the luminescent studies on sodium doped ZnO quantum dots synthesized through electro chemical route with polymer based capping agent. The effect of magnesium doping on the luminescence properties of ZnO has also been widely studied[39]. Amino acid ligands such as histidine and cysteine have been identified as suitable surface capping agents for nanocrystals like CdS and ZnS [40]. Studies on amino acid capped ZnS: Mn with high photoluminescence efficiency and stability for commercial electro-luminescent devices have also been carried out [41].

Colloidal chemistry is a very versatile and flexible route for the synthesis of nanoparticles. The crystallites are grown by chemical reactions in liquid or micelle media or in polymers. The growth can be controlled by choosing the reaction temperature, duration, solvent and concentration of the reacting species. Self assembly is also an important process of spontaneous formation of nanostructures. Self organized quantum dots can be easily incorporated in devices. The field of nanocomposite materials has been recognized as a rapidly emerging research area, facilitating the growth of quantum dots at the interface [42]. Chemically synthesized semiconductor nanocomposites having strong confinement effects possess unique and size dependant linear and nonlinear properties [43].

Colloidal systems of ZnSe, CdSe and CdTe have been extensively studied owing to their excellent size tunable properties. But liberation of free radicals into the blood stream may cause toxicity. Hence these nano crystals as such are not suitable for bio imaging applications. These nanocrystals should be made biocompatible before they can be used for any biological applications. Bio compatible nanosized semiconductors can be covalently linked to biomolecules such as peptides and antibodies, for application as fluorescent probes. Amino acids are promising biocompatible capping agents for the semiconductor nanocrystals.

6.3 Objectives of the present work

This is the millennium of nanoscience and nanotechnology. Nanomaterials exhibiting optical nonlinearity have attracted wide spread research attention in recent times. Aminoacids as well as zinc oxide show optical nonlinearity and can be considered as potential candidates for nonlinear optical studies. The main thrust of the present study is to synthesize and characterize small biocompatible nanoparticles of size less than 10nm, suitable for applications in nanobiotechnology, especially for bio imaging. Nanostructured zinc oxide has been chosen for the present studies, because zinc oxide itself is not toxic and by capping with biocompatible materials such as aminoacids, it is possible to engineer the properties, especially suitable for nanobiotechnology. Nano structured materials showing luminescence in the visible range have wide applications in the nanobiotechnology regime. For biological applications of semiconductor quantum dots, proper surface modification has to be achieved which can be brought about by capping with suitable aminoacids. The main objective of the present investigations on aminoacid capped nanocrystals is to study in detail the modifications in the

structural, optical and luminescent characteristics of zinc oxide nanocrystals as a result of capping with aminoacids such as L-histidine, L-citrulline, L-arginine and the complexes L-histidine tartrate and L-citrulline oxalate.

6.4 Studies on various amino acid capped ZnO

6.4.1 Synthesis of aminoacid capped ZnO

Synthesis by chemical route has the advantage of being simple and more economical compared to the complex epitaxial methods. In addition, various capping agents can be used to prevent growth and modify the size and shape of the nanoparticles. The synthesis of zinc oxide nano particles using the wet chemical route has already been reported [44]. However the same type of synthesis modified by the incorporation of biocompatible aminoacid based capping agents has not been reported earlier.

The structural, electrical and optical properties of nano materials are sensitive to the preparation conditions. In the present work, the synthesis of aminoacid capped ZnO nano crystals was carried out through wet chemical route using zinc acetate and sodium hydroxide as precursors. All the reagents were of analytical grade and used without further purification. The entire process was carried out in distilled water at room temperature and ambient conditions. The different aminoacids used for capping were L-histidine, L-citrulline, L-arginine and the complexes L-histidine tartrate and L-citrulline oxalate.

Aminoacid capped ZnO was synthesized as follows. Zinc acetate(0.1M) was dissolved in 50 ml methanol to which 0.025M aminoacid was mixed at room temperature. Thereafter 0.2M sodium hydroxide was added and the mixture was stirred continuously for 2 hrs at room temperature. The white precipitate obtained was filtered out and dried in an oven at 60⁰C to

get the aminoacid capped ZnO nanocrystals. Schematic diagram of capped nanocrystals is shown in Fig: 6.1

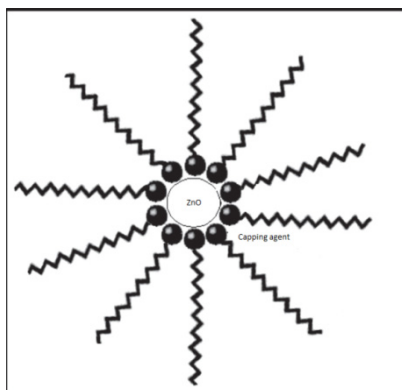


Fig: 6.1 Schematic diagram of capped nanocrystals

6.4.2 Powder X-ray diffraction

Powder X-ray diffraction studies were carried out for the zinc oxide samples capped with different aminoacids like L-histidine, L-citrulline, L-arginine and the complexes L-histidine tartrate and L-citrulline oxalate.

The structural composition of the samples was confirmed by XRD studies. All the prominent peaks of ZnO can be clearly seen in the XRD patterns of the different aminoacid capped ZnO nanocrystals as shown in Fig: 6.2. The particle size was estimated using Scherrer equation

$$d = k\lambda / \beta \cos\theta \quad (6.1)$$

k is a constant equal to 0.89, λ , the wavelength of X-rays used = 0.15496 nm, β , the full width at half maximum and θ , half of diffraction angle. The capped ZnO crystals are found to have an average size ranging from 4 to 7 nm.

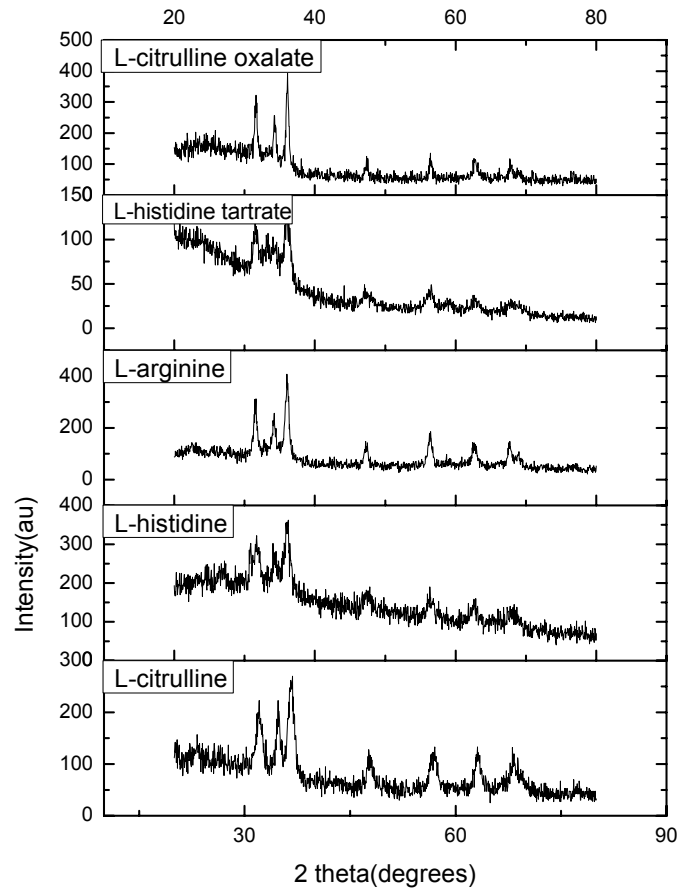


Fig: 6.2 X-ray diffraction patterns of ZnO nanocrystals capped with various aminoacids

6.4.3 Transmission electron microscope images

Transmission electron microscopy (TEM) is a technique to visualize nanostructured materials. The TEM images of the capped nanocrystals were taken using JEOL 3010 microscope. The studies were carried out to confirm the formation of nanosized particles. The images are displayed in Fig: 6.3. The size estimated from the TEM images of aminoacid capped ZnO is around 8 nm.

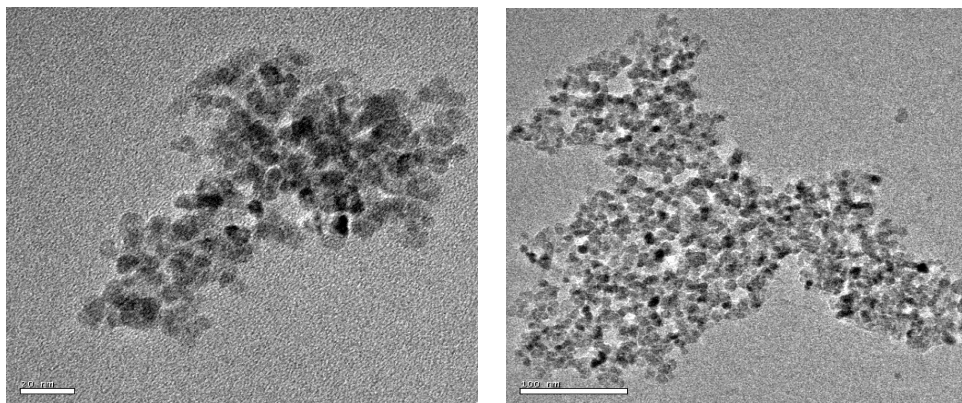


Fig: 6.3 TEM images of L-histidine capped ZnO nanocrystals

6.4.4 UV-Vis Absorption spectral analysis

The optical absorption measurements were recorded using JascoV-570 spectrophotometer. The UV-Vis absorption spectra of the aminoacid capped ZnO recorded are shown in Fig: 6.4. The excitonic peak is found to be blue shifted with respect to bulk ZnO. The absorption edge of L-histidine capped ZnO shows the maximum blue shift compared to other aminoacid capped ZnO, establishing the formation of nano crystals of lesser size.

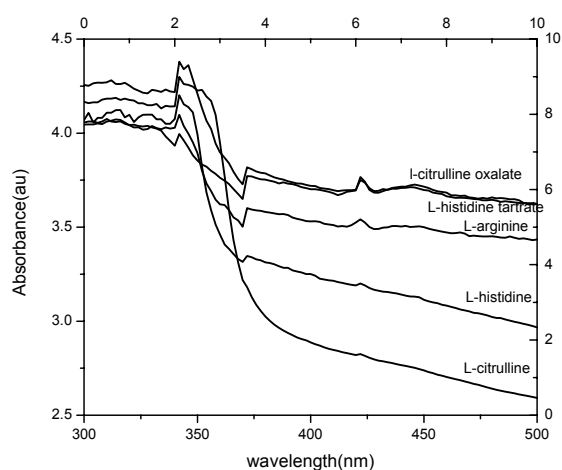


Fig: 6.4 UV-Vis absorption spectra of ZnO nanocrystals capped with different aminoacids

The size of the nanocrystals (d) was evaluated from the absorption spectra using the formula

$$1240/\lambda_{1/2} = 3.301 + 294/d^2 + 1.09/d \quad (6.2)$$

where $\lambda_{1/2}$ is the wavelength (nm) corresponding to half of absorption at shoulder and d is the size in Å [35,45]

The size of the various amino acid capped ZnO nanocrystals calculated from X-ray diffraction patterns using Scherrer formula and that from UV-Vis absorption spectra is given in Table 6.1. The size calculated in both cases is below 7nm. The capping agents have played a significant role in controlling the size and size distribution of capped ZnO nanocrystals.

Table 6.1. Size of the nanocrystals from XRD and UV absorption spectra

Capping agent	Size from XRD (nm)	Size from absorption spectra(nm)
L-citrulline	6.54	4.79
L-histidine	5.9	3.94
L-arginine	6.6	4.9
L-histidine tartrate	7.09	4.95
L-citrulline oxalate	7.5	5.28

6.4.5 Photoluminescence (PL) spectral analysis

The Photoluminescence spectra of various amino acid capped zinc oxide were recorded using Fluoramax-3 spectrofluorimeter and are shown in Fig:6.5. The intensity of the PL spectrum is maximum for L-citrulline capped ZnO, while for L-histidine capped ZnO, the UV band edge emission has been suppressed to a large extent.

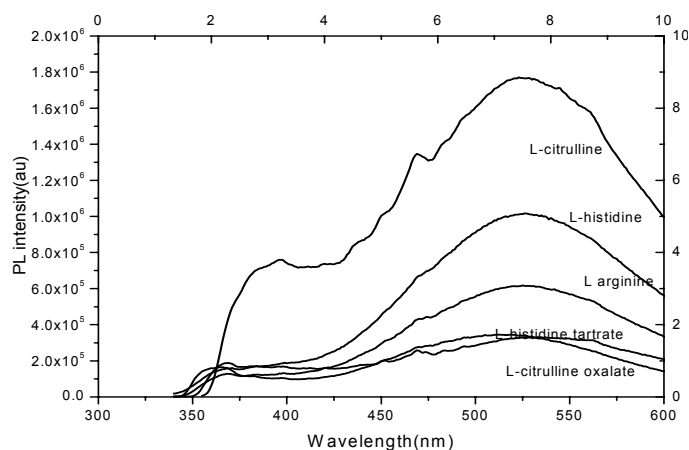


Fig: 6.5 PL spectra of ZnO nano crystals capped with various aminoacids

Photoluminescence spectrum of ZnO is normally characterized by a near-band-edge (NBE), ultra-violet (UV) emission and at least one broad band emission due to deep defect levels, extending from above 400nm up to 750 nm, *i.e.*, the whole visible spectrum. The deep lying defect levels of ZnO are divided into extrinsic and intrinsic defect levels. The possible intrinsic ‘native’ deep defect levels in ZnO are due to oxygen vacancies (VO), zinc vacancies (VZn), oxygen interstitials (Oi), zinc interstitials (Zni), oxygen anti-sites (OZn), and zinc anti-sites (ZnO). The native defects often directly or indirectly control the extent of doping, compensation, minority carrier lifetime and luminescent efficiency in semiconductors. Zinc vacancies have the lowest formation energy of all of the native defects in n-type ZnO and have been observed in many as-grown n-ZnO materials and are more favorable when growth is performed in oxygen-rich conditions [46]. Zinc vacancies are situated 0.9 eV above the valence band maxima, and hence a transition from the conduction band (or from a shallow donor) would yield a luminescence around 2.4 eV. This corresponds to the green luminescence appearing at 2.4–2.5 eV and is observed in ZnO samples grown by many techniques. Hence, zinc vacancies are widely accepted as contributing to the broad band emission

at the green wavelength, although oxygen vacancies are also suggested to be the source of the green emission. In the present study, the observed enhanced luminescence in the green region, when ZnO is capped with the amino acid L-histidine can be due to the growth of the nanocrystals in the presence of oxygen rich environment, provided by the amino acid, which consequently creates a favorable atmosphere for the generation of more Zn vacancies. The broadness of the band results from the fact that it represents a superposition of emissions from many different deep defect levels emitting at the same time.

Among the various aminoacids used for capping, it is found that L-histidine is most effective in reducing the size of the nanocrystals formed, as evident from the XRD patterns and the absorption spectra. The PL spectra highlight the possibility of using L-histidine capped ZnO for bioimaging studies, since the UV band edge emission is almost suppressed for this sample thereby confining the PL emission exclusively to the visible region. Hence further studies have been carried out with L-histidine capped zinc oxide.

6.5 Characterization of capped ZnO with L-histidine in various molar ratios

Solution chemistry is a very versatile and flexible technique to tune the size of nanocrystals to the desired range. ZnO nanocrystals capped with L-histidine in various molar ratios, 0.0125M (sample a), 0.025M (sample b) and 0.05M (sample c) were synthesized and their properties investigated.

6.5.1 X-ray diffraction patterns

The structural composition of the samples was confirmed from XRD studies. All the prominent peaks of ZnO can be clearly seen in the XRD patterns of the capped samples, shown in Fig: 6.6. The particle size was

estimated using Scherrer equation (6.1). The capped crystals have an average size ranging from 4 to 7 nm.

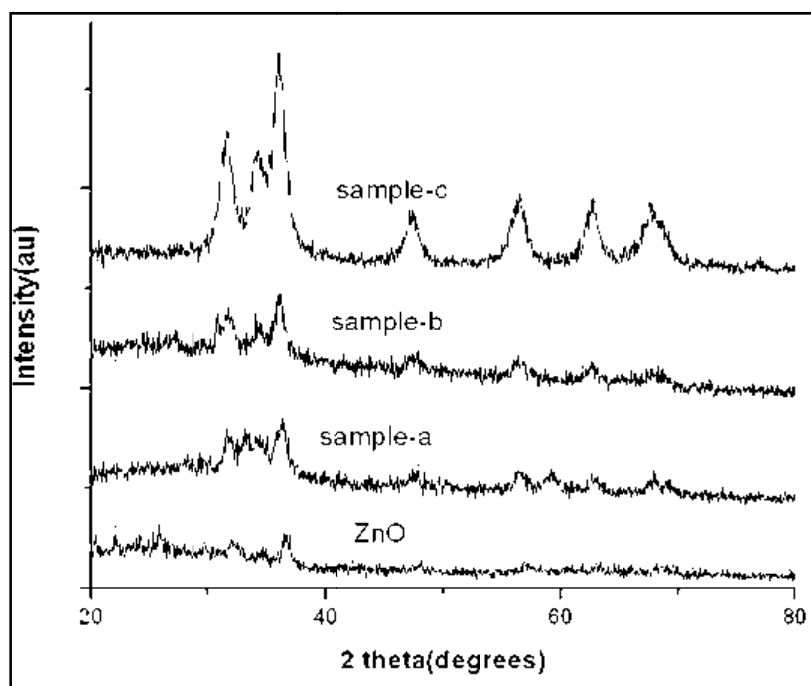


Fig: 6.6 X-ray diffraction patterns of capped ZnO nanocrystals with L-histidine in various molar ratios

6.5.2 UV-Vis absorption spectra

The UV-Vis absorption spectra of ZnO capped with L-histidine in various molar ratios are shown in Fig: 6.7 and a comparison is made with the spectrum of uncapped ZnO. For uncapped ZnO nanoparticles, the absorption starts at 384 nm while for the capped ZnO, the absorption starts at 357nm. There is a wide window of UV absorption of width 157 nm for all the three capped ZnO samples. Compared to uncapped ZnO, the absorption spectra show a blue shift which suggests that surface modification has enabled the formation of nanoparticles of lesser size.

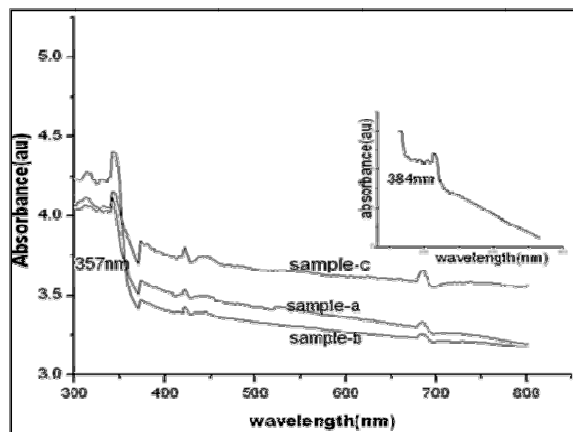


Fig: 6.7 UV-Vis absorption spectra of ZnO nano crystals capped with L-histidine in different molar ratios and uncapped ZnO (inset)

The size of the L-histidine capped ZnO nanocrystals calculated from X-ray diffraction patterns using Scherrer formula and that from UV-Vis absorption spectra is shown in Table. 6.2. The size calculated in both cases is below 8nm.

Table.6.2 Size of capped ZnO from XRD and absorption spectra

Samples	Size from XRD(nm)	Size from absorption spectra (nm)
Sample (a)	6.61	3.94
Sample (b)	5.9	3.9
Sample(c)	7.72	4.17

6.5.3 Transmission Electron Microscopy

The TEM images, shown in Fig-6.8(a, b), reveal the nanostructure of L-histidine capped ZnO. The size of the nanocrystals estimated from TEM images is of the order of 8 nm which is in good agreement with that calculated from the XRD analysis. Fig:-6.8(c) depicts the atomic scale imaging of capped

ZnO. The d value estimated from HRTEM is around 2.63 \AA . The hkl planes identified based on SAED patterns are shown in fig: 6.8(d).

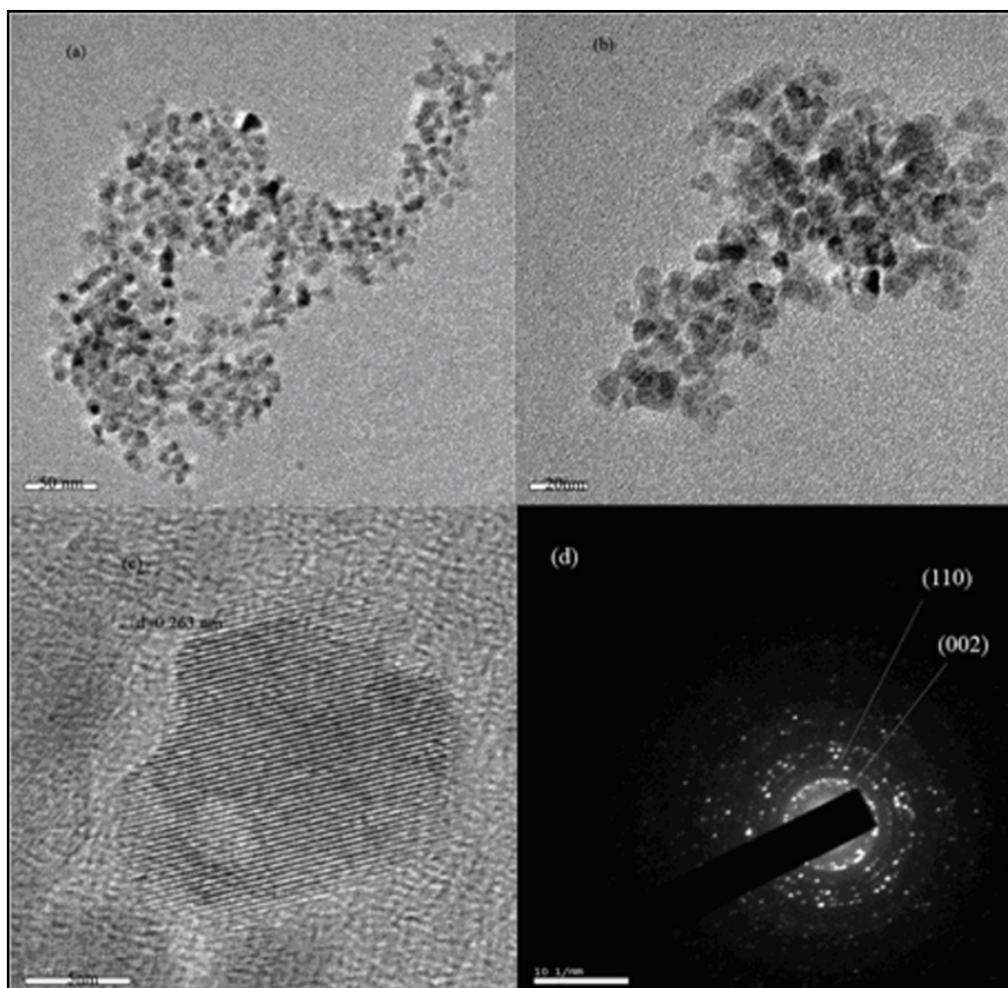


Fig:6.8 TEM (a, b), HRTEM(c) images and (d) SAED pattern of L-histidine capped ZnO nano crystals

6.5.4 EDX spectra

The EDX spectrum (Fig 6.9)of the capped samples shows the presence of carbon, hydrogen and nitrogen of L-histidine, confirming that capping has

been effective and also the presence of zinc and oxygen indicating the formation of L-histidine capped ZnO nanocrystals.

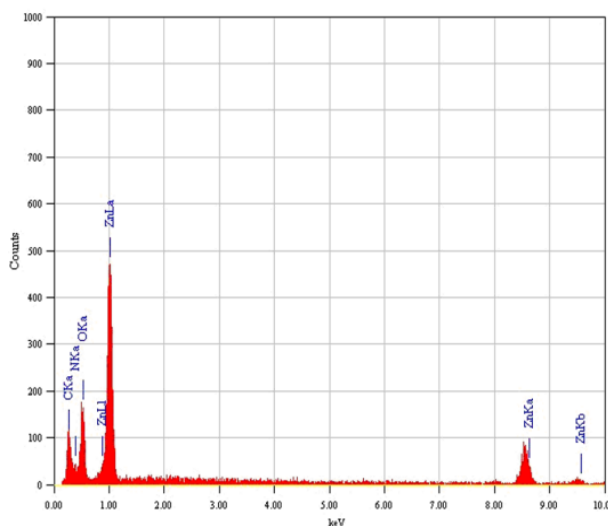


Fig: 6.9- EDX spectrum of L-histidine capped ZnO nano crystals

6.5.5 Fourier Transform Infra red Spectroscopy Studies

The FTIR spectrum of the capped ZnO shows all the vibrational bands of zinc oxide and L-histidine as shown in figure 6.10. For uncapped ZnO, bands observed at 424, 483 and 531 cm^{-1} are assigned to Zn-O vibrations [47-49]. In addition to these bands, strong bands observed at 1327 cm^{-1} , 1400 cm^{-1} and 1568 cm^{-1} can be attributed to the stretching vibrations of C=O, C=C and C-H groups respectively in acetate species of the zinc acetate precursor. The broad absorption peak centered at 3321 cm^{-1} corresponds to OH group of H₂O indicating the existence of water adsorbed on the surface of the nanocrystals. For the L-histidine capped ZnO nanocrystals also, characteristic Zn-O vibrations are observed. The band around 3315 cm^{-1} corresponds to the NH₂ stretching vibrations of the amino acid. Band at 1043 cm^{-1} is that of rocking

CH₂ and that at 1117 cm⁻¹ corresponds to the wagging NH₂ vibrations of the amino acid. These observations confirm the presence of the capping agent in the capped ZnO nanocrystals.

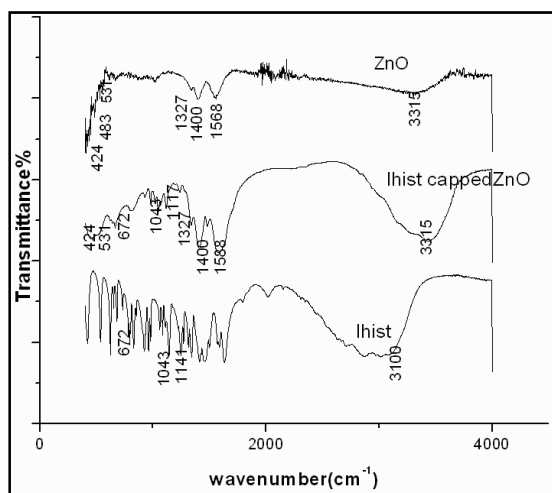


Fig: 6.10 FTIR spectra of L-histidine , ZnO and L-histidine capped ZnO nano crystals

6.5.6 PL spectra

The PL spectra of ZnO capped with L-histidine in various molar ratios are shown in Fig:6.11.

The PL spectrum of uncapped ZnO (Fig:6.11 inset) shows a wide emission band extending from UV to visible region with almost the same intensity, while for the capped ZnO, the UV band edge emission has been suppressed to a large extent. The shoulder peak at 427nm has been quenched for samples (b) and (c) which contain higher amount of L-histidine than sample (a) where the quenching is not appreciable. The green emission at 527nm has become sharper without much change in intensity in the capped samples. For bio imaging applications, PL emission with considerable intensity in the visible region is preferred. The presence of almost sharp and

highly intense green emission for capped ZnO makes it suitable for bioimaging applications. L-histidine capped ZnO nanocrystals are found to have excellent colloidal stability for days together without settling down. Capping with the nontoxic L-histidine is found to provide a hydrophilic and bio compatible surface coating, capable of rendering good colloidal stability to ZnO nanocrystals. These biocompatible nanocrystals having average size less than the size of the protein molecules offer prospects as promising biolabels in bioimaging applications.

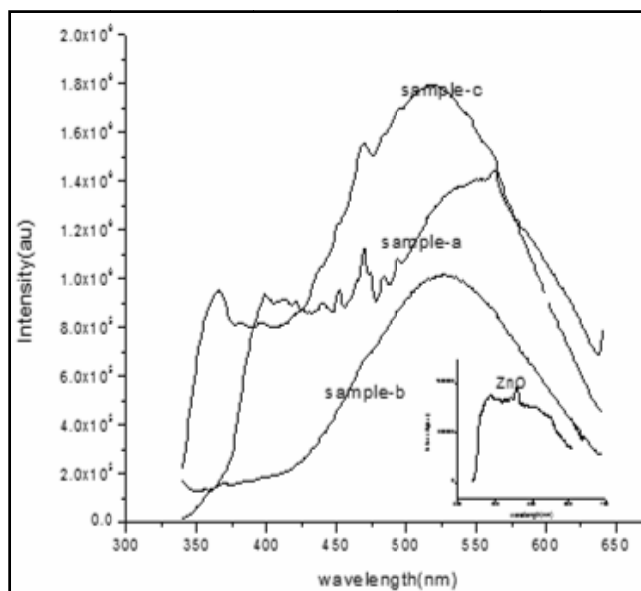


Fig: 6.11 PL spectra of ZnO nano crystals capped with L-histidine in different molar ratios and uncapped ZnO (inset)

6.5.7 Open aperture Z scan

This single beam technique developed by Sheik Bahe [50] is based on the principle of spatial beam distortion. Open aperture z-scan technique is employed to measure nonlinear absorption such as two photon absorption

which is manifested as a transmission minimum at the focal point. Zinc oxide nanocrystals show significantly high optical nonlinearity. Many of the aminoacids also exhibit optical nonlinearity. In the present work, attempts were hence made to investigate the nonlinear optical properties of L-histidine capped ZnO using open aperture z scan. The z scan curve is shown in Fig:6.12. The nonlinear absorption coefficient β is calculated to be $= 3.76 \times 10^{-9}$ m/W which is comparable with that of nano sized ZnO. The dip of the z scan curve is at 0.4 which indicates that L-histidine capped ZnO can be used as an efficient optical limiter.

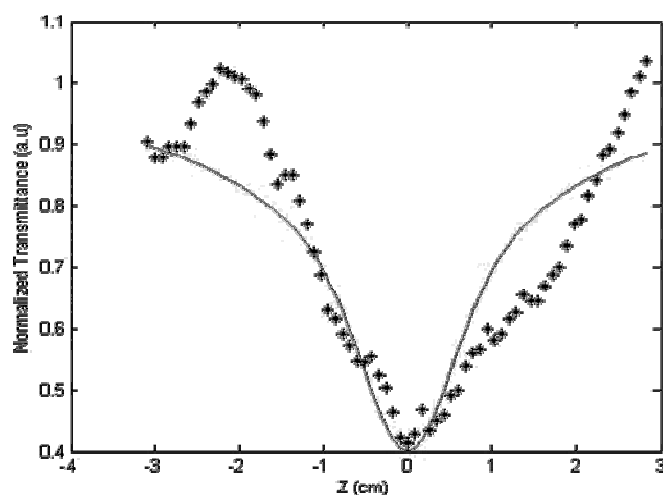


Fig: 6.12 Open aperture z scan of L- histidine capped ZnO

6.6 Studies of L- histidine capped ZnO by varying the molarity of NaOH

The size of the nanocrystals depends on various factors. The molarity of the precursors, zinc acetate and sodium hydroxide plays a vital role in deciding the size of the nano crystals. Studies on the size variation, shift in the absorption spectra and the variation in the intensity of the PL spectrum of L-

histidine capped ZnO, prepared by varying the molarity of the precursor, were carried out.

6.6.1 Synthesis

Synthesis by chemical route has many advantages as it is simple and cost effective compared to the complex epitaxial methods. The structural, electrical and optical properties of nano materials are sensitive to the preparation conditions. The synthesis of ZnO capped with L- histidine by varying the molarity of the precursor sodium hydroxide was carried out as follows.

Zinc acetate(0.1 M) and sodium hydroxide in various molar ratios (0.25M,0.2M,0.15M, and0.1M) were mixed in 50ml methanol to which 0.025M L- histidine, was added and stirred for two hours. The resulting precipitate was filtered out and dried to get L-histidine capped ZnO samples in powder form.

6.6.2 XRD studies

The powder XRD patterns of the synthesized zinc oxide samples are shown in Fig: 6.13.From the graphs it can be inferred that the size of the nanocrystals varies with the molarity of sodium hydroxide. As the molarity of NaOH decreases, the size of the nanocrystals also decreases. Hence capped ZnO nanocrystals of varying size can be synthesized by changing the molarity of the precursor NaOH.

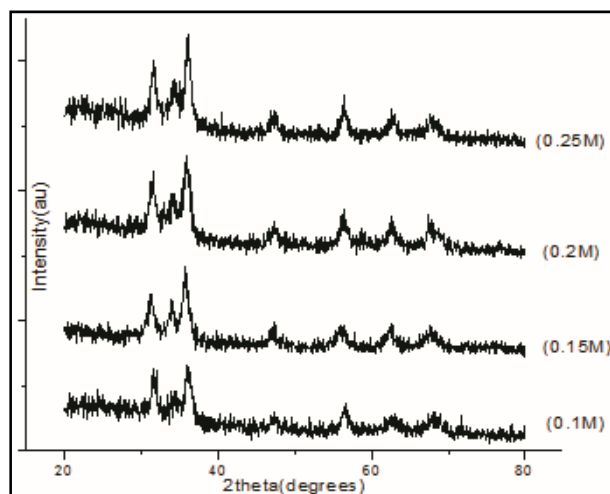


Fig: 6.13 XRD patterns of L-histidine capped ZnO, synthesized with NaOH in different molarity

6.6.3 UV-Vis absorption spectra

Figure 6.14 shows the UV-Vis absorption spectra of capped ZnO samples, synthesized with NaOH in different molarity. The size of the nanocrystals was also estimated from the UV-Vis spectra using the formula (6.2).

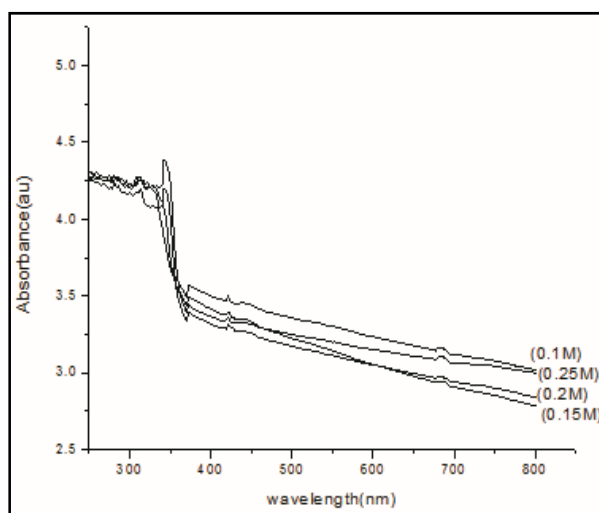


Fig: 6.14 UV-Vis absorption spectra of capped ZnO nano crystals with NaOH in various molarity

The size of the nanocrystals calculated from the XRD and UV-Vis absorption spectra is shown in Table-6.3.

Table-6.3 Size of nanocrystals determined by the two methods

Molarity of NaOH	Size from XRD(nm)	Size from UV-Vis abs spectrum(nm)
0.25M	6.2	4.1
0.2M	5.94	3.9
0.15M	4.5	3.5
0.1M	4	3.2

6.6.4 PL spectra

The PL emission spectra of capped ZnO nanocrystals of various sizes are depicted in Fig: 6.15. The PL spectrum of uncapped ZnO (Fig: 6.11 inset) shows a wide emission band extending from UV to visible region with almost the same intensity. When zinc oxide is capped with L-histidine, the UV band edge emission has been suppressed to a large extent and the green emission at 527nm has become sharper. In the samples prepared by varying the molarity of the precursor NaOH, it is found that the emission intensity increases with increase in the molarity of NaOH. For bio imaging applications, PL emission with considerable intensity in the visible region is preferred. The presence of almost sharp and highly intense green emission for capped ZnO makes it suitable for bioimaging applications. When the molarity of the precursor NaOH is varied, there is considerable change in the PL emission intensity even though the variation in the crystallite size is not significant.

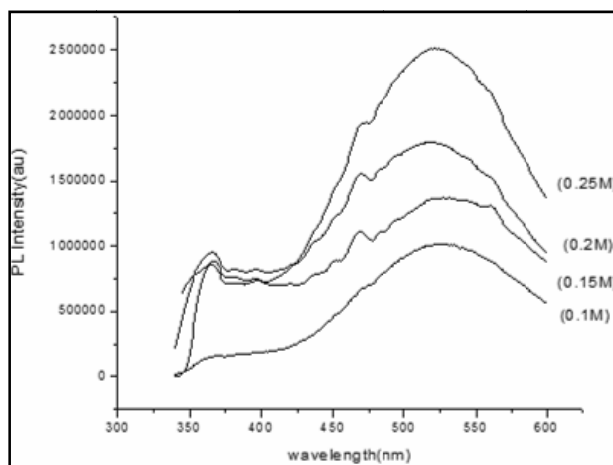


Fig: 6.15 PL spectra of capped ZnO nano crystals with NaOH in various molarity

6.6.5 Biocompatibility studies

Aminoacids which are essential for the growth of human body are generally biocompatible. Hence the aminoacid, L-histidine capped zinc oxide nanocrystals are representatives of biocompatible nanocrystals. The biocompatibility has been roughly assessed by growing bengal gram seeds with and without the presence of L-histidine capped zinc oxide. The seeds were grown in distilled water with the incorporation of capped ZnO in two different ratios of 5% and 30%. The photographs showing the growth of the seeds are displayed in Fig: 6.16. It is found that the rate of growth of the seeds is faster for 5% inclusion of capped ZnO, compared to that without the presence of any inclusions. This shows that the presence of small percentage of capped ZnO solution promotes the growth process. It is also worthy to point out that the growth is not inhibited by increasing the concentration of the capped solution which is an indication that the capped ZnO nano crystals are highly biocompatible. These biocompatible nanocrystals having average size

comparable to the size of the bio molecules offer prospects as promising biolabels in imaging applications.



Fig: 6.16 Seeds grown with (a) no inclusions(b) 5%(c) 30% inclusion of capped ZnO solution

6.7 Nanocomposite films

Nanocomposites are highly promising organic/inorganic complexes for various applications in light-emitting diodes, photodiodes, photovoltaic cells, smart microelectronic devices, gas sensors etc [51-52]. The properties of nanocomposite films can be easily adjusted by varying the composition of the filler materials. The growth of polymer nanocomposite films shares the advantages of organic device technology, such as low production cost and the possibility of device fabrication on large areas and flexible substrates.

Polymer based nano composites are of current interest due to their ability to modify the optical and mechanical properties of the host polymer. It unfolds the advantages of both polymers and filler components leading to a wide spectrum of applications. Nanocomposites play a key role in tailoring the properties to suit any technology. Nano-sized fillers have properties that are often significantly different from their counterparts with “ordinary size”. The inclusion of nano sized ZnO into polymers can influence the electrical,

mechanical and optical properties of the polymers due to strong interfacial interaction between the organic polymer and the inorganic nanoparticles[53-55]. Semiconductor nano crystals capped with amino acid ligands find applications in advanced biotechnology areas due to their unique physical, chemical and optical properties[56-58]. The optical properties of the nanocrystals can be varied according to the size of the nanocrystals with the same elemental compositions [59,60]. Modification of the surface of the nanocrystals by capping with biocompatible amino acids increases the quantum efficiency and thermal stability. Quantum dots of II-VI semiconductors show unique characteristics due to quantum confinement effects. Their band structure is reduced into discrete quantum levels due to the increasing proximity of electrons and holes on entering into the nano domain. The characteristic features of the polymer matrices and the capped ZnO nano filler material can be blended to synthesize capped ZnO/polymer nano composite films with prospects of possible applications as optical limiters, UV and NIR radiation protectors, switches and biolabels. The present study is focused on the optical absorption and photoluminescent characteristics of L-histidine tartrate capped zinc oxide/polyvinyl alcohol (PVA) nanocomposite films. The surface passivation effect of the polymer matrix has resulted in better optical absorption and luminescent properties so that these nanocomposite films can be of application as UV filters and efficient UV emitters.

6.7.1 Preparation of capped ZnO nanoparticles

The synthesis of nano sized ZnO, capped with the amino acid complex, L-histidine tartrate was carried out using the procedure reported earlier. L-histidine tartrate crystals were grown by solution growth technique using L-histidine and tartaric acid in stoichiometric ratio. The photograph of the

grown crystals is shown in Fig: 6.17. The crystals show thermal stability upto 230 °C and are found to be non hygroscopic and air stable. This crystal is chosen as capping agent for ZnO in the present study mainly because it is a biocompatible and non toxic amino acid complex showing good air and thermal stability.

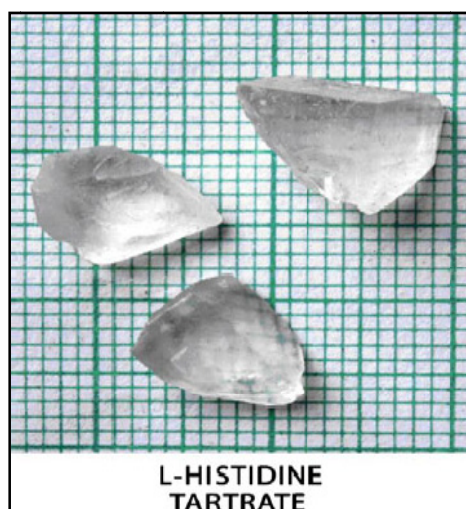


Fig: 6.17 Photograph of L-histidine tartrate crystals

6.7.2 Powder X-ray diffraction studies

L-histidine tartrate capped ZnO nano crystals were structurally characterized using Rigaku X-ray diffractometer with Cu-K α radiation of wavelength, 0.1542 nm. The XRD spectrum is displayed in Fig:6.18. The significant peaks of ZnO can be seen in the sample spectrum and the nano crystals have a particle size of ~ 7 nm, calculated using the Scherrer relation (6.1).

The diffused reflectance spectrum (DRS) of the capped ZnO powder was recorded and the plot of $(k/s \cdot hv)^2$ Vs hv (in eV), is shown in Fig: 6.19. Here k/s is a constant given by

$$k/s = (1 - R)^2 / 2R \quad (6.3)$$

where R is the absolute reflectance. The optical band gap calculated comes to 3.4 eV. There is a slight increase in the band gap compared to bulk ZnO confirming the formation of nano sized ZnO.

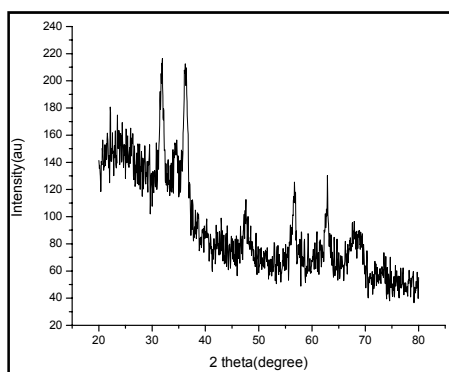


Fig: 6.18 XRD pattern of capped ZnO nano crystals

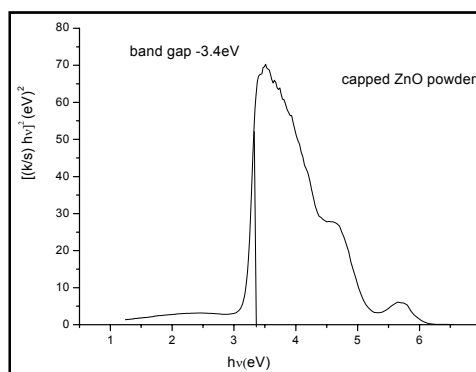


Fig: 6.19 DRS spectrum of capped ZnO powder

6.7.3 UV-Vis absorption spectra of capped ZnO nanocrystals

The UV-Vis absorption spectrum of the capped ZnO colloid (Fig:6.20) shows sharp absorption in the UV region (370nm) and a blue shift compared to bulk ZnO, which is characteristic of nanostructure. For pure ZnO, the absorption starts from 384 nm (shown in Fig:6.7) while for the capped ZnO, the absorption starts at 370nm. There is a wide window of UV absorption of width 107 nm for the capped ZnO sample. Compared to pure ZnO, the absorption edge of the capped ZnO shows a blue shift which suggests that capping has enabled the formation of nanoparticles of lesser size.

6.7.4 PL spectra of capped ZnO nanocrystals

The photo luminescence (PL) spectrum of capped ZnO (Fig: 6.21) shows emission in the UV region (368nm) followed by comparatively stronger emission in the green-yellow region. The photo luminescence (PL) spectrum

of the uncapped colloid shows emission from middle UV to the full visible range. The broad PL band in the visible region has been reported in bulk ZnO as well as in ZnO quantum dots by many researchers [61–64].

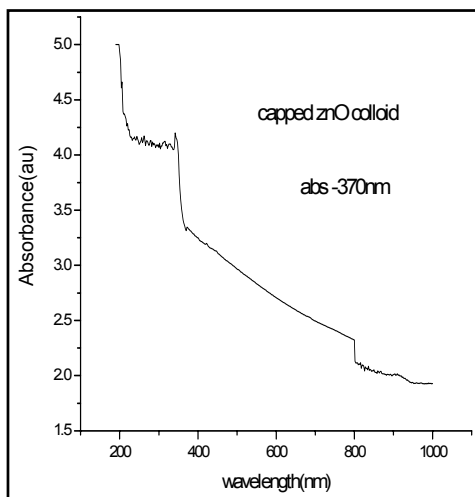


Fig: 6.20 UV-Vis absorption spectrum of capped ZnO nanocolloid

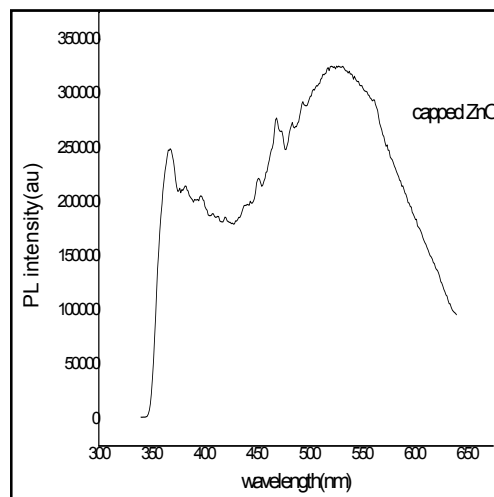


Fig: 6.21 PL spectrum of capped ZnO nanocolloid

6.8 Studies on L-histidine tartrate capped ZnO/PVA nano composite films

The nanocomposite films were grown on glass substrates using the following procedure. Poly vinyl alcohol was dissolved in water under stirring for 4 hours to obtain a 10 % w/v solution. Appropriate amount of capped ZnO powder was added to the PVA solution to have 10%, 20% and 30% by weight of the ZnO powder in the PVA matrix. The solution was stirred for ½ an hour and then sonicated for 5 minutes and films were deposited on glass substrates by spin coating technique. In the present work the spin coater(spin 150)was used with a spin speed of 5000 rpm.

6.8.1 UV-Vis absorption spectra of the nanocomposite films

The UV-Vis absorption spectra of the nanocomposite films are shown in Fig:6.22. It is found that the onset wavelength of absorption of nanocomposite films has red shift with increase in the weight % of ZnO added. The absorption intensity of the ZnO/PVA nano composite films has increased considerably compared to that of PVA alone. The absorption peak wavelength (290nm) of the nanocomposite films is substantially blue shifted relative to that of the uncapped and capped ZnO [65].

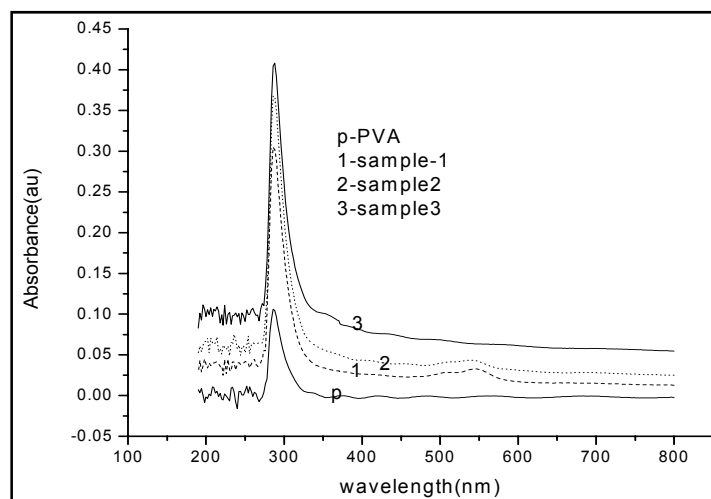


Fig: 6.22 UV-Vis Absorption spectra of ZnO/PVA nanocomposite films

The optical band gap of these films is estimated as shown in Fig: 6.23. The band gap of these films varies from 4.11eV to 3.98eV suggesting that the band gap decreases with increase in the ZnO content. The sharp increase in the intensity of UV absorption for the ZnO/PVA nano composite films, offers prospects of applications of these nanocomposite films for UV filtering.

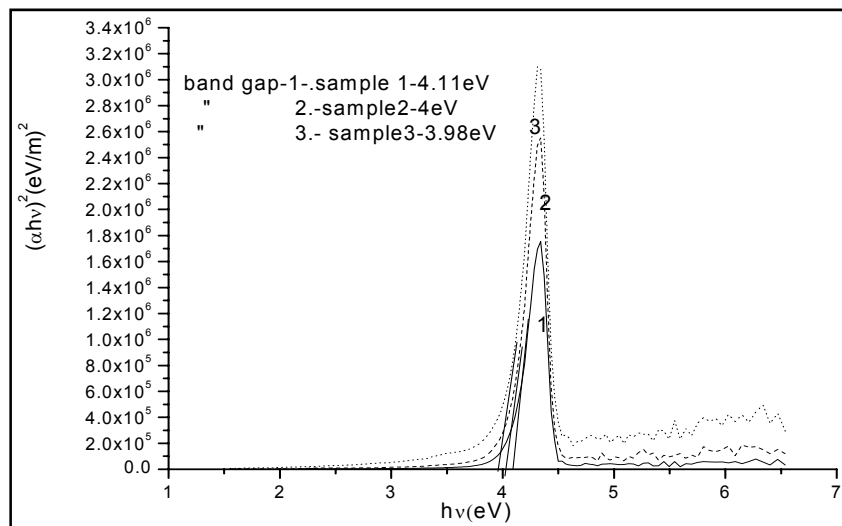


Fig: 6.23 Band gap determination of nanocomposite films

6.8.2 PL Studies of the nanocomposite films

The PL spectra of these nanocomposite films are shown in Fig:6.24.

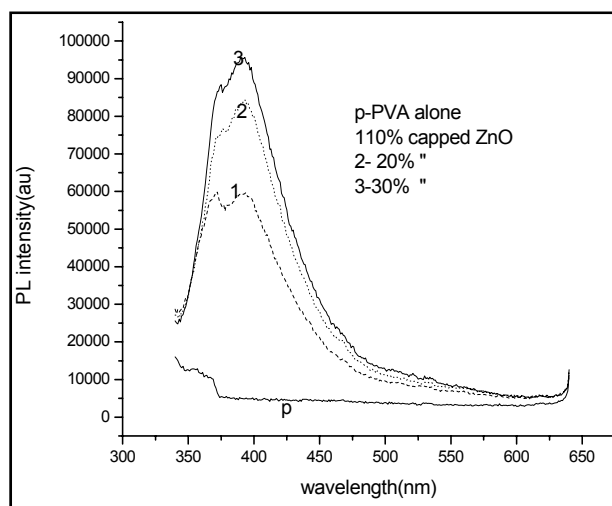


Fig: 6.24 PL spectra of nanocomposite films

The intensity of the PL emission increases with increase in the ZnO content in the films. Also the green-yellow emission of the capped ZnO has

been completely quenched in the films, confirming the surface modification of ZnO by the polymer matrix. For the nanocomposite films, the emission has been confined to the UV region, which highlights the possibilities of applications of these nanocomposite films as efficient UV emitters. All the films used in the present work have thickness around 1.505 μm , determined using the Dektak 6m Veeco thickness profiler.

6.9. Conclusions

6.9.1 Summary of aminoacid capped ZnO nanocrystals

The synthesis of ZnO nano crystals in the presence of capping agents with the perspective of biological applications has attracted wide spread attention recently. In the present work, nanocrystals of ZnO capped with different biocompatible aminoacids have been synthesized, by the wet chemical route which is a simple and cost effective method. It is found that capping with aminoacid L-histidine is effective in modifying the size and size distribution and also the PL emission characteristics of capped zinc oxide nanocrystals, compared to pure ZnO. The effective capping with the amino acid, L-histidine has been confirmed from the FTIR and EDX studies. The size and nano structure of L-histidine capped ZnO could very well be estimated from XRD and UV-Vis absorption studies and TEM analysis. The presence of L-histidine has brought about significant surface modification of ZnO, resulting in the formation of nanocrystals of smaller size. The PL spectrum of L-histidine capped ZnO shows an intense emission around 527nm in the visible region. The L-histidine capped ZnO nanocrystals are found to have excellent colloidal stability for days together without settling down. The intense PL emission in the green region, excellent colloidal stability,

biocompatibility and size comparable to that of biomolecules, observed in L-histidine capped ZnO, highlight the prospects of applications as biolabels in imaging techniques.

6.9.2 Nanocomposite films

Transparent films of ZnO nano particles capped with the biocompatible amino acid complex-L-histidine tartrate, embedded in PVA matrix have been grown on glass substrates using spin coating technique. The capping of the amino acid has enabled the formation of nano particles of smaller size. From the optical absorption and PL studies of the capped ZnO/ PVA nanocomposite films, it is clear that the PVA matrix brings about considerable surface modification of ZnO. The nanocomposite films exhibit much pronounced UV absorption at about 290nm compared to PVA films. These nanocomposite films can therefore be of application as efficient UV filters. The PL spectra of these films show a strong UV band edge emission with complete quenching of the green-yellow emission observed in the capped ZnO. This quenching of the green yellow emission in the ZnO/PVA nanocomposite films can be attributed to the fact, that surface passivation has been brought about by the polymer matrix. The intense UV band edge emission observed in the nano composite films can be of application in the realization of efficient UV emitting devices.

6.10 References

- [1] Ekimov,Elfros,Ounuchenko, Solid State Commun,56(1985)921.
- [2] Potter.B.G,Simmons.J.H,Phys.RevB 37(1988)10838.
- [3] K.D.Brinker,Sol-gel Science,Academic press,Ltd1990.
- [4] Sphanhel and Anderson, J.Am.Chem.Soc,113(1991)2826.

- [5] Nosaka, Ohta and Miyama, *J. Phys. Chem.*, 94(1990)3752.
- [6] Tennakone et al, *Chem. Phys. Lett.*, 117(1987)593
- [7] Micic et al. *J. Phys. Chem* 91, (1991)1295
- [8] Brus. L. E, *J. Chem. Phys.* 90(1986)2555.
- [9] VanDijken, E. A. Mueulenkamp, D. Vanmaekelbergh, A. Meijerink, *J Luminescence*, 90(2000)123.
- [10] Ranjani Viswanatha, D. D. Sharma et al *J. Mat. Chem.*, 14(2004)661.
- [11] A. P. Alivisatos, W. W. Gu, C. Larabell, *Ann. Rev. Biomed. Eng.*, 7(2005), 55
- [12] W. C. W. Chan, *Biol. Blood Marrow Transplant.* 12, (2006), 87.
- [13] M. Bruchez, M. Moronne, P. Gin, S. Wies and A. P. Alivisatos, *Science*, 281, (1998), 2013.
- [14] Wang Z, *J Matter* 16:(2004), 829.
- [15] W. C. W. Chan and S. Nie, *Science*, 281, (1998), 2016.
- [16] R. Elghanian, J. J. Storhoff, R. C. Mucic, R. L. Letsinger and C. A. Mirkin, *Science*, 277, (1997), 1078.
- [17] C. B. Murray, D. J. Norris, M. G. Bawendi, *J Am. Chem. Soc.* 115, (1993), 8706.
- [18] A. P. Alivisatos, *Science* 271, (1996), 933.
- [19] C. Donega, S. G. Hickey, S. F. Wuister, D. Vanmaekelbergh, A. Meijerink, *J. Phys. Chem. B* 107, (2003), 489.
- [20] Z. Adam Peng and Xiao gang Peng, *J. Am. Chem. Soc.* 123, (2001), 1389.

- [21] R. Cohen, L. Kronik, A. Shanzer, D. Cahen, A. Liu, Y. Rosenwaks, J. K. Lorenz, and A. B. Ellis, *J. Am. Chem. Soc.* 121 (1999), 10545.
- [22] Lanlan Chen, Yang Jiang, Chun Wang, Xinmei Liu, Yan Chen, Jiansheng Jie, *J Exp Nanosci* 5, (2010) , 106 .
- [23] J. Riegler, T. Nann, *Anal. Bioanal. Chem.* 379, (2004), 913.
- [24] B.D. Butkus, *Biophotonics Int.* 11, (2004), 34.
- [25] A.M. Derfus, C.W.W. Chan, N. Bhatia, *Nano Lett.* 4, (2004), 11.
- [26] W.C.W. Chan, S.M. Nie, *Science* 281, (1998), 2016.
- [27] H. Mattoussi, J.M. Mauro, E.R. Goldman, G.P. Anderson, V.C. Sundar, F.V. Mikulec, M.G. Bawendi, *J. Am. Chem. Soc.* 122, (2000) , 12142.
- [28] Yin, Hong, Casey, Philip S, McCall, Maxine, *J. Nanosci. Nanotechnol* 10, (2010)7565.
- [29] Yuan Q, Hein S, Misra RD , *Acta Biomater* 6, (2010)2732
- [30] P.Zu, Z.K.Tang, G.K.L.Wong, M.Kawasaki, A.Ohtomo, H.Koinuma, *Solid State Communications*, 103, (1997)459.
- [31] H.Cao, J.Y.Xu, E.W.Seelig, R.P.H.Chang, *J.Appl. Phys. Lett*, 76, (2000)2997.
- [32] Wen-Ching Shih, Mu-Shieng Wu, *J. Cryst. Growth*, 137(1994)319
- [33] Koch U, Fojtic A, Weller H, Henglein, *Chem Phys Lett* 122, (1985)507.
- [34] D. W. Bahnemann, C. Kormann, and M. R. Hoffmann, *Journal of Physical Chemistry*, vol. 91, no. 14, (1987)3789.
- [35] Meulenkamp EA, *J Phys Chem B* 102(1998)5566

- [36] M. S. Tokumoto, S. H. Pulcinelli, C. V. Santilli, and V. Briois, *J. Phys. Chem. B*, 107, (2003)568
- [37] L.Liao, J.C.Li, D.F.Wang, C.Liu, C.S.Liu, Q.Fu and L.X.Fan, *Nanotech*, 16, (2005) 985.
- [38] S.D.Kshir sagar, V.V.Nikesh and S.Mahamuni, *Appl. Phys.Lett.* 89, (2006)31.
- [39] Chen, X.L, Xu, C.S, Liu. Y.X, Qiao, H.Q.; Xu, H.T, Ning,Y.H, Liu, Y.C, *J. Nanosci. Nanotechnol*, 10, (2010) 2185.
- [40] Dabbousi, B. O.; Bawendi, M. G.; Onitsuka, B. O., Rubner, M. F. 66, (1995)1316.
- [41] Hwang, J. M.; Oh, M. O.; Kim, I.; Lee, J. K.; Ha, C.S, *Curr. Appl. Phys.* 5, (2005)31.
- [42] T. Yao and J.C.Woo, *Physics and applications of semiconductor quantum structures*, IOP publishing Bristol and Philadelphia, 2001.
- [43] A.Nakamura, Y.L.Lee, T.Tokizaki, *J.Luminescence*, 376 (1994) 60.
- [44] B. Vinitha, K. Manzoor, R. S. Ajimsha, P. M. Aneesh, M. K. Jayaraj, *Nano- MetalChem* 131, (2008)126.
- [45] Ranjani Viswanatha, Sameer Sapra, Subhra Sen Gupta, B. Satpati, P. V. Satyam, B. N. Dev, D. D. Sarma, *J. Phys. Chem. B*108, (2004)6303.
- [46] Janotti. A,van de Walle, *Phys. Rev. B*76, (2007)165202.
- [47] Sumetha Suwanboon, *Science Asia* 34, (2008) 031.
- [48] Yong Jae Kwon, Kyoung Hun Kima, Chang Sung Limb and Kwang, Bo Shim, *Journal of Ceramic Processing Research* 3, (2002)146.

- [49] R. Siddheswaran, R. Sankar, M. Ramesh Babu, M. Rathnakumari, R. Jayavel, P. Murugakoothan, and P. Suresh Kumar, *Crystal Res. Technol.* 41 (2006) 446.
- [50] M.S. Bahae, A.A. Said, T.H. Wei, D.J. Hagan and E.W. Van Stryland, *IEEE J. Quantum Electron.* 14(1990)760.
- [51] Godovsky DY, *Adv. Polym. Sci.* 153 : (2000)163
- [52] Chiara Ingrosso, AnnaMaria Panniello, Roberto Comparelli, Maria Lucia Curri, Marinella Striccoli *Materials* 3: (2010)1316
- [53] Lee J, Bhattacharyya D, Eastal AJ, Metson JB *Curr. Appl. Phys.* 8: (2008) 42
- [54] Sui XM, Shao CL, Liu YC *Appl. Phys. Lett.* 87: (2005)113
- [55] Xiong M, Gu G, Youn B, Wu L *J. Appl. Polym. Sci.* 153: (2000)37
- [56] Milliron D. J, Alivisatos AP, Pitois C, Edder C, Frechet JM J. *Adv. Mater.* 15: (2003)58.
- [57] Jaiswal JK, Mattoussi H., Mauro JM., Simon SM. *Nature Biotechnol.* 21: (2002)47.
- [58] Heath JR. *Acc. Chem. Res.*: 32. (1999)415.
- [59] Hoffman AJ, Mills G, Yee H, Hoffmann MR *J. Chem. Phys.* 96: (1992) 5546.
- [60] Kanemoto M., Shiragami T, Pac C, Yanagida S *J. Phys. Chem.* 96: (1992) 3521.
- [61] Gong V, Gertrude TA, Neumark F, Stephen O'Igor L *Nanoscale Res Lett* 2: (2007)297.

- [62] Guo L, Yang S, Yang C, Yu P, Wang J, Ge W, Wong GKL *Appl Phys Lett* 76: (2000)2901
- [63] Wu L, Wu Y, Pan X, Kong F *Opt Mater* 28: (2006)418.
- [64] Zhang SB, Wei SH., Zunger A *Phys Rev B* 63: (2001)75205.
- [65] Haase M, Weller H, Henglein A. *J Phys Chem* 92: (1988)482.



7.1 Summary
7.2 Scope for future work

7.1 Summary

Nonlinear optical crystals play a very powerful role in photonics and optoelectronics. The search for new NLO materials is a never ending process. Nonlinear optics has been a fascinating area, currently due to the exciting properties exhibited by materials having nonlinear response. Organic amino acid family crystals have been the centre of focus for their NLO properties.

Organic crystals possess extremely large optical nonlinearity compared to inorganic crystals. Also organic compounds have the amenability for synthesis and scope for introducing desirable characteristics by inclusions. A wide variety of organic materials having electron donor and acceptor groups, generate high order of nonlinearity.

In the present work, a new nonlinear optical crystal, L-citrulline oxalate (LCO) based on the aminoacid L-citrulline was grown using slow evaporation technique. Structural characterization was carried out by single crystal XRD. It crystallizes in the noncentrosymmetric, orthorhombic structure with space group $P2_1 P2_1 P2_1$. Functional groups present in the sample were identified by

Fourier transform infra red (FTIR) and FT-Raman spectral analysis. On studying the FTIR and Raman spectra of the precursors L-citrulline and oxalic acid, used for growing L-citrulline oxalate crystal, it is found that the significant peaks of the precursors are present in the spectra of the L-citrulline oxalate crystal. This observation along with the presence of NH_3^+ group in the spectra of L-citrulline oxalate, confirms the formation of the charge transfer complex.

Thermo gravimetric analysis (TGA) of LCO was carried out using a simultaneous thermal analyzer. The crystal is found to be highly stable up to 165°C and there after the decomposition starts. The compound starts to lose single molecules of water of crystallization around 100°C . Optical transmittance of LCO was measured in the range 200- 1000 nm and the crystal is found to possess a wide transparency region extending from 311 nm to the far IR region. Using pulsed Nd: YAG laser, the second harmonic signal generated by the crystal was confirmed by the emission of green radiation. The open aperture z-scan studies reveal the third order nonlinearity.

The dielectric studies performed show that the dielectric constant decreases with increase in frequency and has a comparatively high value at very low frequencies. The grown LCO crystal exists as a charge transfer complex, which contributes mostly for polarization in the direction of the applied field. L-citrulline oxalate is not encountered with any microbial growth even after 3 months. This favorable property makes it suitable for device applications. This crystal showing wide transparency, significant dielectric properties and moderate thermal stability can be a potential candidate as a NLO material.

Many of the optical properties can be considerably improved using lithium as the dopant. Literature survey on lithium doped materials show that many of the inherent properties of amino acid based materials can be modified by doping with lithium. Crystals of L-citrulline oxalate doped with lithium (LCOL) were grown and characterized. The structure was determined from powder XRD, refined by single crystal XRD data for LCO. The presence of the dopant lithium in the doped LCO sample was confirmed from ICPAES studies.

The presence of functional groups in lithium doped L- citrulline oxalate was established based on FT-IR and FT-Raman spectral analysis.

The recorded absorption spectrum of lithium doped LCO crystals shows a better transparency window in the visible region which is about 20nm wider than that of the pure sample. The thermo gravimetric analysis of Li doped LCO crystals was done in nitrogen atmosphere in the temperature range of 28⁰C–800⁰C. The decomposition of pure LCO sample begins at 165°C. But for lithium doped L-citrulline oxalate crystals, the decomposition starts at 205°C. The increment in the decomposition temperature is evident for the doped crystals, suggesting that the substitution of lithium enhances the thermal stability.

The SHG efficiency of doped LCO crystal is 0.9 times that of KDP. Thus, the presence of lithium metal has increased the SHG efficiency of pure LCO to a value almost comparable with that of KDP. Due to the presence of the metallic dopant in the crystal lattice, there is an increase in polarizability of the molecule, which tends to increase the SHG efficiency.

Good mechanical properties, excellent optical quality, moderate thermal stability and SHG efficiency comparable to that of KDP, make the Li doped LCO crystals a strong candidate for NLO device applications.

Potassium dihydrogen phosphate (KDP) is a well known nonlinear optical (NLO) material for various optoelectronic applications. The amino acids, the famous organic materials, play a vital role in the field of nonlinear optical crystal growth. They have proton donor COOH and proton acceptor NH₂ groups and intermolecular charge transfer is possible, which is one of the prime factors contributing to the non linear optical properties. In the present work, detailed studies were carried out to analyze the effects of aminoacid doping on the properties of KDP.

Single crystals of amino acid, L-citrulline (CKDP) and L-lysine (LKDP) doped Potassium dihydrogen phosphate (KDP) were grown by slow evaporation. The structure of the doped samples was determined from powder XRD and refined by single crystal XRD data of pure KDP. The thermal stability has also increased for both the doped samples. The UV-absorption spectrum shows a wide transparency region extending from the middle UV to the IR region for both the doped samples. The SHG efficiency of CKDP has increased to more than double the efficiency of KDP and that of LKDP to 1.4 times. It can be concluded that doping potassium dihydrogen phosphate with the aminoacids have significantly modified the nonlinear optical properties.

The pursuit for new nonlinear optical materials has resulted in the growth of a new NLO crystal L-citrulline oxalate of moderate nonlinearity, whose NLO properties are found to be considerably enhanced by lithium doping to form lithium doped L- citrulline oxalate. Also L-citrulline and

L-lysine doped potassium dihydrogen phosphate crystals are found to be promising NLO candidates better than KDP.

In a different direction, the search for NLO materials resulted in the investigations on nanostructured zinc oxide capped with aminoacids. The present work highlights the benefits of using aminoacids as capping agents for ZnO.

Nanostructured materials have conquered the new era due to their varied applications in all fields of science and technology. Photo stable fluorescent quantum dots show promise as alternatives to organic dyes for fluorescent biological labeling. For biological applications of quantum dots (QD), proper surface modification has to be achieved.

In the present work, nanocrystals of ZnO capped with different aminoacids, L-histidine, L-arginine, L-citrulline and the complexes L-citrulline oxalate and L-histidine tartrate were synthesized. It is found that capping with L-histidine is effective in modifying the size and size distribution and also the PL emission characteristics of zinc oxide nanocrystals. The effective capping with the amino acid, L-histidine was confirmed from the FTIR and EDX studies. The size and nano structure of L-histidine capped ZnO could very well be estimated from XRD and UV-Vis absorption spectra and TEM analysis. The presence of L-histidine has brought about significant modification of ZnO, resulting in the formation of nanocrystals of smaller size. The PL spectrum of L-histidine capped ZnO shows an intense green emission around 527nm which can be of practical application in imaging techniques. The capped ZnO nanocrystals are found to have excellent colloidal stability for days together without settling down. These biocompatible nanocrystals having average size less than the size of the protein molecules offer prospects as

promising biolabels in bioimaging applications. Different sized nanocrystals were also synthesized by varying the molarity of the precursor NaOH. As the molarity of NaOH was decreased, the size of the nanocrystals was also reduced resulting in the formation of quantum dots. These quantum dots offer promise as alternatives to organic dyes for fluorescent biological labeling.

Polymer nanocomposites have a significant role in tailoring the properties to suit any technology. They have the ability to modify the electrical, optical and mechanical properties of the host polymer. Present study is focused on the optical absorption and photoluminescence (PL) characteristics of the nanocomposite films of L-histidine tartrate capped zinc oxide in polyvinyl alcohol (PVA). Zinc oxide (ZnO) nanocrystals capped with the amino acid complex, L-histidine tartrate, having an average size of about 10 nm were prepared by wet chemical route at room temperature and blended with polyvinyl alcohol (PVA) in various weight percentages by solution mixing. From the PL studies of the nanocomposite films, it is observed that, the green yellow emission of ZnO has been completely quenched in the films, confining the emission entirely to the UV region. The surface modification brought about by the polymer matrix, has resulted in better optical absorption and luminescent properties. These nanocomposite films offer prospects as efficient UV filters and UV emitters.

7.2 Scope for future work

The search for new NLO materials is a treasure hunt and a never ending process. The present studies show that NLO properties of aminoacid based compounds can be very efficiently modified by doping with lithium. Detailed

investigations in this direction incorporating other metallic dopants can be carried out.

The present work highlights the benefits of using aminoacids as capping agents for ZnO.

Semiconductor quantum dots with different biocompatible capping agents can be synthesized and studied for nanophotonic and bioimaging applications.

One of the aminoacids, L-citrulline has been found to be quite effective in making Mn doped ZnS biocompatible. These biocompatible, capped, fluorescent nanoparticles can be attached to biological species such as Lysine bacillus fusi formis bacteria for visualization, having applications in metal detection, for the removal of metal components from industrial waste. Studies in this direction are of high significance in the nano biotechnology regime.
